

University of Groningen

Imaging of tumor vascularization and related hypoxia

Mees, Gilles

IMPORTANT NOTE: You are advised to consult the publisher's version (publisher's PDF) if you wish to cite from it. Please check the document version below.

Document Version

Publisher's PDF, also known as Version of record

Publication date:

2012

[Link to publication in University of Groningen/UMCG research database](#)

Citation for published version (APA):

Mees, G. (2012). Imaging of tumor vascularization and related hypoxia. [S.n.].


Copyright

Other than for strictly personal use, it is not permitted to download or to forward/distribute the text or part of it without the consent of the author(s) and/or copyright holder(s), unless the work is under an open content license (like Creative Commons).

Take-down policy

If you believe that this document breaches copyright please contact us providing details, and we will remove access to the work immediately and investigate your claim.

Downloaded from the University of Groningen/UMCG research database (Pure): <http://www.rug.nl/research/portal>. For technical reasons the number of authors shown on this cover page is limited to 10 maximum.



**Imaging of tumor vascularization
and related hypoxia :
preclinical and clinical studies.**

Gilles Mees

CMB



rijksuniversiteit
groningen

Imaging of tumor vascularization and related hypoxia

Preclinical and clinical studies

Proefschrift

ter verkrijging van het doctoraat in de
Medische Wetenschappen
aan de Rijksuniversiteit Groningen
op gezag van de
Rector Magnificus, dr. E. Sterken,
in het openbaar te verdedigen op
maandag 17 september 2012
om 16.15 uur

door

Gilles Mees

geboren op 26 april 1984
te Gent, België

Centrale	U
Medische	M
Bibliotheek	C
Groningen	G

Centrale	U
Medische	M
Bibliotheek	C
Groningen	G

Stellingen behorend bij het proefschrift

“Imaging of tumor vascularization and related hypoxia: preclinical and clinical studies.”

“It remains difficult to discern whether hypoxia and/or HIF-1 activation are a cause or a contributing factor in aerobic glycolysis.”

“The relationship found between CA IX expression and [¹⁸F]FDG-PET imaging suggests that in the future it may be possible to identify NSCLC patients that are most likely to benefit from CA IX targeting therapy on the basis of [¹⁸F]FDG-PET imaging.”

“Possibly, in situations where [¹⁸F]FDG-PET imaging is less successful due to low [¹⁸F]FDG-avidity or a low or decreased tumor-to-background ratio, imaging after pharmacological HIF-1 activation might increase sensitivity.”

“Imaging using ^{99m}Tc-(CO)₃ His-CNA35 allows selective imaging of tumor vasculature through a mechanism in which the characteristic leakiness and immaturity of tumor blood vessels allows binding of subendothelial collagen IV.”

“Given its mechanism of binding, CNA35 might be an ideal candidate to identify the time frame of the ‘normalisation window’ of antiangiogenic therapy and thereby identify the ideal moment to administer chemotherapy.”

"Biological processes rarely have absolute truth; it's only our artificial constructs of those truths that tend to be absolute." - unknown

"Common sense is what tells us the Earth is flat and the Sun goes around it." - Stuart Chase

“In science one tries to tell people, in such a way as to be understood by everyone, something that no one ever knew before. But in poetry, it's the exact opposite.” - Paul Dirac

“Good judgement comes from experience. Experience comes from bad judgement.” - Jim Horning

"Laugh at your problems; everybody else does." - unknown

Promotores:

Prof. dr. C. Van de Wiele
Prof. dr. R.A.J.O. Dierckx

Beoordelingscommissie:

Prof. dr. J.A. Langendijk
Prof. dr. P.M. Kluin
Prof. dr. A. Signore



ISBN: 978-90-367-5682-2

Cover illustration: Dougal Haston on the summit of mount Everest after the first successful ascent of the south-west face, september 25th 1975. Photo courtesy of Doug Scott.

“We walked up side by side the last few paces to the top, arriving there together the entire world lay before us. That summit was everything and more that a summit should be. My usually reticent partner became expansive, his face broke out in a broad, happy smile and we stood there hugging each other and thumping each other’s backs.”

Table of contents

List of abbreviations.....	7
Summary	9
Samenvatting	11
Chapter 1: Introduction and Aims	13
1.1 Hypoxia: definition	15
1.2 Tumor hypoxia: definition and causative factors	16
1.3 Tumor hypoxia: consequences	18
1.4 Tumor hypoxia: detection	20
1.4.1 Invasive detection of tumor hypoxia	20
1.4.2 Non-invasive detection of tumor hypoxia.....	22
1.4.2.1 Non-invasive detection of tumor hypoxia with PET.....	24
1.4.2.2 Non-invasive detection of tumor hypoxia with SPECT.....	34
1.5 Tumor hypoxia and tumor metabolism	39
1.6 References	42
1.7 Outline and objectives	59
Chapter 2: Tumor Hypoxia and Glucose Metabolism.....	61
2.1 Research article: Combined effect of EPO and radiotherapy on the expression of endogenous molecular markers of tumour metabolism and metastasis.	63
2.2 Research article: Pharmacological activation of tumor hypoxia: a means to increase tumor [¹⁸ F]FDG-uptake?	81
2.3 Research article: Metabolic correlates of tumour hypoxia in malignant canine mammary carcinoma.	101
2.4 Research article: CA-IX expression correlates with FDG-uptake by primary NSCLC.	111
Chapter 3: Tumor Hypoxia and Vasculature	123
Research article: ^{99m} Tc-labeled tricarbonyl His-CNA35 as an imaging agent for the detection of tumor vasculature.	125

Chapter 4: General Discussion	145
Chapter 5: Conclusions and Future Perspectives	153
References	159
Curriculum Vitae	165
Acknowledgements	169

List of abbreviations

ANOVA	analysis of variance
ARCON	accelerated fractionated radiotherapy combined with carbogen
α SMA	alpha smooth muscle actin
ATP	adenosine triphosphate
ATSM	diacetyl-bis(N ⁴ -methylthiosemicarbazone)
BSA	bovine serum albumin
CA IX	carbonic anhydrase IX
CBP	CREB (cAMP-response-element-binding protein)-binding protein
CIT	citrate
CNA	collagen-binding adhesion protein
CoCl ₂	cobalt chloride
COX	cytochrome c oxidase
CT	computed tomography
DAB	diaminobenzidine
DCE	dynamic contrast enhanced
DMOG	dimethylloxalylglycine
DNA	deoxyribonucleic acid
ECM	extracellular matrix
ED	effective dose
EDE	effective dose equivalent
EDTA	ethylenediaminetetraacetic acid
ELISA	enzyme-linked immunosorbent assay
EMT	epithelial to mesenchymal transformation
FAZA	fluoroazomycin-arabinofuranoside
FBS	fetal bovine serum
FDG	2-deoxy-2-fluoro-D-glucose
FET	O-(2-fluoroethyl)-L-tyrosine
FETA	fluoroetanidazole
FETNIM	fluoroerythronitromidazole
FIH-1	factor inhibiting HIF-1
FLSD	Fisher's protected least significant differences
FLT	3'-fluoro-3'-deoxy-L-thymidine
FMISO	fluoromisonidazole
FOV	field of view
G6P	glucose-6-phosphatase
GLUT	glucose transporter
H-score	histological score
HIF-1	hypoxia-inducible factor 1
HK	hexokinase
HMBS	hydroxymethylbilane synthase
HPLC	high-performance liquid chromatography
HRP	horseradish peroxidase
IAZA	iodoazomycin arabinoside
ID	injected dose
IFP	interstitial fluid pressure
ip	intraperitoneal(ly)

ITLC	instant thin layer chromatography
IU	international unit
iv	intravenous(ly)
LDH-A	lactate dehydrogenase-A
MIRD	medical internal radiation dose
MRI	magnetic resonance imaging
mRNA	messenger ribonucleic acid
MVD	microvessel density
N-CAD	N-cadherin
NSCLC	non-small-cell lung carcinoma
OG	oxoglutarate
PBS	phosphate-buffered saline
PDH	pyruvate dehydrogenase
PDK1	pyruvate dehydrogenase kinase 1
PET	positron emission tomography
PHD	prolyl hydroxylase
pi	post-injection
rhEPO	recombinant human erythropoietin
RT	radiotherapy
sc	subcutaneous(ly)
SD	standard deviation
SDHA	succinate dehydrogenase complex subunit A
SDS-PAGE	sodium dodecyl sulphate polyacrylamide gel electrophoresis
SEM	standard error of the mean
SPECT	single photon emission computed tomography
SUV	standardized uptake value
TAC	time-activity curve
T/B ratio	tumour-to-background ratio
TBS	tris-buffered saline
TCA	tricarboxylic acid
VDAC	voltage-dependent anion channel
VEGF	vascular endothelial growth factor
VHL	von Hippel-Lindau
VMI	vessel maturity index
VOI	volume of interest

Summary

Tumor hypoxia is a characteristic feature of locally advanced solid tumors which has been described in a wide range of tumor types. It is the consequence of the tumor's uncontrolled growth and structural and functional abnormalities of its blood vessels. Its presence is associated with a negative prognosis and impairs the effectiveness of common anti-cancer therapies. Despite the existence of a number of specialized PET tracers for the detection of tumor hypoxia, their use is limited. The most widely used PET tracer for tumor detection, staging and evaluating therapy response is the glucose analogue [^{18}F]FDG, which exploits the inherent dependence of the tumor cell on glycolysis (Warburg effect). As the proteins responsible for [^{18}F]FDG-uptake are under control of HIF-1, the master transcription factor regulating the hypoxic response, the degree of [^{18}F]FDG-uptake might indirectly reflect the level of tumor hypoxia and vice versa. Detection of tumor hypoxia under certain circumstances using [^{18}F]FDG would obviate the need for more specialized hypoxia radiotracers. Additionally, as there are a number of situations where [^{18}F]FDG-PET imaging is less than ideal (high physiological uptake, low tumor metabolic rate, high tumor G6P-levels), insight into the close relation between tumor hypoxia and tumor metabolism might provide opportunities to increase tumor [^{18}F]FDG-uptake and thereby improve imaging. In this work the effects of a modification of tumor oxygenation on tumor metabolism and with it the possible consequences and benefits for functional imaging using [^{18}F]FDG-PET, were studied and a new marker of tumor vasculature was validated. In Chapter 2, partim 2.1, the effects of an increase in tumor oxygenation on tumor metabolism were studied by investigating changes in expression of proteins important for tumor metabolism, survival and spread in a rat colorectal xenograft after treatment with rhEPO. This study showed the detrimental effects of the combination of rhEPO treatment with RT. In Chapter 2, partim 2.2, the effects of a decrease in tumor oxygenation or a direct HIF-1 activation on tumor metabolism were studied by investigating [^{18}F]FDG-uptake in an *in vitro* and *in vivo* model of human colorectal carcinoma. Activation of HIF-1 and subsequent transcription of proteins responsible for [^{18}F]FDG-uptake, increased [^{18}F]FDG-uptake in HT29-cells. Although physical induction of hypoxia in an *in vivo* model of human colorectal carcinoma using hydralazine did not result in an increase in tumor [^{18}F]FDG-uptake, systemic administration of a chemical inhibiting HIF-1 α breakdown resulted in a significant increase in SUVmax and SUVmean. In Chapter 2, partim 2.3, the distribution of the exogenous nitroimidazole hypoxia

marker pimonidazole was compared with the expression of GLUT1 and 3, HK2 and CA IX in a spontaneous canine mammary gland tumor and a statistically significant correlation was found between pimonidazole staining and GLUT1 expression. In Chapter 2, partim 2.4, a significant correlation was found between SUVmax and SUVmean values of patients suffering from NSCLC and the expression of the endogenous hypoxia marker CA IX. Although our results suggest that [^{18}F]FDG-uptake might reflect tumor hypoxia, the use of [^{18}F]FDG as a reliable non-invasive marker of tumor hypoxia seems questionable. Nevertheless, insights into the relationship between tumor hypoxia and tumor metabolism can create opportunities to increase tumor [^{18}F]FDG-uptake in situations where diagnostic accuracy is suboptimal. In Chapter 3, a new radiotracer ($^{99\text{m}}\text{Tc}(\text{CO})_3$ His-CNA35) that selectively binds tumor vasculature was evaluated. Our results indicated the convenient preparation of a stable, functional and specific radiotracer that gives a reliable estimate of existing tumor vasculature through the binding of subendothelial collagen IV due to the characteristic leakiness and immaturity of tumor blood vessels in a human HT29 colorectal carcinoma xenograft. Non-invasive detection of tumor vasculature might (i) offer a tool to provide a reliable assessment of tumor vasculature and thus provide a means for the management and planning of anti-angiogenic therapy and (ii) might provide insights into tumor hypoxia.

Samenvatting

Tumorale hypoxie is een karakteristiek fenomeen dat is beschreven in verscheidene tumor types. Het is het gevolg van een ongecontroleerde tumorale groei en structurele en functionele abnormaliteiten van de tumorale bloedvaten. De aanwezigheid van tumorale hypoxie is geassocieerd met een negatieve prognose en vermindert de efficiëntie van standaard oncologische behandelingen zoals radio- en chemotherapie. Ondanks het bestaan van verscheidene gespecialiseerde PET tracers voor de detectie van tumorale hypoxie, is hun gebruik eerder beperkt. De meest gebruikte PET tracer voor kanker detectie, staging en nagaan van therapie respons is het glucose analog $[^{18}\text{F}]\text{FDG}$, welke de inherente afhankelijkheid van de tumor cel op glycolyse voor z'n energieproductie (Warburg effect) uitbuit. Omdat de eiwitten die verantwoordelijk zijn voor $[^{18}\text{F}]\text{FDG}$ -opname onder de controle staan van HIF-1, de centrale transcriptiefactor die de hypoxische respons regelt, zou de mate van hypoxie deels worden weergegeven door de mate van $[^{18}\text{F}]\text{FDG}$ -opname en omgekeerd. Detectie van hypoxie door middel van $[^{18}\text{F}]\text{FDG}$ zou gespecialiseerde hypoxie tracers overbodig maken. Bijkomend zouden in situaties waarin beeldvorming dmv. $[^{18}\text{F}]\text{FDG}$ -PET minder ideaal is (hoge fysiologische opname, lage metabole activiteit, hoge tumorale G6P activiteit), de inzichten in deze relatie mogelijkheden kunnen bieden om tumorale $[^{18}\text{F}]\text{FDG}$ -opname te verhogen en op die manier beeldvorming kunnen verbeteren. In dit werk werden de effecten van een modificatie van de oxygenatie op het metabolisme van de tumor nagegaan en daarmee de mogelijke gevolgen en voordelen voor functionele beeldvorming dmv. $[^{18}\text{F}]\text{FDG}$ -PET. Bijkomend werd een nieuwe merker voor tumorale vasculatuur gevalideerd. In Hoofdstuk 2, partim 2.1 werden de effecten van een stijging van de tumorale oxygenatie op de expressie van een aantal metabole eiwitten nagegaan. Deze studie toonde de negatieve invloed aan van de combinatie van rhEPO - behandeling en radiotherapie. In Hoofdstuk 2, partim 2.2 werd tumorale $[^{18}\text{F}]\text{FDG}$ opname nagegaan na chemische inductie van hypoxie en chemische activatie van HIF-1 in een *in vitro* en *in vivo* model van colorectale kanker. Activatie van HIF-1 en de daaropvolgende transcriptie van eiwitten die verantwoordelijk zijn voor de opname van $[^{18}\text{F}]\text{FDG}$, leidde tot een stijging van $[^{18}\text{F}]\text{FDG}$ opname in HT29 cellen. Waar fysische inductie van hypoxie in een *in vivo* model van colorectale kanker dmv. hydralazine niet resulteerde in een stijging van de tumorale $[^{18}\text{F}]\text{FDG}$ opname, resulteerde systemische toediening van geneesmiddelen die de afbraak van HIF-1 inhibeerden, in een significante stijging van SUVmax en SUVmean. Deze resultaten geven aan dat, in situaties waar

[¹⁸F]FDG-PET beeldvorming minder ideaal is, voorbehandeling met geneesmiddelen die de afbraak van HIF-1 inhiberen, mogelijk tumorale [¹⁸F]FDG-opname kunnen doen stijgen. In Hoofdstuk 2, partim 2.3 werd een gelijkaardig expressiepatroon gevonden van eiwitten die verantwoordelijk zijn voor [¹⁸F]FDG-opname en pimonidazole, een exogene hypoxie merker, in een spontaan borstcarcinoom in honden. In Hoofdstuk 2, partim 2.4 werd een significante correlatie gevonden tussen de SUV_{max} en SUV_{mean} waarden van patiënten die lijden aan longkanker en de expressie van CA IX, een endogene merker van hypoxie. Hoewel onze resultaten suggereren dat [¹⁸F]FDG-opname en hypoxie in hoge mate verbonden zijn, lijkt het gebruik van [¹⁸F]FDG als betrouwbare merker voor hypoxie twijfelachtig. Wel kunnen inzichten in deze relatie de mogelijkheid bieden om tumorale [¹⁸F]FDG-opname te vergroten in situaties waarin de diagnostische accuraatheid suboptimaal is. In Hoofdstuk 3 werd een nieuwe tracer (^{99m}Tc-(CO)₃ His-CNA35) geëvalueerd, die selectief bindt aan tumorale bloedvaten. Onze resultaten gaven aan dat deze radiotracer gemakkelijk te produceren is, stabiel en functioneel is, en een betrouwbare inschatting geeft van de bestaande tumorale vasculatuur door de binding van de subendotheliale collageen IV laag als gevolg van de structurele abnormaliteiten van tumorale bloedvaten in een HT29 colorectaal carcinoom xenograft. Niet-invasieve detectie van tumorale bloedvaten kan: (i) een mogelijkheid bieden om op een betrouwbare manier anti-angiogene therapie te plannen (ii) inzichten bieden in het proces van tumorale hypoxie.

Chapter 1: Introduction and Aims

1.1 Hypoxia: definition

Maintaining a normal oxygen (O_2) homeostasis is a key prerequisite for the development, growth and normal function of all mammals. In every mammalian cell, O_2 is used in aerobic respiration to generate energy in the form of ATP (adenosine triphosphate) and other energy-carrying molecules. Under normal aerobic conditions, this happens through the succession of glycolysis and Krebs cycle (alternatively known as the TCA (tricarboxylic acid) cycle) where oxidative phosphorylation is completed. The former takes place in the cytosol and does not require O_2 , the latter takes place in the mitochondria and requires O_2 . In the absence of O_2 , the end product of glycolysis (pyruvate) does not enter the Krebs cycle but is broken down (to lactic acid) in a process yielding considerable less energy than aerobic respiration (Lodish et al. 2004). Oxygen thus ensures an efficient cellular energy production. Normal physiological pO_2 -values across the body range from 150 mmHg in the upper airway to 66-24 mmHg in different tissues/organs (see Table 1).

Tissue / Position	pO_2 (mmHg)	reference
Sea level	159 mmHg	
Upper airway	150 mmHg	
Alveolar blood	100 mmHg	Stainsby et al., 1988
Arterial blood	95 mmHg	Stainsby et al., 1988
Venous blood	40 mmHg	Stainsby et al., 1988
Tissue, organ dependent	66-24 mmHg	Vaupel, 1989
Malignancies	≤ 20 mmHg	Vaupel, 1989
Anoxia	0 mmHg	

Table 1. pO_2 -levels across the body.

When there is an imbalance between O_2 supply and demand, tissue hypoxia arises. It can be caused by a number of factors such as low O_2 partial pressure in arterial blood (hypoxemic hypoxia), reduced ability of blood to carry O_2 (anaemic hypoxia), reduced tissue perfusion (circulatory or ischemic hypoxia), deterioration of the diffusion geometry (diffusional hypoxia), and the inability of cells to use O_2 due to intoxication (histotoxic or cytotoxic hypoxia). In normal physiological circumstances, an increase in O_2 -consumption is matched by an increase in blood flow and, therefore, does not lead to hypoxia (Hockel et al. 2001).

1.2 Tumor hypoxia: definition and causative factors

As apposed to normal mammalian cells, tumor cells are characterized by their uncontrolled growth due to self-sufficiency in growth signals, insensitivity to antigrowth signals, limitless replicative potential, sustained angiogenesis, tissue invasion and metastasis, and evasion of apoptosis (Hanahan et al. 2000). As a result of this uncontrolled growth, a tumor outgrows the vasculature and resources it relies on and intratumoral hypoxia arises. The occurrence of heterogeneously distributed, clinically relevant areas of hypoxia and/or anoxia is a characteristic feature of locally advanced solid tumors which has been described in a wide range of tumor types and in approximately 50-60% of all solid tumors. The pretherapeutic oxygenation status assessed in cancers of the breast, uterine cervix and head and neck is lower than in their respective normal counterpart and is independent of clinical size, stage, histology, grade, nodal status and a series of other tumor characteristics or patient demographics. Tumor-to-tumor variability in oxygenation is greater than intra-tumor variability and there doesn't seem to be a topological distribution of pO_2 values within the tumor. Local recurrences have a higher hypoxic fraction than the respective primary tumors and there is no difference in oxygenation status between primary and metastatic malignancies (Vaupel et al. 1989, Hockel et al. 2001, Vaupel et al. 2007). Although no sharp threshold exists between hypoxia and normoxia and no single hypoxic treshold is generally applicable, a median O_2 partial pressure in the tumor of approximately 8-10 mmHg appears to represent a critical threshold below which detrimental changes associated with reduced O_2 consumption have been described and intracellular acidosis, ATP depletion, and a drop in energy supply will occur. The threshold O_2 partial pressure below which oxidative phosphorylation, and thus ATP formation, will cease, is dependent on cell line and experimental setup and is believed to lie between 0.5 and 10 mmHg (Hockel et al. 2001).

Commonly, three major pathogenetic mechanisms involved in the emergence of tumor hypoxia are described, respectively chronic hypoxia, acute hypoxia and anaemic hypoxia.

Chronic or diffusion-related hypoxia is believed to be the result of increased diffusion distances between the nutritive blood vessels and the tumor cells or deterioration of diffusion geometry. As a consequence, O_2 -supply (and nutrient supply) for cells distant ($> 70\mu m$) from nutritive blood vessels, is obstructed.

Acute or perfusion-related hypoxia is an often transient form of hypoxia which is caused by an inadequate blood flow in the tumor and is believed to be the result of an abnormal structure

and function of the tumoral microvessels. The formation of these vessels is achieved through the process of angiogenesis in which, through a multistep process that relies on the tumor-driven production of pro-angiogenic factors, new blood vessels are formed from existing ones (Carmeliet et al. 2000). These resulting new blood vessels however, are structurally and functionally deficient when compared to normal ones. Anatomically, tumor blood vessels are disorganized, dilated, tortuous and leaky. Unlike the blood vessels of normal tissue, which have an organized and regular branching order, tumor blood vessels display irregular interconnections and branching, and are heterogeneous in their spatial distribution within the tumor. At the cellular level, the endothelial cells that line the tumor blood vessels have an irregular, disorganized morphology, leading to an incomplete endothelial lining with large inter-endothelial junctions and an increased number of fenestrations (Baluk et al. 2005, Fukumura et al. 2007, Carmeliet et al. 2011). In addition, perivascular cells (pericytes and vascular smooth muscle cells), that normally surround and support the endothelium, have an abnormal morphology and a heterogeneous association with tumor vessels. These cells usually lie within the vessel basement membrane and interact closely with endothelial cells to prevent vessel leakage (Baluk et al. 2005, Fukumura et al. 2007, Carmeliet et al. 2011). Finally, the vascular basement membrane in tumor tissue also displays abnormal characteristics. It has a loose association with endothelial cells and is characterized by multiple redundant layers, irregular thickness, focal holes and broad extensions into the tumor stroma (Baluk et al. 2005). These structural and functional deficiencies of tumor vasculature lead to heterogeneous blood flow, hypoxia, acidosis and elevated interstitial fluid pressure (IFP) with a disturbed tumor microenvironment as a result (Fukumura et al. 2007). The molecular mechanisms underlying this abnormal vasculature characteristics are not entirely clear, but an imbalance between pro- and anti-angiogenic factors as the tumor grows, is believed to be a key contributor (Jain et al. 2005).

Finally, a third type of hypoxia (anaemic hypoxia) is sometimes described which is the result of reduced O₂ transport capacity of the blood due to the presence of disease- or treatment-related anaemia which frequently accompanies cancer (Vaupel et al. 2007).

1.3 Tumor hypoxia: consequences

Cancer cells adapt to hypoxic conditions by the induction of target genes involved in glucose metabolism, angiogenesis, erythropoiesis and apoptosis in an effort to overcome their compromised situation. Many of these adaptations are coordinated by the transcription factor hypoxia-inducible factor (HIF) - 1, which has been verified as a master regulator of oxygen homeostasis under hypoxic conditions (Semenza et al. 2000). HIF-1 is a heterodimer consisting of HIF-1 α and HIF-1 β . Its biological activity is determined by the expression and activity of HIF-1 α which is constantly expressed and subsequently rapidly destroyed under normal oxygen conditions. This involves a mechanism where post-translational hydroxylation of specific proline residues (Pro⁴⁰² and Pro⁵⁶⁴) by prolyl hydroxylases (PHD) allows binding of the von Hippel-Lindau (VHL) tumor suppressor protein which in turn leads to ubiquitination by an E3 ubiquitin-protein ligase and subsequent proteosomal degradation. Additionally, factor inhibiting HIF-1 (FIH-1) hydroxylates an asparagine residue (Asn⁸⁰³) within HIF-1 α and thereby blocks its interaction with the co-activators p300 and CBP [CREB (cAMP-response-element-binding protein)-binding protein] (Mahon et al. 2001, Lando et al. 2002). Under hypoxic conditions however, stabilization of HIF-1 α occurs through inactivation of the PHDs, allowing it to translocate to the nucleus where it can bind with the constitutively expressed HIF-1 β to form a functional transcription factor that will transactivate several target genes (Vaupel et al. 2004, Kim et al. 2007, Semenza et al. 2007). These target genes include amongst others vascular endothelial growth factor (VEGF), facilitative glucose transporters (GLUTs), hexokinases (HKs), erythropoietin (EPO), carbonic anhydrase IX (CAIX), ... The resulting adaptive changes in the proteome and genome of the tumor cells are, after selection and clonal expansion, believed to lead to a more adapted and aggressive tumor cell population. Accordingly, the presence of tumor hypoxia impairs the effectiveness of common anti-cancer therapies like radiotherapy (RT) and chemotherapy. Hypoxia-induced radioresistance is multifactorial. Besides the above mentioned proteomic and genomic changes that most likely contribute to resistance by increasing the number of mutated cells that are more resistant to apoptosis or have an increased proliferative and metastatic potential, and by causing upregulation of several repair enzymes and stress proteins (Hockel et al. 2001, Harrison et al. 2004), the main reason for radioresistance is the intrinsic dependence of RT on oxygen to cause damage to the tumor cell. As oxygen has a very high electron affinity, it stabilizes the DNA-damaging radicals that are formed after the interaction of radiation with intracellular water. Additionally, oxygen stabilizes ('fixes') the radicals that are formed after

direct interaction of radiation with the DNA (Harrison et al. 2004). This effect, widely known as the 'oxygen enhancement ratio', implies that the radiation dose needed to acquire the same biologic effect is two to three times higher in the absence of oxygen than in the presence of oxygen (Gray et al. 1953). Hypoxia has also been shown to reduce chemotherapeutic efficacy by causing cells within hypoxic regions to cycle more slowly, and by providing a selection mechanism for cells with reduced susceptibility for apoptosis and upregulation of several repair enzymes and stress proteins (Hickman et al. 1994, Hockel et al. 2001). Also, several chemotherapeutic agents like cyclophosphamide, carboplatin and doxorubicin have been shown to be oxygen dependent in *in vitro* and *in vivo* conditions (Teicher 1990 et al., Hockel et al. 2001, Harrison et al. 2004). Additionally, due to limited drug penetration within solid tumors, hypoxic regions are often protected from the cytotoxic effects of chemotherapeutic agents further reducing drug efficacy (Hockel et al. 2001, Durand et al. 2001). All these mechanisms together ensure that tumor hypoxia is a negative prognostic factor. Accordingly, tumor hypoxia measured with invasive oxygen electrodes has been associated with an aggressive tumor phenotype, poor response to radio- and chemotherapy, and worse prognosis in advanced squamous cell carcinoma of the cervix (Hockel et al. 1996, Fyles et al. 1998), head and neck (Nordsmark et al. 1996, Brizel et al. 1997, Nordsmark et al. 2005), and soft-tissue sarcomas (Brizel et al. 1996).

In order to increase success of RT and chemotherapy, attempts have been made to reduce tumor hypoxia and its effects. A first approach is to directly increase the oxygen supply to the tumor. This can be done by the use of hyperbaric oxygen and accelerated fractionated radiotherapy combined with carbogen (ARCON) or by the correction of anaemia by blood transfusion or the administration of recombinant human erythropoietin (rhEPO). A second approach is the development of chemicals that mimic oxygen and sensitize hypoxic cells to radiation of which the nitroimidazole compounds are the best known. Further, attempts have been made to selectively target hypoxic cells through the use of hypoxia-specific cytotoxins. These bioreductive drugs are reduced by biological enzymes to their toxic and active metabolites in the absence of oxygen (Hoogsteen et al. 2007).

1.4 Tumor hypoxia: detection

Given its importance in tumor biology and in order to predict outcome and identify patients with a worse prognosis and/or patients that would benefit from appropriate treatments, *in vivo* measurement of tumor hypoxia is required. Several different approaches exist for the detection of tumor hypoxia including invasive (oxygen electrodes, endogenous markers, exogenous markers) and non-invasive methods (MRI, PET-, SPECT-imaging).

1.4.1 Invasive detection of tumor hypoxia.

At present, the best-known technique for direct *in vivo* determination of tumor oxygenation is the real-time measurement of oxygen tension in tissues with invasive oxygen electrodes such as the Eppendorf™ polarographic needle electrode (Fyles et al. 1998, Olive et al. 2001, Nordmark et al. 2005) and the OxyLite™ fiber-optic probe (Bussink et al. 2000, Jarm et al. 2002, Brurberg et al. 2003). Although both have a different mode of action, they allow direct measurement of oxygen concentrations at different positions in the tumor. Whereas the Eppendorf™ polarographic needle electrode consumes oxygen during its operation and is moved throughout the tissue during measurements, providing multiple samplings, the OxyLite™ fiber-optic probe does not consume oxygen and can be left at one position for a longer period of time making it more suitable for the detection of temporal fluctuations in pO₂. Tumor oxygenation measurements obtained using the Eppendorf™ polarographic needle electrode correlated well with clinical outcome in several clinical trials (Hockel et al. 1996, Brizel et al. 1996, Nordmark et al. 1996, Brizel et al. 1997, Fyles 1998, Nordmark 2005). As a consequence, this technique has been considered the “gold standard” for oxygenation measurements in human tumors. Nonetheless, this technically demanding procedure has a number of drawbacks and limitations like its sensitivity for sampling errors, large inter-observer variability, its invasive nature, failure to distinguish necrotic areas from viable tumor tissue and the fact that only easy accessible tumors can be studied.

Several different proteins that are involved in the hypoxic response, of which the most important are HIF-1 α , CA IX, GLUT1 and GLUT3, have emerged as possible endogenous markers of hypoxia.

As a part of the transcription factor HIF-1, HIF-1 α seems the most obvious choice as an endogenous marker of tumor hypoxia. Exposure of HeLaS3 cells to hypoxia for less than 2 min already revealed nuclear HIF-1 α protein induction. Reoxygenation reduced HIF-1 DNA

binding within 2 min, and nuclear HIF-1 α protein levels within 4 to 8 min, down to a level below the detection limit within 32 min (Jewell et al. 2001). This quick hypoxic response would make HIF-1 α the ideal hypoxic endogenous marker for detection of chronic as well as acute hypoxia. Unfortunately, studies trying to identify a correlation between immunohistochemical HIF-1 α expression and electrode measurements have reported only a weak (Haugland et al. 2002, Hutchison et al. 2004) or lack of (Mayer et al. 2004) correlation. The transmembrane zinc metalloenzyme carbonic anhydrase IX (CA IX) catalyzes the reversible hydration of carbon dioxide to carbonic acid and is involved in respiration and acid-base balance (Potter et al. 2004). The gene for CA IX has been shown to be the most strongly hypoxia-inducible gene of 25504 transcripts on a gene array (Lal et al. 2001). A study by Vordermark et al. showed that hypoxia-induced CA IX protein expression was delayed (detectable level of expression after 6h of hypoxia, highest level of expression after 24h of hypoxia) and that the protein was stable for 96h after reoxygenation in human fibrosarcoma and human pharyngeal carcinoma cells (Vordermark et al. 2005). As a result, it appears that CA IX is more suited as a marker of chronic hypoxia than as a marker of acute hypoxia. Several studies investigated a possible correlation of CA IX expression with oxygenation status in several types of cancer with mixed results. Whereas some studies reported on a positive correlation between these two (Loncaster et al. 2001, Le et al. 2006, Iakovlev et al. 2007), other studies found no such correlation (Hedley et al. 2003, Mayer et al. 2005, Jankovic et al. 2006).

Also controlled by HIF-1 and of interest as endogenous markers of hypoxia are the facilitative glucose transporters (GLUTs) 1 and 3 which mediate the transport of glucose and other monosaccharides across the plasma membrane of mammalian cells. As the timescale for GLUT1 expression appears to be similar to that of CA IX (Rafajova et al. 2004), GLUT1 is also expected to be mainly a marker of chronic hypoxia. Again, conflicting results were found when comparing GLUT1 expression with oxygenation status (Airley et al. 2001, Mayer et al. 2005, Sakata et al. 2006).

To date, it remains unclear whether the conflicting results when looking for a correlation between the expression of endogenous hypoxia markers and direct tumor oxygenation measurements have a methodological or biological cause. Probably, the combination of the above mentioned limitations and drawbacks associated with the use of invasive oxygen electrodes taken together with the influence of hypoxia-independent microenvironmental parameters such as differentiation, pH, glucose availability, oncogene activation, ... on the

expression of proteins downstream of HIF-1, is responsible for the mixed results (Bussink et al. 2003).

The most studied invasive marker for qualitative and quantitative determination of tumor hypoxia in experimental and clinical circumstances is the exogenous hypoxia marker pimonidazole hydrochloride. This 2-nitroimidazole reagent is reduced under hypoxic conditions and the resulting adducts are irreversibly bound to thiol-containing proteins in viable hypoxic cells with functional nitro-reductase enzymes. After it has been reduced and bound in tumor tissue, loss of the marker mainly occurs through cell loss (Ljungkvist et al. 2005). It shows a steep increase in the amount of reduction below a pO_2 of 10 mmHg (Gross et al. 1995). This was confirmed in a study by Raleigh et al. in which pimonidazole binding was compared with micro-electrode pO_2 measurements. They found that the correlation was strongest when the pimonidazole hypoxic fraction was compared with the percentage of pO_2 values below 10 mmHg (Raleigh et al. 1999). Other studies that compared pimonidazole binding with invasive oxygen measurements have yielded inconsistent results (Bussink et al. 2000, Olive et al. 2001, Nordmark et al. 2003). Necrosis is thought to be the main confounding factor. As pimonidazole staining is usually seen at a distance from blood vessels (Janssen et al. 2002), it is believed that it mainly detects chronic (diffusion-related) hypoxia. Although numerous studies reported on correlations between pimonidazole staining and HIF-1 α expression (Hutchinson et al. 2004, Jankovic et al. 2006, Russel et al. 2009), CA IX expression (Hoskin et al. 2003, Jankovic et al. 2006, Shin et al. 2007, Russel et al. 2009) and GLUT1 expression (Airley et al. 2003, Hoskin et al. 2003) in several tumor types, other studies proved negative in this regard (Janssen et al. 2002, van Laarhoven et al. 2006, Goethals et al. 2006). Besides analysis of a possible correlation by correlating fractions of positively stained areas and intensities, some of these studies performed a more qualitative analysis taking into account the degree of colocalization.

1.4.2 Non-invasive detection of tumor hypoxia

In nuclear medicine, the distribution of a previously administered radiolabeled molecule is studied by means of specialized instrumentation to assist in the diagnosis and treatment of disease. In contrast to anatomical imaging modalities like CT (computed tomography) and MRI (magnetic resonance imaging), which provide morphological information of the studied object, nuclear medicine techniques attempt to provide functional and biological information.

A gamma camera or SPECT (single photon emission computed tomography) camera detects scintillations that result from the interaction of SPECT radioisotopes (e.g. technetium-99m (^{99m}Tc), iodine-123 (^{123}I)) emitted gamma rays with a sodium iodide crystal in front of the camera. A lead collimator placed in front of this crystal ensures that only gamma rays that are travelling perpendicularly to the crystal face can enter. In this way a projection of the distribution of the radiopharmaceutical in the body can be obtained. By the use of specific reconstruction algorithms, the planar images that are obtained at different angles by rotating the camera around the patient, are reconstructed to tomographic images (Eberl et al. 1998, Bailey et al. 1998). The same principle is used in PET (positron emission tomography) where images are acquired through the indirect detection of PET radioisotopes (e.g. fluorine-18 (^{18}F), carbon-11 (^{11}C), oxygen-15 (^{15}O)) emitted positrons. When positrons emitted from positron emitting molecules interact with an electron in its surrounding, annihilation of both takes place and electromagnetic radiation in the form of two high-energy (511 keV) photons emitted 180° away from each other is generated. Simultaneous detection of these photons by detectors on opposite sides of the object allows mapping of the distribution of the annihilations ('coincidence detection') (Meikle et al. 1998). The half-lives of SPECT radioisotopes is usually longer than that of PET radioisotopes, allowing longer acquisition times. This short half-life of PET radioisotopes raises the need for an on-site cyclotron and specialized radiosynthesis facilities, whereas the production of SPECT radiopharmaceuticals is less expensive and less cumbersome. On the other hand, PET cameras have a superior spatial resolution and PET allows more accurate quantification (Van de Wiele 2006). Nuclear medicine has proven its role in today's clinical practice were it is used for a variety of applications. One of the major applications is in oncology where different radiopharmaceuticals are used for cancer detection, staging and monitoring of response and recurrence in several tumor types. For these purposes, a variety of radiopharmaceuticals are available to allow evaluation of tumor metabolism, cell death, cell proliferation, tumor hypoxia, Below is an overview of the most important radiopharmaceuticals to detect tumor hypoxia which was published as a review (Molecular imaging of hypoxia with radiolabeled agents. *European Journal of Nuclear Medicine and Molecular Imaging*. 2009;36:1674-1686.)

1.4.2.1

Non-invasive detection of tumor hypoxia with PET

1) Nitroimidazole compounds

These compounds are reduced into reactive intermediary metabolites by intracellular reductases in a process which is directly related to the level of oxygenation/hypoxia. This causes a gradient which is favourable for detection of hypoxic cells. Subsequently, these metabolites covalently bind to thiol groups of intracellular proteins and thereby accumulate within viable hypoxic cells. When labelled with a PET-tracer, these chemicals can be detected using PET-imaging methods. Several nitroimidazole compounds with different properties and labelled with different PET radionuclides have been described (Lee et al. 2007, Krohn et al. 2008).

A) [^{18}F]FMISO ([^{18}F]fluoromisonidazole)

Preclinical data: Kubota et al. evaluated the tumour imaging potential of [^{18}F]FMISO in an AH109A tumour rat xenograft and examined the correlation between intratumoural distributions of [^{18}F]FMISO, ^{14}C -2-deoxyglucose and ^{14}C -methionine. Hypoxic and radioresistant tumours could be identified by increased [^{18}F]FMISO uptake. A large overlap in the distribution of [^{18}F]FMISO and ^{14}C -2-deoxyglucose and a small overlap in the distribution of [^{18}F]FMISO and ^{14}C -methionine were observed (Kubota et al. 1999). In a study by Rasey et al., an attempt was made to define the relationship between [^{18}F]FMISO uptake and radiobiologically hypoxic fraction in a 36B10 glioma rat xenograft. Although the relationship between classically defined radiobiologically hypoxic fraction and [^{18}F]FMISO time-activity data remained to be clarified, [^{18}F]FMISO retention provided useful correlations with the degree of hypoxia (Rasey et al. 2000). Bentzen et al. compared [^{18}F]FMISO uptake with invasive Eppendorf electrode pO_2 measurements in a C3H mammary carcinoma mouse xenograft and found no direct correlation between both methods (Benten et al. 2002).

A number of studies compared [^{18}F]FMISO uptake with immunohistochemical staining techniques. In a study by Dubois et al., [^{18}F]FMISO uptake was compared with the exogenous hypoxia marker pimonidazole and the endogenous hypoxia marker carbonic anhydrase IX (CA IX) in a rhabdomyosarcoma rat xenograft. A statistically significant correlation was obtained between the hypoxic volumes defined with [^{18}F]FMISO PET and the volumes

derived from the pimonidazole- and CA IX-stained tumour sections, indicating the value of [^{18}F]FMISO PET to measure hypoxia (Dubois et al. 2004). Troost et al. tried to validate [^{18}F]FMISO PET by comparing [^{18}F]FMISO uptake with pimonidazole staining in several xenograft models in two different studies. Both studies found a correlation between [^{18}F]FMISO uptake and pimonidazole immunohistochemistry (Troost et al. 2006, Troost et al. 2008).

In a number of studies [^{18}F]FMISO uptake was compared with [^{18}F]FDG uptake. Most of these studies demonstrated the feasibility and utility of [^{18}F]FMISO PET imaging to identify tumour hypoxia whereas [^{18}F]FDG PET imaging seemed less suitable for this purpose (Bentzen et al. 2000, Wyss et al. 2006, Zanzonico et al. 2006, Oswald et al. 2007, Dence et al. 2008).

Clinical data: Valk et al. were the first to demonstrate the feasibility of [^{18}F]FMISO PET to detect tumour hypoxia in three patients with malignant glioma (Valk et al. 1992). Rasey et al. assessed pretreatment hypoxia in a variety of human tumours using [^{18}F]FMISO PET and concluded that human tumour hypoxia is widely prevalent and highly variable between different tumours of the same histology and also between regions within the same tumour (Rasey et al. 1996). In a study by Bruehlmeier et al. where hypoxia was measured in eleven patients with various brain tumours, it was concluded that late [^{18}F]FMISO PET images provide a spatial description of tumour hypoxia which may develop irrespective of the magnitude of perfusion as measured with ^{15}O - H_2O PET (Bruehlmeier et al. 2004).

A number of studies compared [^{18}F]FMISO uptake with invasive Eppendorf electrode pO_2 measurements. In some of these studies, [^{18}F]FMISO uptake in renal cell carcinoma and head and neck cancer correlated well with pO_2 measurements from polarographic needle oxygen electrodes, confirming the use of [^{18}F]FMISO PET to measure tumour hypoxia (Lawrentschuk et al. 2005, Zimny et al. 2006, Gagel et al. 2007, Gagel et al. 2004, Bentzen et al. 2003). Bentzen et al., however found no correlation between [^{18}F]FMISO uptake and pO_2 measurements in human soft tissue tumours (Bentzen et al. 2003). Some of the above mentioned studies also compared uptake of [^{18}F]FDG and [^{18}F]FMISO in patients with head and neck cancer. They found no correlation between [^{18}F]FDG uptake and pO_2 measurements whereas an association between [^{18}F]FMISO uptake and pO_2 measurements existed (27-29). Further comparison of [^{18}F]FDG and [^{18}F]FMISO indicated that no correlation exist between both tracers as both represent different tumour characteristics (Rajendran et al. 2003, Rajendran et al. 2004, Cherk et al. 2006, Cher et al. 2006, Thorwarth et al. 2006).

Several clinical studies have used [^{18}F]FMISO PET as a prognostic indicator in oncology. In a study by Rajendran et al., the prognostic effect of pretherapy [^{18}F]FMISO PET on survival was investigated in 73 patients with head and neck cancer and pretreatment [^{18}F]FMISO uptake proved to be an independent prognostic factor (Rajendran et al. 2006). Another study of 12 patients with head and neck carcinoma who received a preradiotherapy [^{18}F]FMISO PET scan, concluded that [^{18}F]FMISO uptake was predictive of treatment response to radiotherapy (Thorwarth et al. 2006). Similarly, in forty patients with advanced head and neck cancer and non-small cell lung cancer, outcome after radiotherapy could be predicted on the basis of kinetic behaviour of [^{18}F]FMISO in tumour tissue (Eschmann et al. 2005). Two studies investigating the prognostic significance of [^{18}F]FMISO PET in patients with head and neck cancer receiving chemoradiation in combination with the hypoxia sensitizer tirapazamine concluded that [^{18}F]FMISO uptake can predict prognosis and is associated with a high risk of locoregional failure (Hicks et al. 2005, Rischin et al. 2006). Cher et al. showed that in patients with malignant glioma, [^{18}F]FMISO uptake is prognostic for treatment outcome in the majority of patients (Cher et al. 2006). In a study with eight patients with non-small cell lung cancer receiving chemotherapy and/or radiotherapy, changes in [^{18}F]FMISO uptake measured early response to therapy and may predict freedom from disease as well as overall survival (Gagel et al. 2006). A recent study that was conducted to evaluate the reproducibility of [^{18}F]FMISO intratumour distribution in 20 patients with head and neck cancer showed considerable variability in the intratumour uptake that can occur between repeated [^{18}F]FMISO PET scans performed 3 days apart (Nehmeh et al. 2008).

B) [^{18}F]FAZA ([^{18}F]fluoroazomycin-arabinofuranoside)

Preclinical data: Sorger et al. compared the selective uptake of [^{18}F]FMISO and [^{18}F]FAZA in hypoxic cells *in vitro* and in a Walker 256 rat sarcoma model. The *in vitro* study showed that [^{18}F]FAZA is able to indicate reduced oxygen supply in the same order of magnitude of [^{18}F]FMISO. The *in vivo* study however, indicated that [^{18}F]FMISO displayed a slightly higher standardized uptake value and tumour-to-muscle ratio compared to [^{18}F]FAZA though the elimination of the latter was much faster (Sorger et al. 2003). Two other studies also compared [^{18}F]FMISO and [^{18}F]FAZA in various tumour mice xenografts and reported superior biokinetics for [^{18}F]FAZA compared with [^{18}F]FMISO. In both studies [^{18}F]FAZA displayed higher tumour-to-background, tumour-to-muscle and tumour-to-blood ratios due to its more rapid clearance from blood and non-target tissues (Piert et al. 2005, Reischl et al.

2007). Beck et al. evaluated the predictive value of [^{18}F]FAZA PET for success of radiotherapy in combination with tirapazamine in EMT6 tumour mice xenografts. High [^{18}F]FAZA uptake was identified as an independent adverse prognostic factor for tumour progression and hypoxia imaging with [^{18}F]FAZA PET was able to predict the success of radiochemotherapy (Beck et al. 2007). In a study by Busk et al., [^{18}F]FAZA uptake was compared with Eppendorf electrode measurements and the hypoxia marker pimonidazole. The distribution of [^{18}F]FAZA proved to be consistent with tumour hypoxia, as identified with the Eppendorf electrode measurements and the hypoxia marker pimonidazole (Busk et al. 2008). The same group compared the *in vitro* hypoxia specificity of cellular [^{18}F]FDG and [^{18}F]FAZA retention and tested tracer distribution between hypoxic and non-hypoxic areas in different mice xenografts. As well the *in vitro* as the *in vivo* experiments indicated that [^{18}F]FAZA is an excellent marker for tumour hypoxia, whereas [^{18}F]FDG is not (Busk et al. 2008).

Clinical data: Souvatzoglou et al. evaluated the feasibility of [^{18}F]FAZA PET for the imaging of tumour hypoxia in eleven patients with head and neck cancer and concluded that PET imaging with [^{18}F]FAZA is feasible and that adequate image quality is achieved (Souvatzoglou et al. 2007). Another study, that included 18 patients with advanced squamous cell head and neck cancer, evaluated the role of [^{18}F]FAZA PET imaging to identify hypoxia in order to plan radiation treatment. It was concluded that radiation treatment planning and intensity-modulated radiotherapy based on [^{18}F]FAZA uptake measurements is feasible (Grosu et al. 2007).

C) [^{18}F]FETA ([^{18}F]fluoroetanidazole)

In a study by Rasey et al., four cultured rodent cell lines were incubated with [^{18}F]FETA for various times under graded O_2 concentrations. The biodistributions of [^{18}F]FETA and [^{18}F]fluoromisonidazole (FMISO) at 2h and 4h postinjection in C3H mice bearing KHTn tumours were also compared. [^{18}F]FMISO and [^{18}F]FETA demonstrated similar oxygen dependency of binding in cultured cells. However, differences in biodistribution suggested advantages of [^{18}F]FETA over [^{18}F]FMISO because [^{18}F]FETA appeared to be less metabolized *in vivo* than [^{18}F]FMISO (Rasey et al. 1999). In another study, the cellular transport and retention of [^{18}F]FETA was determined *in vitro* under air and nitrogen and the biodistribution and metabolism was determined in mice bearing several different xenografts. It was concluded that [^{18}F]FETA has suitable physicochemical properties and is stable to non-

hypoxic degradation *in vivo*. It was also demonstrated that the tumour retention of the radiotracer is related to radiobiological hypoxia and pO_2 status as determined with polarographic needle oxygen electrodes (Barthel et al. 2004).

D) [^{18}F]FETNIM ([^{18}F]fluoroerythronitromodazole)

Preclinical data: Yang et al. reported on the synthesis and evaluation of [^{18}F]FETNIM. Their results indicated that at 4h after injection, tumour-to-blood and tumour-to-muscle ratios in mammary tumour-bearing rats were significantly higher with [^{18}F]FETNIM than with [^{18}F]FMISO (Yang et al. 1995). In a later study by Grönroos et al. where the pharmacokinetic properties and metabolite formation of [^{18}F]FETNIM were studied, [^{18}F]FETNIM showed low peripheral metabolism, little defluorination, and possible metabolic trapping in hypoxic tumour tissue (Grönroos et al. 2001). In a pre-clinical study by the same group, the hypoxia imaging ability of [^{18}F]FETNIM was compared with that of [^{18}F]FMISO in a C3H mammary carcinoma mice xenograft under different oxygenation conditions. Additionally, the biodistribution of both markers in normal tissues was assessed under similar conditions. Uptake of both tracers correlated with the oxygenation status in the tumours, but [^{18}F]FETNIM showed a low and favourable background signal in normal tissues as compared with [^{18}F]FMISO (Grönroos et al. 2004).

Clinical data: Most of the clinical studies with [^{18}F]FETNIM were performed in patients with head and neck cancer. A study investigating the accurate radiation dosimetry in 27 patients with head and neck cancer concluded that the effective dose of [^{18}F]FETNIM PET is well within the range of several related nuclear medicine procedures (Tolvanen et al. 2002). A lot of clinical studies were performed by researchers at the University of Turku in Finland. They found that [^{18}F]FETNIM uptake in the early phase of tissue accumulation, as measured using [^{15}O]H₂O and PET, was highly variable and depended for the most part on perfusion (Lehtiö et al. 2001). Tumour-to-plasma ratio provided the best estimate for tumour hypoxia (Lehtiö et al. 2004). In another study the radiotherapy response was assessed by hypoxia imaging with [^{18}F]FETNIM PET in 21 patients with head and neck cancer and high uptake of [^{18}F]FETNIM prior to radiation therapy was associated with a trend towards poor overall survival (Lehtiö et al. 2004).

E) [^{18}F]EF5

In a study by Ziemer et al., the biodistribution of [^{18}F]EF5 was assessed using hepatoma and glioma rodent tumour models. [^{18}F]EF5 was rapidly and uniformly distributed to all tissues. This together with its high drug stability *in vivo* suggests that [^{18}F]EF5 is a promising agent for the noninvasive assessment of tumour hypoxia (Ziemer et al. 2003). Another study investigated hypoxia in androgen-dependent, androgen-independent and regressing Shionogie tumours using [^{18}F]EF5. Differences in hypoxia between the different types of tumours could be detected with [^{18}F]EF5 (Yapp et al. 2007). Recently, the first human study with [^{18}F]EF5 was performed in 15 patients with squamous cell carcinoma of the head and neck (HNSCC) in which the time course of [^{18}F]EF5 uptake after intravenous injection was evaluated to determine the most suitable PET protocol (Komar et al. 2008).

F) [^{18}F]EF3

Preclinical data: In the framework of the preclinical evaluation, Mahy et al. studied the pharmacokinetics, biodistribution, metabolism and specificity for hypoxia of [^{18}F]EF3 in different tumour bearing C3H mice breathing carbogen (5% CO_2 , 95% O_2), 21% oxygen and 10% oxygen. They also compared [^{18}F]EF3 uptake and EF5 adducts detected by immunofluorescence in the same model. [^{18}F]EF3 uptake was inversely correlated with oxygen concentration and a significant correlation was found between the [^{18}F]EF3 tumour-to-muscle ratio and the fluorescence intensity of EF5 (Mahy et al. 2004, Mahy et al. 2006). Pharmacokinetics, biodistribution and metabolism of [^{18}F]EF3 were assessed and compared with [^{18}F]FMISO uptake in rodent tumour models. It was concluded that both exhibited similar pharmacokinetics, biodistribution and metabolism and that [^{18}F]FMISO was able to detect tumour hypoxia to a similar extent than [^{18}F]EF3, although it seemed less specific than the latter tracer (Mahy et al. 2008). The same group tried to increase tumour-to-noise ratio in C3H mice by increasing [^{18}F]EF3 elimination. Several chemicals increasing renal filtration rate, decreasing tubular reabsorption or stimulating gastro-intestinal elimination were tested. Only phenobarbital induced a trend toward an increase in tumour-to-noise ratio (Christian et al. 2007). In another study, [^{18}F]EF3 was quantitatively compared with [^{18}F]FMISO in rats bearing syngeneic rhabdomyosarcoma tumours. It was showed that [^{18}F]EF3 is cleared faster from the blood compared to [^{18}F]FMISO. Both had a similar tumour uptake at 4h post injection, a similarly fast and uniform distribution in normal tissues and a comparable intra-tumoural distribution, indicating that [^{18}F]EF3 is not superior to [^{18}F]FMISO (Dubois et al. 2009).

Clinical data: In a recent phase I study by Mahy et al., pharmacokinetics, biodistribution and metabolism of [^{18}F]EF3 were assessed in ten patients with head and neck squamous cell carcinoma. Administration of [^{18}F]EF3 seemed feasible and safe in head and neck cancer patients. Uptake and retention of the tracer was observed in the tumour, indicating the presence of hypoxia (Mahy et al. 2007).

G) [^{18}F]EF1

Imaging with this marker was studied in 2 rat tumour types whereby the drug's biodistribution was assessed and optimized. [^{18}F]EF1 proved an excellent radiotracer for noninvasive imaging of tumour hypoxia (Evans et al. 2000).

H) [^{124}I]IAZA ([^{124}I]iodoazomycin arabinoside)

Although IAZA has been frequently labelled with gamma rays-emitting isotopes of iodine ([^{123}I] and [^{125}I]), several studies report on the use of IAZA labelled with [^{124}I]. In a recent study by Reischl et al., the hypoxia imaging capacities of [^{124}I]IAZA, [^{18}F]FAZA and [^{18}F]FMISO were compared in female Balb/c nude mice bearing A431 tumours with a small animal PET scanner. [^{18}F]FAZA displayed significantly higher tumour-to-background ratio compared to [^{18}F]MISO and [^{124}I]IAZA. Although tumour-to-background ratio for [^{124}I]IAZA increased with time, ratios were still lower than these for [^{18}F]FAZA at shorter time periods. The study demonstrated the superior biokinetics of [^{18}F]FAZA compared to [^{18}F]FMISO and [^{124}I]IAZA (Reischl et al. 2007).

Newer agents based on the azomycin-nucleoside structure such as iodoazomycin galactoside (IAZG) (Zanzonico et al. 2004, Riedl et al. 2007), iodoazomycin galactopyranoside (IAZGP) (Riedl et al. 2008) have been developed and evaluated. Two studies compared [^{124}I]IAZG uptake with [^{18}F]FMISO uptake. Zanzonico et al. studied the use of [^{124}I]IAZG as a hypoxia imaging agent in MCa and FsaII tumour bearing mice using microPET imaging by comparing it with [^{18}F]FMISO imaging and provided data showing the potential of this tracer for hypoxia imaging (Zanzonico et al. 2004). A similar study by Riedl et al. in Morris hepatoma (RH7777) bearing nude rats however, found that although [^{18}F]FMISO localized in the same intra-tumoural regions as [^{124}I]IAZG, a superior diagnostic image quality was obtained with [^{18}F]FMISO (Riedl et al. 2007). A recent study evaluated hypoxia imaging using [^{124}I]IAZGP in a Morris hepatoma RH7777 tumour rat model by comparing it with fluorescence fiberoptic oxygen probe measurements, pimonidazole and EF5 distribution, and tried to determine the

optimal time after injection to depict hypoxia. [^{124}I]IAZG distribution correlated positively with pimonidazole and EF5 distributions and the optimal ratio between signal intensity and tumour-to-liver contrast occurred 6 hours after tracer administration (Riedl et al. 2008).

2) Non-imidazole imaging agents

A) [^{18}F]FDG (2-Deoxy-2- [^{18}F]fluoro-D-glucose)

[^{18}F]FDG-PET is a non-invasive functional imaging method that is routinely used for cancer detection, staging and monitoring of response in several tumour types. Because the uptake of [^{18}F]FDG during FDG-PET imaging relies largely on the expression of proteins that are under control of HIF-1, the degree of [^{18}F]FDG-uptake by tumours might indirectly reflect the level of hypoxia. Reports trying to relate [^{18}F]FDG-uptake with tumour hypoxia have, however, given inconsistent results. *In vitro* studies have suggested that FDG should be accumulated in hypoxic cancer cells compared to normoxic cancer cells because of changed metabolism (Oswald et al. 2007, Busk et al. 2008, Clavo et al. 1995, Minn et al. 1996, Burgman et al. 2001, Pedersen et al. 2001, Hara et al. 2006). However, *in vivo* experiments (pre-clinical and clinical) have given conflicting results when showing a correlation between the uptake of [^{18}F]FDG and the existence of hypoxia in tumours (Bentzen et al. 2000, Wyss et al. 2006, Zanzonico et al. 2006, Dence et al. 2008, Zimney et al. 2006, Gagel et al. 2007, Gagel et al. 2004, Rajendran et al. 2004, Cherk et al. 2006, Cher et al. 2006, Thorwarth et al. 2006, Gagel et al. 2006, Dearling et al. 2004, Pugachev et al. 2005, Scigliano et al. 2008, Obata et al. 2003, Tanaka et al. 2006, Dietz et al. 2008). A recent review by Dierckx et al., addresses this subject matter (Dierckx et al. 2008).

B) Cu-ATSM

Another alternative PET agent for hypoxia imaging that holds great promise is based on a metal complex of radioactive copper with ATSM, diacetyl-bis(N^4 -methylthiosemicarbazone). Cu(II)-ATSM is a neutral lipophilic molecule, which is highly membrane permeable. It can undergo reduction by cellular reducing equivalents and can be converted to [Cu(I)-ATSM], which becomes entrapped in cells because of its negative charge when cells are hypoxic. There are four different positron-emitting copper isotopes that each have their own decay scheme: ^{60}Cu ($t_{1/2} = 0,40\text{h}$), ^{61}Cu ($t_{1/2} = 3,32\text{h}$), ^{62}Cu ($t_{1/2} = 0,16\text{h}$), ^{64}Cu ($t_{1/2} = 12,7\text{h}$) (Vavere et al. 2007).

Preclinical data: After reports on the use of Cu⁶²-ATSM to detect hypoxia in hypoxic myocardial tissue (Fujibayashi et al. 1997), numerous pre-clinical studies have evaluated and validated its use for imaging of hypoxia in tumours. In an *in vitro* study by Dearling et al., several ⁶⁴Cu-labelled bis(thiosemicarbazone) complexes were prepared and tested for tumour hypoxia selectivity by incubation with CHO320 Chinese hamster ovary cells under normoxic and hypoxic conditions. A number of molecules, including ⁶⁴Cu-ATSM, showed significant hypoxia selectivity (Dearling et al. 1998). Later, attempts were made to improve the hypoxia selectivity of the copper complexes by identification of the physicochemical properties that control hypoxia selectivity (Dearling et al. 2002). Lewis et al. evaluated ⁶⁴Cu-ATSM *in vitro* in the EMT6 carcinoma cell line under varying pO₂ and compared it with [¹⁸F]FMISO and further evaluated ⁶⁴Cu-ATSM *in vivo* in a murine animal model. ⁶⁴Cu-ATSM was selectively trapped *in vitro* in EMT6 cells under hypoxic conditions and *in vivo* in solid EMT6 tumours, confirming its role as an agent to successfully detect tumour hypoxia (Lewis et al. 1999). A study by Burgman et al. indicated, after determining the *in vitro* uptake of ⁶⁴Cu-ATSM as a function of oxygenation conditions and incubation time in several tumour cell lines of rodent and human origin, that the uptake and retention of ⁶⁴Cu-ATSM and their relation to oxygenation conditions were cell line dependent (Burgman et al. 2005). The pO₂ dependence of Cu-ATSM was confirmed in a 9L gliosarcoma rat model by comparison of Cu-ATSM uptake with direct oxygen measurements using needle oxygen electrodes while tumour oxygen concentration was manipulated (Lewis et al. 2001). A study by Yuan et al. on the other hand, concluded after comparing the autoradiographic distributions of ⁶⁴Cu-ATSM with the hypoxia markers EF5, pimonidazole and CAIX in R3230 mammary adenocarcinomas, fibrosarcomas and 9L gliomas that ⁶⁴Cu-ATSM is a suitable PET hypoxia marker in most tumour types, but not for all (Yuan et al. 2006).

A number of studies compared ⁶⁴Cu-ATSM uptake with [¹⁸F]FMISO uptake and [¹⁸F]FDG uptake *in vivo*. O'Donoghue et al. reported that the uptake of ⁶⁴Cu-ATSM 4h after injection in an R3327-AT anaplastic rat prostate tumour model did not correlate with [¹⁸F]FMISO uptake and does not reflect the level of hypoxia, as assessed by pimonidazole immunostaining and invasive oxygen needle probes. ⁶⁴Cu-ATSM imaging at 16-20h after injection however, corresponded with [¹⁸F]FMISO uptake and showed a good correlation with the distribution of tumour hypoxia. In a FaDu tumour model, early and late ⁶⁴Cu-ATSM images were in concordance with [¹⁸F]FMISO imaging, indicating a tumour specific dependence of ⁶⁴Cu-ATSM uptake and retention under hypoxic conditions (O'Donoghue et al. 2005). In another study ⁶⁴Cu-ATSM tumour uptake was unable to predictably detect changes in varying

amounts of tumour hypoxia when oxygenation levels in SCCVII tumours were modulated, whereas [^{18}F]FMISO tumour uptake was more responsive to changing levels of hypoxia. Tumour hypoxia was also assessed independent using pimonidazole (Matsumoto et al. 2007). Two studies comparing ^{64}Cu -ATSM uptake with [^{18}F]FDG uptake in different animal models concluded that both tracers have a different distribution pattern (Obata et al. 2003, Tanaka et al. 2006). ^{64}Cu -ATSM accumulated in hypoxic but viable tumour cells, whereas [^{18}F]FDG uptake was highest in pre-necrotic regions where the cells were believed to lack the necessary reductive mechanisms to accumulate ^{64}Cu -ATSM (Obata et al. 2003). It was also shown that regions with high ^{64}Cu -ATSM uptake were hypovascular and consisted of tumour cells arrested in the cell cycle, whereas regions with high [^{18}F]FDG uptake were hypervascular and consisted of proliferating cells, as confirmed by histological analysis with Ki67, CD34 and TUNEL assay (Tanaka et al. 2006). Finally Dence et al. compared the regional distribution of ^{64}Cu -ATSM, [^{18}F]FDG and [^{18}F]FMISO in 9L gliosarcoma tumours. It was shown that the regional distribution of [^{18}F]FMISO at 2h correlates highly with the distribution of ^{64}Cu -ATSM at 10 min or 24h. A poor correlation existed however between ^{64}Cu -ATSM (10 min) and [^{18}F]FDG (Dence et al. 2008).

Clinical data: In numerous studies, ^{60}Cu -ATSM uptake proved to be predictive of tumour behaviour and response to therapy in patients with non-small cell lung cancer (Dehdashti et al. 2003), cervical cancer (Dehdashti et al. 2003, Dehdashti et al. 2008) and rectal carcinoma (Dietz et al. 2008). In a study by Dehdashti et al. 14 patients with biopsy proven cervical cancer, an arbitrary selected tumour-to-muscle threshold of 3,5 was able to discriminate those patients that were likely to develop recurrence so that ^{60}Cu -ATSM uptake was inversely related to progression-free survival and overall survival. Additionally, no correlation was found between ^{60}Cu -ATSM uptake and [^{18}F]FDG uptake (Dehdashti et al. 2003). To confirm these results, a study with a larger group of patients was performed by the same group. Tumour ^{60}Cu -ATSM uptake (T/M threshold of 3,5) in 38 patients with cervical cancer was inversely related to progression-free survival and cause-specific survival. Again, no correlation was found between ^{60}Cu -ATSM uptake and [^{18}F]FDG uptake (Dehdashti et al. 2008). Similar results were obtained in a study where semi-quantitative analysis of the ^{60}Cu -ATSM tumour-to-muscle ratio in 14 patients with non-small cell lung cancer was able to discriminate responders from non-responders. However, there was no significant difference in mean tumour SUV of non-responders and responders. Again, no correlation was found between ^{60}Cu -ATSM uptake and [^{18}F]FDG uptake (Dehdashti et al. 2003). In a recent study an effort was made to predict the response of rectal cancers to neoadjuvant

chemoradiotherapy and prognosis in 17 patients. The results of this small pilot study suggested that ^{60}Cu -ATSM tumour-to-muscle ratio may be predictive of survival and, possibly, tumour response. Again, no correlation was found between ^{60}Cu -ATSM uptake and [^{18}F]FDG uptake (Dietz et al. 2008). To determine if hypoxia-related molecular markers were associated with ^{60}Cu -ATSM retention, the PET imaging data of 15 patients with cancer of the cervix were compared with the expression of tissue molecular markers, which included vascular endothelial growth factor (VEGF), cyclo-oxygenase-2 (COX-2), epidermal growth factor receptor (EGFR), carbonic anhydrase IX (CA-9), and apoptotic index. Hypoxia as identified with ^{60}Cu -ATSM imaging was correlated with overexpression of VEGF, EGFR, COX-2, CA-9, an increase in apoptosis, and a poor outcome (Grigsby et al. 2007). Chao et al. further demonstrated the feasibility to use ^{60}Cu -ATSM imaging to identify the hypoxic tumour subvolume through coregistration of CT and ^{60}Cu -ATSM PET images in order to plan a patients' course of radiotherapy and perform intensity-modulated radiation therapy (IMRT) (Chao et al. 2001). As most clinical Cu-ATSM studies used the agent with the short-lived positron-emitting radionuclide of copper, ^{60}Cu , a recent study compared the image quality and tumour uptake of ^{60}Cu -ATSM and ^{64}Cu -ATSM in 10 patients with cervical carcinoma to evaluate the use of Cu-ATSM with one of the longer-lived positron-emitting copper nuclides, ^{64}Cu . It was concluded that ^{64}Cu -ATSM was a safe radiopharmaceutical that can be used to obtain high quality images of tumour hypoxia in human cancers (Lewis et al. 2008).

1.4.2.2 Non-invasive detection of tumor hypoxia with SPECT

1) [^{123}I]IAZA and [^{125}I]IAZA ([^{123}I] / [^{125}I]iodoazomycin arabinoside)

Preclinical data: In one of the first studies with IAZA, its synthesis and labelling with [^{125}I] was described. Its elimination and biodistribution were also studied *in vivo* in EMT-6 tumours in BALB/c mice and it was shown that IAZA undergoes hypoxia-dependent binding in EMT-6 cells *in vitro* (Mannan et al. 1991). Moore et al. investigated the oxygenation status and tumour perfusion of rats with Dunning R3327-AT tumours who were treated with photodynamic therapy (PDT) with [^{123}I]IAZA and [$^{99\text{m}}\text{Tc}$]HMPAO. Increased retention of [^{123}I]IAZA was observed in tumours treated with PDT together with an inverse correlation

between tumour hypoxia as measured with [^{123}I]IAZA and tumour perfusion as measured with [$^{99\text{m}}\text{Tc}$]HMPAO (Moore et al. 1993).

Clinical data: The first clinical study assessing hypoxia with IAZA, investigated the uptake of [^{123}I]IAZA in patients with advanced malignancies. Radiotracer avidity was observed in three out of ten tumours and it was concluded that the use of gamma-emitter labelled 2-nitroimidazoles as diagnostic radiopharmaceuticals is feasible and safe and that metabolic binding of [^{123}I]IAZA is observed in some, but not all tumours (Parliament et al. 1992). In 22 patients, [^{123}I]IAZA uptake showed a significant inverse correlation with the perfusion marker [$^{99\text{m}}\text{Tc}$]-HMPAO and severe perfusion deficits were usually associated with an increased uptake of the hypoxic marker (Groshar et al. 1993). After observing uptake of radioactivity in the brain after administration of [^{123}I]IAZA, a study was undertaken to investigate the proposed metabolites of IAZA in normal and tumour-bearing murine models. Neither of the proposed metabolites' biodistribution did support its involvement in brain radioactivity uptake in patients (Lee et al. 2000). A study investigating the use of [^{123}I]IAZA in 51 human patients with newly diagnosed malignancies demonstrated hypoxia in small cell lung cancer and squamous cell carcinoma of head and neck but not in malignant gliomas. The study did however, demonstrate the feasibility of [^{123}I]IAZA imaging in a clinical setting (Urtasun 1996). Stypinski et al. reported the clinical pharmacokinetics of IAZA, the radiopharmacokinetics of [^{123}I]IAZA, total radioactivity kinetics and the radiation dosimetry estimates for 6 healthy volunteers and concluded that all supported its clinical use for imaging tissue hypoxia (Stypinski et al. 1999, Stypinski et al. 2001).

Newer agents based on the azomycin-nucleoside structure such as iodoazomycin galactoside (IAZG) (Chapman et al. 1996, Iyer et al. 1998), iodoazomycin pyranoside (IAZP) (Mannan et al. 1992), iodoazomycin galactopyranoside (IAZGP) (Iyer et al. 2001, Saitoh et al. 2002), iodoazomycin xylopyranoside (IAZXP) (Chapman et al. 1996) have been developed and evaluated. Iyer et al. demonstrated that microelectrode measurements in R3327-AT tumour bearing rats, did not correlate with [^{125}I]IAZGP uptake (Iyer et al. 2001). Furthermore, a study by Saitoh et al. showed high accumulation of IAZGP in FM3A mouse tumours 24h after administration (Saitoh et al. 2002).

2) [$^{99\text{m}}\text{Tc}$] labelled agents

A) BMS181321

This was the first [^{99m}Tc]-labelled 2-nitroimidazole to be widely studied for imaging (Linder et al. 1994). A number of experimental studies have evaluated the use of BMS 181321 for the detection of ischemic and hypoxic myocardium (Kusuoka et al. 1994, Shi et al. 1995, Rumsey et al. 1995, Fukuchi 1996). Ballinger et al. showed selective accumulation in hypoxic cells *in vitro* and *in vivo* but concluded that BMS 181321 was not optimal for tumour hypoxia imaging because of *in vitro* and *in vivo* instabilities and a high partition coefficient, resulting in slow clearance from the blood and high background levels in normal tissues (Ballinger et al. 1996).

B) BRU59-21

Preclinical data: BRU59-21, previously known as BMS194796, is a second generation analogue of BMS181321 which shows greater stability *in vitro* and more rapid clearance from the circulation *in vivo*, resulting in higher tumour-to-blood and tumour-to-muscle ratios. It showed selective localisation in tumour cells incubated under hypoxic conditions and following intravenous injection in animal models representative of poorly perfused tumours (Melo et al. 2000). In a study by Zhang et al. BRU59-21 and HL91 were compared directly in the same *in vitro* systems. Both tracers proved suitable for hypoxia imaging (Zhang et al. 2001). Clinical data: Hoebbers et al. assessed the safety and biodistribution of [^{99m}Tc]BRU59-21 in 10 patients with head and neck cancer and correlated uptake *in vivo* with pimonidazole staining. *In vivo* evaluation of tumour hypoxia with [^{99m}Tc]BRU59-21 appeared to be safe and feasible and uptake and retention of the marker seemed to be indicative of tumour hypoxia, as confirmed by pimonidazole staining (Hoebbers et al. 2002).

C) [^{99m}Tc]HL-91

Preclinical data: Zhang et al. evaluated the efficacy of [^{99m}Tc]HL91 as a non invasive marker of tumour hypoxia *in vitro* (Chinese hamster ovary cells) and *in vivo* (C3H mice bearing KHT-C tumours) and observed selective accumulation of [^{99m}Tc]HL91 in hypoxic cells and hypoxic tumours (Zhang et al. 1998). A similar study assessed the retention of [^{99m}Tc]HL91 in mice bearing 3 different tumours under control and enhanced oxygenation conditions and correlated these data with the oxygenation status as assessed by Eppendorf pO₂ histogram measurements. A very good correlation between [^{99m}Tc]HL91 retention and hypoxia, as measured by the Eppendorf histogram, was observed (Honest et al. 1998). Yutani et al. found that [^{99m}Tc]HL91 accumulated to significantly higher levels in hypoxic tumour areas and that

[^{99m}Tc]HL91 uptake was strongly correlated with the expression of GLUT1 in the viable cancer cell area (Yutani et al. 1999). In a study by Tatsumi et al., a dual-tracer autoradiography was performed with HL91 and IAP (carbon-14 iodoantipyrine) in Walker 256 tumour bearing rats to elucidate the relationship between hypoxia and blood flow. The study confirmed that high HL91 uptake is related to low blood flow (Tatsumi et al. 1999). Kinuya et al. reported on an increase in [^{99m}Tc]HL91 uptake after exposure to X-ray radiation (Kinuya et al. 2000). Siim et al. examined whether [^{99m}Tc]HL91 uptake could be used as a marker for the inhibition of tumour blood flow by the antivascular agents DMXAA (5,6-dimethylxantenone-4-acetic acid) and CA4P (combrestatin A4 phosphate) and observed that tumour hypoxia as a result of the acute inhibition of blood flow by antivascular agents caused increased tumour uptake of [^{99m}Tc]HL91 (Siim et al. 2000). Another study demonstrated that microelectrode measurements in R3327-AT tumour bearing rats, did not correlate with [^{99m}Tc]HL91 uptake (Iyer et al. 2001). After having determined the biodistribution of [^{99m}Tc]HL91 (129), Suzuki et al. investigated the relationship between [^{99m}Tc]HL91 uptake and tumour response to radiation in athymic mice bearing different human tumours. They concluded that [^{99m}Tc]HL91 uptake did not always relate to their sensitivities to radiation therapy (Suzuki et al. 2003). In a study by Kinuya et al., an attempt was made to determine whether oxygenation status affected [^{99m}Tc]MIBI (sestamibi) uptake. They observed enhanced [^{99m}Tc]HL91 accumulation in hypoxic tumour cells after treatment with N₂-gas (*in vitro*) and hydralazine (*in vivo*) (Kinuya et al. 2002). A recent study by Lee et al. investigated the selectivity of [^{99m}Tc]HL91 for hypoxia *in vitro* in A549 human lung cancer cells and LL2 murine Lewis lung cancer cells under varying oxygen concentrations and *in vivo* in different xenograft mouse models after chemically altering the degree of tumour hypoxia with hydralazine. The *in vitro* studies identified hypoxia-selective uptake of [^{99m}Tc]HL91, with significantly increased uptake in the hypoxic state compared to the normoxic state. The *in vivo* studies showed that [^{99m}Tc]HL91 was markedly increased in mice treated with hydralazine compared with controls (Lee et al. 2008).

Clinical data: Clinical studies concerning the clinical evaluation of [^{99m}Tc]HL91 are limited. In a pilot study, Cook et al. compared [^{99m}Tc]HL91 uptake with [¹⁸F]FDG-PET imaging in 10 patients with a variety of tumours and showed visible [^{99m}Tc]HL91 tumour uptake in all 7 patients where the tumour could be clearly identified with [¹⁸F]FDG PET (Cook et al. 1998). Another phase I pilot study evaluated the usefulness of [^{99m}Tc]HL91 imaging for the visualization of local recurrence in 9 men with squamous cell carcinoma of the head and neck (SCCHN) as compared to CT and biopsy and concluded that [^{99m}Tc]HL91 is a safe

radioligand and that metabolic binding in a large fraction but not all of local SCCN recurrences may be expected (Van de Wiele et al. 2001). Finally, in a study with 32 patients with non-small cell lung cancer, Li et al. showed that hypoxia imaging with [^{99m}Tc]HL91 before radiotherapy may predict tumour response and patient survival (Li et al. 2006).

1.5 Tumor hypoxia and tumor metabolism

More than 50 years ago, Warburg described that even in aerobic conditions, tumor cells prefer to use glycolysis instead of oxidative phosphorylation for their energy/ATP-production (aerobic glycolysis or Warburg effect) (Warburg 1953). As a consequence, tumor cells utilize far more glucose than their normal counterparts to compensate for the use of glycolysis which is inherently inefficient as compared to aerobic degradation of glucose through the Krebs cycle and oxidative phosphorylation. Although several explanations exist, the exact mechanisms and advantages associated with aerobic glycolysis remain unclear and are probably multiple (Bartrons et al. 2007, Kroemer et al. 2008, Denko et al. 2008). This tumor-specific phenomenon is exploited in [^{18}F]FDG-PET (2-Deoxy-2- ^{18}F]fluoro-D-glucose positron emission tomography) imaging. This non-invasive imaging method which is routinely used for cancer detection, staging and monitoring of response in several tumor types, is based upon the accumulation of a radiolabeled glucose analogue in tumor cells as a consequence of this enhanced glucose uptake and glycolysis. Major factors that are considered to play a key role in the higher [^{18}F]FDG uptake by malignant cells appear to be overexpression of different types of GLUTs, a high HK activity and a low glucose-6-phosphatase (G6P) activity (Smith et al. 2001, Ong et al. 2008). The precise determinant however, remains unclear. Overexpression of several types of GLUTs and HKs is a common feature of cancer and has been described extensively (Pastorino et al. 2003, Macheda et al. 2005).

Under hypoxic conditions, tumor cells will further increase their glycolytic ATP-production to compensate for the hypoxia-induced drop in mitochondrially produced ATP (Pasteur effect). The efficiency of the glycolytic response is enhanced by activation of HIF-1 and the downstream expression of metabolic proteins. HIF-1 stimulates glycolytic energy production by transactivating genes involved in glucose transport and glycolytic enzymes. HIF-1 increases the rate of glucose uptake through the induction of the facilitative glucose transporters GLUT1 and GLUT3 (Maxwell et al. 1997, Chen et al. 2001). These transporters (solute carriers SLC2A, protein symbol GLUT) mediate the transport of glucose and other monosaccharides across the plasma membrane of mammalian cells. HIF-1 also increases expression of HK I and II, although it seems that HKII is more important for modifying glucose metabolism under hypoxic conditions (Mathupala et al. 2001). Hexokinases convert glucose to glucose-6-phosphate and allow the tumor cell to maintain a high rate of glycolysis

by maintaining the downhill concentration gradient necessary to move glucose into the cell through glucose transporters. Further, expression of lactate dehydrogenase-A (LDH-A), a protein responsible for the conversion of pyruvate to lactate, is under control of HIF-1 (Semenza et al. 1996, Semenza et al. 2007). Besides stimulating glycolytic energy production, hypoxia also actively suppresses aerobic glucose metabolism by inducing pyruvate dehydrogenase kinase 1 (PDK1) which inactivates pyruvate dehydrogenase (PDH) (Kim et al. 2006, Papandreou et al. 2006, Semenza et al. 2007). As PDH catalyzes the committed, irreversible step in the mitochondria in which pyruvate is broken down into acetyl-CoA and CO₂, access of pyruvate into the TCA cycle is inhibited. Further, an effect of HIF-1 on mitochondrial biogenesis and function through actions on MXI1 and the activity of cytochrome c oxidase (COX), has been described (Denko et al. 2008). All these mechanisms together result in the glycolytic tumor phenotype. It remains however, difficult to discern whether hypoxia and/or HIF-1 activation are a cause or a contributing factor in aerobic glycolysis.

(i) As the proteins responsible for [¹⁸F]FDG-uptake are under control of HIF-1, the degree of [¹⁸F]FDG-uptake might indirectly reflect the degree of tumor hypoxia, obviating the need for more specialized radiopharmaceuticals for hypoxia imaging. Reports trying to find a link between [¹⁸F]FDG-uptake and hypoxia have yielded inconsistent results. Numerous *in vitro* studies in different types of cancer cell lines have reported on an increase in [³H]FDG or [¹⁸F]FDG-uptake after exposure to decreasing oxygen atmospheres (Clavo 1995, Burgman 2001, Pedersen 2001, Oswald 2007). *In vivo* results on the other hand, have proven less straightforward and comparisons of [¹⁸F]FDG with more specialized hypoxia tracers have questioned the use of [¹⁸F]FDG for hypoxia imaging (see Chapter 1, Partim 1.4.2). A review by Dierckx et al. addresses this subject matter (Dierckx 2008).

(ii) As the proteins responsible for [¹⁸F]FDG-uptake are under control of HIF-1, it should be possible to modify tumor [¹⁸F]FDG-uptake by modifying tumor oxygenation state or HIF-1 activation. Despite its widespread use, a number of problems and limitations still exist when using [¹⁸F]FDG-PET imaging. First of all, because glucose is used as an energy substrate throughout the body, [¹⁸F]FDG-uptake in benign tissues and certain physiological processes is common and complicates its oncological use: high uptake in normal brain tissue complicates brain tumor detection, aspecific bladder activity interferes with bladder and prostate cancer diagnosis, and inflammation and infection processes are known to be highly [¹⁸F]FDG avid. Secondly, some tumors such as prostate carcinoma, mucinous carcinoma and hepatocellular

carcinoma display low [^{18}F]FDG-uptake due to low metabolic rates or elevated glucose-6-phosphatase levels (Kellof et al. 2005, Endo et al. 2006). The possibility to increase tumor [^{18}F]FDG-uptake in these situations where diagnostic accuracy is suboptimal, is highly attractive.

1.6 References

- Airley R, Loncaster J, Davidson J, et al. Glucose transporter Glut-1 expression correlates with tumor hypoxia and predicts metastasis-free survival in advanced carcinoma of the cervix. *Clin Cancer Res.* 2001;7:928-934.
- Airley RE, Loncaster J, Raleigh JA, et al. GLUT-1 and CAIX as intrinsic markers of hypoxia in carcinoma of the cervix: relationship to pimonidazole binding. *Int J Cancer.* 2003;104:85-91.
- Bailey DL, Parker JA (1998) Single photon emission computed tomography. In: Murray IPC, Ell PJ (eds) Nuclear medicine in clinical diagnosis and treatment. Churchill Livingstone, Edinburgh, pp 1589-1601.
- Ballinger JR, Kee JWM, Rauth AM. In vitro and in vivo evaluation of a technetium-99m-labeled 2-nitroimidazole (BMS181321) as a marker of tumor hypoxia. *J Nucl Med.* 1996;37:1023-1031.
- Baluk P, Hashizume H, McDonald DM. Cellular abnormalities of blood vessels as targets in cancer. *Current Opinion in Genetics & Development* 2005;15:102-111.
- Barthel H, Wilson H, Collingridge DR, et al. In vivo evaluation of [^{18}F]Fluoroetanidazole as a new marker for imaging tumour hypoxia with positron emission tomography. *Cancer Res UK.* 2004;90:2232-2242.
- Bartrons R, Caro J. Hypoxia, glucose metabolism and the Warburg's effect. *J Bioenerg Biomembr.* 2007;39:223-229.
- Beck R, Röper B, Carlsen JM, et al. Pretreatment ^{18}F -FAZA PET predicts success of hypoxia-directed radiochemotherapy using tirapazamine. *J Nucl Med.* 2007;48:973-980.
- Bentzen L, Keiding S, Horsman MR, et al. Feasibility of detecting hypoxia in experimental Mouse tumours with ^{18}F -fluorinated tracers and positron emission tomography. *Acta Oncol.* 2000;39:629-637.
- Bentzen L, Keiding S, Horsman MR, et al. Assessment of hypoxia in experimental mice tumours by [^{18}F]fluoromisonidazole PET and pO_2 electrode measurements. *Acta Oncol.* 2002;41:304-312.
- Bentzen L, Keiding S, Nordmark M, et al. Tumour oxygenation assessed by ^{18}F -fluoromisonidazole PET and polarographic needle electrodes in human soft tissue tumours. *Radiother Oncol.* 2003;67:339-344.

- Brizel DM, Scully SP, Harrelson JM, et al. Tumor oxygenation predicts for the likelihood of distant metastases in human soft tissue sarcoma. *Cancer Res.* 1996;56:941-943.
- Brizel DM, Sibley GS, Prosnitz LR, et al. Tumor hypoxia adversely affects the prognosis of carcinoma of the head and neck. *Int J Radiation Oncology Biol Phys.* 1997;38:285-289.
- Bruhlmeier M, Roelcke U, Schubiger PA, et al. Assessment of hypoxia and perfusion in human brain tumors using PET with ¹⁸F-fluoromisonidazole and ¹⁵O-H₂O. *J Nucl Med.* 2004;45:1851-1859.
- Brurberg KG, Graff BA, Rofstad EK. Temporal heterogeneity in oxygen tension in human melanoma xenografts. *Br J Cancer.* 2003;89:350-356.
- Burgman P, Odonoghue JA, Humm JL, et al. Hypoxia induced increase in FDG uptake in MCF7 cells. *J Nucl Med.* 2001;42:170-175.
- Burgman P, O'Donoghue JA, Lewis JS, et al. Cell line-dependent differences in uptake and retention of the hypoxia-selective nuclear imaging agent Cu-ATSM. *Nucl Med Biol.* 2005;32:623-630.
- Busk M, Horsman MR, Jakobsen S, et al. Imaging hypoxia in xenografted and murine tumors with ¹⁸F-Fluoroazomycin arabinoside: a comparative study involving microPET, autoradiography, pO₂-polarography, and fluorescence microscopy. *Int J Rad Oncol Biol Phys.* 2008;70:1202-1212.
- Busk M, Horsman MR, Jakobsen S, et al. Cellular uptake of PET tracers of glucose metabolism and hypoxia and their linkage. *Eur J Nucl Med Mol Imaging.* 2008;DOI 10.1007/s00259-008-0888-9.
- Bussink J, Kaanders JHAM, Strik AM, Vojnovic B, van der Kogel AJ. Optical sensor-based oxygen tension measurements correspond with hypoxia marker binding in three human xenograft lines. *Radiat Res.* 2000;154:547-555.
- Bussink J, Kaanders JHAM, van der Kogel AJ. Tumor hypoxia at the micro-regional level: clinical relevance and predictive value of exogenous and endogenous hypoxic cell markers. *Radiother Oncol.* 2003;67:3-15.
- Carmeliet P, Jain RK. Angiogenesis in cancer and other diseases. *Nature.* 2000;407:249-257.
- Carmeliet P, Jain RK. Principles and mechanisms of vessel normalization for cancer and other angiogenic diseases. *Nat Rev.* 2011;10:417-427.
- Chao KSC, Bosch Wr, Mutic S, et al. A novel approach to overcome hypoxic tumor resistance: Cu-ATSM-guided intensity-modulated radiation therapy. *Int J Radiation Oncology Biol Phys.* 2001;49:1171-1182.

- Chapman JD, Coia LR, Stobbe CC, et al. Prediction of tumour hypoxia and radioresistance with nuclear medicine markers. *Br J Cancer Suppl.* 1996;27:S204-S208.
- Chen C, Pore N, Behrooz A, et al. Regulation of glut1 mRNA by hypoxia-inducible factor-1. *J Biol Chem.* 2001;276:9519-9525.
- Cherk MH, Foo SS, Poon AM, et al. Lack of correlation of hypoxic cell fraction and angiogenesis with glucose metabolic rate in non-small cell lung cancer assessed by ^{18}F -fluoromisonidazole and ^{18}F -FDG PET. *J Nucl Med.* 2006;47:1921-1926.
- Cher LM, Murone C, Lawrentschuk N, et al. Correlation of hypoxic cell fraction and angiogenesis with glucose metabolic rate in gliomas using ^{18}F -fluoromisonidazole, ^{18}F -FDG PET, and immunohistochemical studies. *J Nucl Med.* 2006;47:410-418.
- Clavo AC, Brown RS, Wahl RL. Fluorodeoxyglucose uptake in human cancer cell lines is increased by hypoxia. *J Nucl Med.* 1995;36:1625-1632.
- Cook GJR, Houston S, Barrington SF, et al. Technetium-99m-labeled HL91 to identify tumor hypoxia: correlation with fluorine-18-FDG. *J Nucl Med.* 1998;39:99-103.
- Christian N, Bol A, De Bast M, et al. Determination of tumour hypoxia with the PET tracer [^{18}F]EF3: improvement of the tumour-to-background ratio in a mouse tumour model. *Eur J Nucl Med Mol Imaging.* 2007;34:1348-1354.
- Dearling JJJ, Lewis JS, Mullen GED, et al. Design of hypoxia-targeting radiopharmaceuticals: selective uptake of copper-64 complexes in hypoxic cells in vitro. *Eur J Nucl Med.* 1998;25:788-792.
- Dearling JJJ, Lewis JS, Mullen GED, et al. Copper bis(thiosemicarbazone) complexes as hypoxia imaging agents: structure-activity relationships. *J Biol Inorg Chem.* 2002;7:249-259.
- Dearling J, Flynn A, Sutcliffe-Goulden J, et al. Analysis of the regional uptake of radiolabeled deoxyglucose analogs in human tumor xenografts. *J Nucl Med.* 2004;45:101-107.
- Dehdashti F, Mintun MA, Lewis JS, et al. In vivo assessment of tumor hypoxia in lung cancer with ^{60}Cu -ATSM. *Eur J Nucl Med Mol Imaging.* 2003;30:844-850.
- Dehdashti F, Grigsby PW, Mintun MA, et al. Assessing tumor hypoxia in cervical cancer by positron emission tomography with ^{60}Cu -ATSM: relationship to therapeutic response – a preliminary report. *Int J Radiation Oncology Biol Phys.* 2003;55:1233-1238.
- Dehdashti F, Grigsby PW, Lewis JS, et al. Assessing tumor hypoxia in cervical cancer by PET with ^{60}Cu -labeled diacetyl- bis(N^4 -methylthiosemicarbazone). *J Nucl Med.* 2008;49:201-205.

- Dence CS, Ponde DE, Welch MJ, et al. Autoradiographic and small-animal PET comparisons between ^{18}F -FMISO, ^{18}F -FDG, ^{18}F -FLT and the hypoxic selective ^{64}Cu -ATSM in a rodent model of cancer. *Nucl Med Biol.* 2008;35:713-720.
- Denko NC. Hypoxia, HIF1 and glucose metabolism in the solid tumour. *Nat Rev.* 2008;8:705-713.
- Dierckx RA, Van De Wiele C. FDG uptake, a surrogate of tumor hypoxia? *Eur J Nucl Med Mol Imaging.* 2008;35:1544-1549.
- Dietz DW, Dehdashti F, Grigsby PW, et al. Tumor hypoxia detected by positron emission tomography with ^{60}Cu -ATSM as a predictor of response and survival in patients undergoing neoadjuvant chemoradiotherapy for rectal carcinoma: a pilot study. *The ASCRS.* 2008;51:1641-8.
- Dubois L, Landuyt W, Haustermans K, et al. Evaluation of hypoxia in an experimental rat tumour model by [^{18}F]fluoromisonidazole PET and immunohistochemistry. *Br J Can.* 2004;91:1947-1954.
- Dubois L, Landuyt W, Cloetens L, et al. [^{18}F]EF3 is not superior to [^{18}F]FMISO for PET-based hypoxia evaluation as measured in a rat rhabdomyosarcoma tumour model. *Eur J Nucl Med Mol Imaging.* 2008;DOI 10.1007/s00259-008-x
- Durand RE. Intermittent blood flow in solid tumours – an under-appreciated source of ‘drug resistance’. *Cancer Metastasis.* 2001;20:57-61.
- Eberl S, Zimmerman RE (1998) Nuclear medicine imaging instrumentation. In: Murray IPC, Ell PJ (eds) Nuclear medicine in clinical diagnosis and treatment. Churchill Livingstone, Edinburgh, pp 1559-1569
- Eschmann SM, Paulsen F, Reimold M, et al. Prognostic impact of hypoxia imaging with ^{18}F -misonidazole PET in non-small cell lung cancer and head and neck cancer before radiotherapy. *J Nucl Med.* 2005;46:253-260.
- Evans SM, Kachur AV, Shiue CY, Hustinx R, Jenkins WT, Shive GG, Karp JS, Alavi A, Lord EM, Dolbier WR, Koch CJ. Noninvasive detection of tumor hypoxia using the 2-nitroimidazole [^{18}F]EF1. *J Nucl Med.* 2000;41:327-336.
- Fujibayashi Y, Taniuchi H, Yonekura Y, et al. Copper-62-ATSM: a new hypoxia imaging agent with high membrane permeability and low redox potential. *J Nucl Med.* 1997;38:1155-1160.
- Fukuchi K, Kusuoka H, Watanabe Y, et al. Ischemic and reperfused myocardium detected with technetium-99m-nitroimidazole. *J Nucl Med* 1996;37 :761-6.

- Fukumura D, Jain RK. Tumor microvasculature and microenvironment: targets for anti-angiogenesis and normalization. *Microvasc Res.* 2007;74:72-84.
- Fyles AW, Milosevic M, Wong R, et al. Oxygenation predicts radiation response and survival in patients with cervix cancer. *Radiother Oncol.* 1998;48:149-156.
- Gagel B, Reinartz P, DiMartino E, et al. pO₂ polarography versus positron emission tomography ([¹⁸F] fluoromisonidazole, [¹⁸F]-2-fluoro-2-deoxyglucose). An appraisal of radiotherapeutically relevant hypoxia. *Strahlenther Onkol.* 2004;180:616-622.
- Gagel B, Reinartz P, Demirel C, et al. [¹⁸F] fluoromisonidazole and [¹⁸F] fluorodeoxyglucose positron emission tomography in response evaluation after chemo-/radiotherapy of non-small-cell lung cancer: a feasibility study. *BMC Cancer.* 2006;6:51-58.
- Gagel B, Piroth M, Pinkawa M, et al. pO polarography, contrast enhanced color duplex sonography (CDS), [¹⁸F] fluoromisonidazole and [¹⁸F] fluorodeoxyglucose positron emission tomography: validated methods for the evaluation of therapy-relevant tumor oxygenation or only bricks in the puzzle of tumor hypoxia? *BMC Cancer.* 2007;7:113-122.
- Goethals L, Debuquoy A, Perneel C, et al. Hypoxia in human colorectal adenocarcinoma: comparison between extrinsic and potential intrinsic hypoxia markers. *Int J Radiation Oncology Biol Phys.* 2006;65:246-254.
- Gray LH, Conger AD, Ebert M, et al. The concentration of oxygen dissolved in tissues at the time of irradiation as a factor in radiotherapy. *Br J Radiol.* 1953;26:638-648.
- Grigsby PW, Malyapa RS, Higashikubo R, et al. Comparison of molecular markers of hypoxia and imaging with ⁶⁰Cu-ATSM in cancer of the uterine cervix. *Mol Imaging Biol.* 2007;9:278-283.
- Grönroos T, Eskola O, Lehtiö K, et al. Pharmacokinetics of [¹⁸F]FETNIM: a potential hypoxia marker for PET. *J Nucl Med.* 2001;42:1397-1404.
- Grönroos T, Bentzen L, Marjamäki P, et al. Comparison of the biodistribution of two hypoxia markers [¹⁸F]FETNIM and [¹⁸F]FMISO in an experimental mammary carcinoma. *Eur J Nucl Med Mol Imaging* 2004;31:513-520.
- Groshar D, McEwan AJB, Parliament MB, et al. Imaging tumor hypoxia and tumor perfusion. *J Nucl Med.* 1993;34:885-888.
- Gross MW, Karbach U, Groebe K, et al. Calibration of misonidazole labeling by simultaneous measurement of oxygen tension and labeling density in multicellular spheroids. *Int J Cancer.* 1995;61:567-573.

- Grosu AL, Souvatzoglu M, Röper B, et al. Hypoxia imaging with FAZA-PET and theoretical considerations with regard to dose painting for individualization of radiotherapy in patients with head and neck cancer. *Int J Radiation Oncology Biol Phys.* 2007;69:541-551.
- Hanahan D, Weinberg RA. The hallmarks of cancer. *Cell.* 2000;100:57-70.
- Hara T, Bansal A, DeGrado TR. Effect of hypoxia on the uptake of [methyl-³H]choline, [1-¹⁴C] acetate and [¹⁸F]FDG in cultured prostate cancer cells. *Nucl Med Biol.* 2006;33:977-984.
- Haugland HK, Vukovic V, Pintilie M, et al. Expression of hypoxia-inducible factor-1 α in cervical carcinomas: correlation with tumor oxygenation. *Int J Radiation Oncology Biol Phys.* 2002;53:854-861.
- Hedley D, Pintilie M, Woo J, et al. Carbonic anhydrase IX expression, hypoxia, and prognosis in patients with uterine cervical carcinomas. *Clin Can Res.* 2003;9:5666-5674.
- Hickman JA, Potten CS, Merritt AJ, et al. Apoptosis and cancer chemotherapy. *Philos Trans R Soc Lond B Biol Sci.* 1994;345:319-325.
- Hicks RJ, Rischin D, Fisher R, et al. Utility of FMISO PET in advanced head and neck cancer treated with chemoradiation incorporating a hypoxia-targeting chemotherapy agent. *Eur J Nucl Med Mol Imaging.* 2005;32:1384-1391.
- Höckel M, Schlenger K, Aral B, et al. Association between tumor hypoxia and malignant progression in advanced cancer of the uterine cervix. *Cancer Res.* 1996;56:4509-4515.
- Höckel M, Vaupel P. Tumor hypoxia: definitions and current clinical, biologic, and molecular aspects. *J Natl Cancer Inst.* 2001;93:266-276.
- Hoogsteen IJ, Marres HAM, van der Kogel AJ, et al. The hypoxic microenvironment, patient selection and hypoxia-modifying treatments. *Clin Oncol.* 2007;19:385-396.
- Hoebers FJP, Janssen HLK, Olmos RAV, et al. Phase I study to identify tumour hypoxia in patients with head and neck cancer using technetium-99m BRU 59-21. *Eur J Nucl Med.* 2002;29:1206-1211.
- Honess DJ, Hill SA, Collingridge DR, et al. Preclinical evaluation of the novel hypoxic marker ^{99m}Tc-HL91 (prognox) in murine and xenograft systems in vivo. *Int J Radiat Oncol Biol Phys.* 1998;42:731-735.
- Hoskin PJ, Sibtain A, Daley FM, et al. GLUT1 and CAIX as intrinsic markers of hypoxia in bladder cancer: relationship with vascularity and proliferation as predictors of outcome of ARCON. *Br J Can.* 2003;89:1290-1297.

- Hutchison GJ, Valentine HR, Loncaster JA, et al. Hypoxia-inducible factor 1 α expression as an intrinsic marker of hypoxia: correlation with tumor oxygenation, pimonidazole measurements, and outcome in locally advanced carcinoma of the cervix. *Clin Can Res.* 2004;10:8405-8412.
- Iakovlev VV, Pintilie M, Morrison A, et al. Effect of distributional heterogeneity on the analysis of tumor hypoxia based on carbonic anhydrase IX. *Lab Invest.* 2007;87:1206-1217.
- Iyer RV, Kim E, Schneider RF, et al. A dual hypoxic marker technique for measuring oxygenation change within individual tumors. *Br J Cancer.* 1998;78:163-169.
- Iyer RV, Haynes PT, Schneider RF, et al. Marking hypoxia in rat prostate carcinomas with β -D-[¹²⁵I]azomycin galactopyranoside and [^{99m}Tc]HL-91: correlation with microelectrode measurements. *J Nucl Med.* 2001;42:337-344.
- Jain RK. Normalization of tumor vasculature: an emerging concept in antiangiogenic therapy. *Science* 2005;307:58-62.
- Jankovic B, Aquino-Parsons C, Raleigh JA, et al. Comparison between pimonidazole binding, oxygen electrode measurements, and expression of endogenous hypoxia markers in cancer of the uterine cervix. *Clin Cytom.* 2006;70B:45-55.
- Janssen HLK, Haustermans KMG, Sprong D, et al. HIF-1 α , pimonidazole, and iododeoxyuridine to estimate hypoxia and perfusion in human head-and-neck tumors. *Int J Radiation Oncology Biol Phys.* 2002;54:1537-1549.
- Jarm T, Sersa G, Miklavcic D. Oxygenation and blood flow in tumors treated with hydralazine: evaluation with a novel luminescence-based fiber-optic sensor. *Technol Health Care.* 2002;10:363-380.
- Jewell UR, Kvietikova I, Scheid A, et al. Gassmann. Induction of HIF-1 α in response to hypoxia is instantaneous. *FASEB J.* 2001;15:1312-1314
- Kim JW, Tchernyshyov I, Semenza GL, et al. HIF-1-mediated expression of pyruvate dehydrogenase kinase: a metabolic switch required for cellular adaptation to hypoxia. *Cell Metab.* 2006;3:177-185.
- Kim JW, Gao P, Dang CV. Effects of hypoxia on tumor metabolism. *Cancer Metastasis Rev.* 2007;26:291-298.
- Kinuya S, Yokoyama K, Konishi S, et al. Increased uptake of ^{99m}Tc-HL91 in tumour cells exposed to X-ray radiation. *Ann Nucl Med.* 2000;14:139-140.
- Kinuya S, Yokoyama K, Li XF, et al. Hypoxia-induced alteration of tracer accumulation in cultured cancer cells and xenografts in mice: implications for pre-therapeutic prediction

- of treatment outcomes with ^{99m}Tc -sestamibi, ^{201}Tl chloride and ^{99m}Tc -HL91. *Eur J Nucl Med.* 2002;29:1006-1011.
- Komar G, Seppänen M, Eskola O, et al. 18F-EF5: a new PET tracer for imaging hypoxia in head and neck cancer. *J Nucl Med.* 2008;49:1944-1951.
- Kroemer G, Pouyssegur J. Tumor cell metabolism: cancer's Achilles' heel. *Cancer Cell.* 2008;13:472-482.
- Krohn KA, Link JM, Mason RP. Molecular imaging of hypoxia. *J Nucl Med.* 2008;49:129S-48S.
- Kubota K, Tada M, Yamada S, et al. Comparison of the distribution of fluorine-18 fluoromisonidazole, deoxyglucose and methionine in tumour tissue. *Eur J Nucl Med.* 1999;26:750-757.
- Kusuoka H, Hashimoto K, Fukuchi K, et al. Kinetics of a putative hypoxic tissue marker, technetium-99m-nitroimidazole (BMS181321), in normoxic, hypoxic, ischemic and stunned myocardium. *J Nucl Med.* 1994;35:1371-1376.
- van Laarhoven HWM, Kaanders JHAM, Lok J, et al. Hypoxia in relation to vasculature and proliferation in liver metastases in patients with colorectal cancer. *Int J Radiation Oncology Biol Phys.* 2006;64:473-482.
- Lal A, Peters H, St Croix B, et al. Transcriptional response to hypoxia in human tumors. *J Natl Cancer Inst.* 2001;93:1337-1343.
- Lando D, Peet DJ, Whelan DA, et al. Asparagine hydroxylation of the HIF-transactivation domain: a hypoxic switch. *Science.* 2002;295:858-861.
- Lawrentschuk N, Poon AM, Foo SS, et al. Assessing regional hypoxia in human renal tumours using ^{18}F -fluoromisonidazole positron emission tomography. *BJU Int.* 2005;96:540-546.
- Le QT, Chen E, Salim A, et al. An evaluation of tumor oxygenation and gene expression in patients with early stage non-small cell lung cancers. *Clin Cancer Res.* 2006;12:1507-1514.
- Lee HC, Kumar P, McEwan AJ, et al. Synthesis, radiolabeling, and biodistribution of putative metabolites of iodoazomycin arabinoside. *Nucl Med Biol.* 2000;27:61-68.
- Lee ST, Scott AM. Hypoxia positron emission tomography imaging with ^{18}F -fluoromisonidazole. *Semin Nucl Med.* 2007;37:451-461.
- Lee BF, Chiu NT, Hsia CC, et al. Accumulation of Tc-99m HL91 in tumor hypoxia: in vitro cell culture and in vivo tumor model. *Kaohsiung J Med Sci.* 2008;24:461-472.

- Lehtiö K, Oikinen V, Grönroos T, et al. Imaging of blood flow and hypoxia in head and neck cancer: initial evaluation with [^{15}O]H $_2$ O and [^{18}F]fluoroerythronitromidazole PET. *J Nucl Med.* 2001;42:1643-1652.
- Lehtiö K, Oikonen V, Nyman S, et al. Quantifying tumour hypoxia with fluorine-18 fluoroerythronitromodazole ([^{18}F]FETNIM) and PET using the tumour to plasma ratio. *Eur J Nucl Med Mol Imaging.* 2003;30:101-108.
- Lehtiö K, Eskola O, Viljanen T, et al. Imaging perfusion and hypoxia with PET to predict radiotherapy response in head-and-neck cancer. *Int J Radiation Oncology Biol Phys.* 2004;59:971-982.
- Lewis JS, McCarthy DW, McCarthy TJ, et al. Evaluation of ^{64}Cu -ATSM in vitro and in vivo in a hypoxic tumor model. *J Nucl Med.* 1999;40:177-183.
- Lewis JS, Sharp TL, Laforest R, et al. Tumor uptake of copper-diacetyl-bis(N^4 -methylthiosemicarbazone): effect of changes in tissue oxygenation. *J Nucl Med.* 2001;42:655-661.
- Lewis JS, Laforest R, Dehdashti F, et al. An imaging comparison of ^{64}Cu -ATSM and ^{60}Cu -ATSM in cancer of the uterine cervix. *J Nucl Med.* 2008;49:1177-1182.
- Li L, Yu J, Xing L, et al. Serial hypoxia imaging with $^{99\text{m}}\text{Tc}$ -HL91 SPECT to predict radiotherapy response in non small cell lung cancer. *Am J Clin Oncol.* 2006;29:628-633.
- Linder KE, Chan YW, Cyr JE, et al. TcO(PnA.O-1-(2-nitroimidazole)) [BMS-181321], a new technetium-containing nitroimidazole complex for imaging hypoxia: synthesis, characterisation, and xanthine oxidase-catalyzed reduction. *J Med Chem.* 1994;37:9-17.
- Ljunkvist ASE, Bussink J, Kaanders JHAM, et al. Hypoxic cell turnover in different solid tumor lines. *Int J Radiation Oncology Biol Phys.* 2005;62:1157-1168.
- Lodish H, Berk A, Matsudaira P, et al. Molecular Cell Biology. Chapter 8: Cellular energetics (2004). Freeman, New York, pp 301-350
- Loncaster JA, Harris AL, Davidson SE, et al. Carbonic anhydrase (CA IX) expression, a potential new intrinsic marker of hypoxia: correlations with tumor oxygen measurements and prognosis in locally advanced carcinoma of the cervix. *Cancer Res.* 2001;61:6394-6399.
- Macheda ML, Rogers S, Best JD. Molecular and cellular regulation of glucose transporter (GLUT) proteins in cancer. *J Cell Phys.* 2005;202:654-662.
- Mahon PC, Hirota K, Semenza G. FIH-1: a novel protein that interacts with HIF-1 α and VHL to mediate repression of HIF-1 transcriptional activity. *Genes Dev.* 2001;15:2675-2686.

- Mahy P, De Bast M, Leveque PH, et al. Preclinical validation of the hypoxia tracer 2-(2-nitroimidazol-1-yl)-N-(3,3,3-[¹⁸F]trifluoropropyl)-acetamide, [¹⁸F]EF3. *Eur J Nucl Med Mol Imaging*. 2004;31:1263-1272.
- Mahy P, De Bast M, Gillart J, et al. Detection of tumour hypoxia: comparison between EF5 adducts and [¹⁸F]EF3 uptake on an individual mouse tumour basis. *Eur J Nucl Med Mol Imaging*. 2006;33:553-556.
- Mahy P, De Bast M, de Groot T, et al. Comparative pharmacokinetics, biodistribution, metabolism and hypoxia-dependent uptake of [¹⁸F]-EF3 and [¹⁸F]-FMISO in rodent tumor models. *Radiother Oncol*. 2008;doi:10.1016/j.radonc.2008.06.008
- Mahy P, Geets X, Lonnew M, et al. Determination of tumour hypoxia with [¹⁸F]EF3 in patients with head and neck tumours: a phase I study to assess the tracer pharmacokinetics, biodistribution and metabolism. *Eur J Nucl Med Mol Imaging*. 2008;35:1282-1289.
- Mannan RH, Somayaji VV, Lee J, et al. Radioiodinated 1-(5-iodo-5-deoxy-β-D-arabinofuranosyl)-2-nitroimidazole (iodoazomycin arabinoside: IAZA): a novel marker of tissue hypoxia. *J Nucl Med*. 1991;32:1764-1770.
- Mannan RH, Mercer JR, Wiebe LI, et al. Radioiodinated azomycin pyranoside (IAZP): a novel non-invasive marker for the assessment of tumor hypoxia. *J Nucl Biol Med*. 1992;36:60-67.
- Mathupala SP, Rempel A, Pedersen PL. Glucose catabolism in cancer cells. Identification and characterization of a marked activation response of the type II hexokinase gene to hypoxic conditions. *J Biol Chem*. 2001;276:43407-43412.
- Matsumoto KI, Szajek L, Krishna MC, et al. The influence of tumor oxygenation on hypoxia imaging in murine squamous cell carcinoma using [⁶⁴Cu]Cu-ATSM or [¹⁸F]fluoromisonidazole positron emission tomography. *Int J Oncol*. 2007;30:873-881.
- Maxwell PH, Dachs GU, Gleadle JM, et al. Hypoxia-inducible factor-1 modulates gene expression in solid tumors and influences both angiogenesis and tumor growth. *Proc Natl Acad Sci USA*. 1997;94:8104-8109.
- Mayer A, Wree A, Höckel M, et al. Lack of correlation between expression of HIF-1α protein and oxygenation status in identical tissue areas of squamous cell carcinomas of the uterine cervix. *Cancer Res*. 2004;64:5876-5881.
- Mayer A, Höckel M, Wree A, et al. Microregional expression of glucose transporter-1 and oxygenation status: lack of correlation in locally advanced cervical cancers. *Clin Cancer Res*. 2005;11:2768-2773.

- Mayer A, Höckel M, Vaupel P. Carbonic anhydrase IX expression and tumor oxygenation status do not correlate at the microregional level in locally advanced cancers of the uterine cervix. *Clin Cancer Res.* 2005;11:7220-7225.
- Meikle SR, Dahlbom M (1998) Positron emission tomography. In: Murray IPC, Ell PJ (eds) Nuclear medicine in clinical diagnosis and treatment. Churchill Livingstone, Edinburgh, pp 1603-1616
- Melo T, Duncan J, Ballinger JR, et al. BRU59-21, a second-generation ^{99m}Tc -labeled 2-nitroimidazole for imaging hypoxia in tumors. *J Nucl Med.* 2000;41:169-176.
- Minn H, Clavo AC, Wahl RL. Influence of hypoxia on tracer accumulation in squamous-cell carcinoma: in vitro evaluation for PET imaging. *Nucl Med Biol.* 1996;23:941-946.
- Moore RB, Chapman JD, Mercer JR, et al. Measurement of PDT-induced hypoxia in dunning prostate tumors by iodine-123-iodoazomycin arabinoside. *J Nucl Med.* 1993;34:405-413.
- Nehmeh SA, Lee NY, Schröder H, et al. Reproducibility of intratumor distribution of ^{18}F -fluoromisonidazole in head and neck cancer. *Int J Radiation Oncology Biol Phys.* 2008;70:235-242.
- Nordmark M, Overgaard M, Overgaard J. Pretreatment oxygenation predicts radiation response in advanced squamous cell carcinoma of the head and neck. *Radiother Oncol.* 1996;41:31-39.
- Nordmark M, Loncaster J, Aquino-Parsons C, et al. Measurements of hypoxia using pimonidazole and polarographic oxygen-sensitive electrodes in human cervix carcinomas. *Radiother Oncol.* 2003;67:35-44.
- Nordmark M, Bentzen SM, Rudat V, et al. Prognostic value of tumor oxygenation in 397 head and neck tumors after primary radiation therapy. An international multi-center study. *Radiother Oncol.* 2005;77:18-24.
- Obata A, Yoshimoto M, Kasamatsu S, et al. Intra-tumoral distribution of ^{64}Cu -ATSM: a comparison study with FDG. *Nucl Med Biol.* 2003;30:529-534.
- O'Donoghue JA, Zanzonico P, Pugachev A, et al. Assessment of regional tumor hypoxia using ^{18}F -fluoromisonidazole and ^{64}Cu (II)-diacetyl- bis(N^4 -methylthiosemicarbazone) positron emission tomography: comparative study featuring microPET omaging, pO_2 probe measurement, autoradiography, and fluorescent microscopy in the R3327-AT and FaDu rat tumor models. *Int J Radiation Oncology Biol Phys.* 2005;61:1493-1502.
- Olive PL, Banath JP, Aquino-Parsons C. Measuring hypoxia in solid tumors. Is there a gold standard? *Acta Oncol.* 2001;40:917-923.

- Ong LC, Jin Y, Song IC, et al. PKH. 2-[¹⁸F]-2-deoxy-D-glucose (FDG) uptake in human tumor cells is related to the expression of GLUT-1 and hexokinase II. *Acta Radiol.* 2008;49:1145-1153.
- Oswald J, Treite F, Hasse C, et al. Experimental hypoxia is a potent stimulus for radiotracer uptake in vitro: comparison of different tumor cells and primary endothelial cells. *Cancer Lett.* 2007;254:102-110.
- Papandreou I, Cairns RA, Fontana L, et al. HIF-1 mediates adaptation to hypoxia by actively downregulating mitochondrial oxygen consumption. *Cell Metab.* 2006;3:187-197.
- Parliament MB, Chapman JD, Urtasun RC, et al. Non-invasive assessment of human tumour hypoxia with ¹²³I- iodoazomycin arabinoside: preliminary report of a clinical study. *Br J Cancer.* 1992;65:90-95.
- Pastorino JG, Hoek JB. Hexokinase II: the integration of energy metabolism and control of apoptosis. *Curr Med Chem.* 2003;10:1535-1551.
- Pedersen MW, Holm S, Lund EL, et al. Coregulation of glucose uptake and vascular endothelial growth factor (VEGF) in two small-cell lung cancer (SCLC) sublines in vivo and in vitro. *Neoplasia.* 2001;3:80-87.
- Piert M, Machulla HJ, Picchio M, et al. Hypoxia-specific tumor imaging with ¹⁸F-Fluoroazomycin arabinoside. *J Nucl Med.* 2005;46:106-113.
- Potter C, Harris AL. Hypoxia inducible carbonic anhydrase IX, marker of tumor hypoxia, survival pathway and therapy target. *Cell Cycle.* 2004;3:164-167.
- Pugachev A, Ruan S, Carlin S, et al. Dependence of FDG uptake on tumor microenvironment. *Int J Radiation Oncology Biol Phys.* 2005;62:545-553.
- Rafajova M, Zatovicova M, Kettman R, et al. Induction by hypoxia combined with low glucose or low bicarbonate and high posttranslational stability upon reoxygenation contribute to carbonic anhydrase IX expression in cancer cells. *Int J Oncol.* 2004;24:995-1004.
- Rajendran JG, Wikson DC, Conrad EU, et al. [¹⁸F]FMISO and [¹⁸F]FDG PET imaging in soft tissue sarcomas: correlation of hypoxia, metabolism and VEGF expression. *Eur J Nucl Med Mol Imaging.* 2003;30:695-704. Rajendran JG, Mankoff DA, O'Sullivan F, et al. Hypoxia and glucose metabolism in malignant tumors: evaluation by [¹⁸F]Fluoromisonidazole and [¹⁸F]Fluorideoxyglucose positron emission tomography imaging. *Clin Canc Res.* 2004;10:2245-2252.

- Rajendran JG, Schwartz DL, O'Sullivan J, et al. Tumor hypoxia imaging with [F-18] fluoromisonidazole positron emission tomography in head and neck cancer. *Clin Cancer Res.* 2006;12:5435-5441.
- Raleigh RA, Chou SC, Arteel GE, et al. Comparisons among pimonidazole binding, oxygen electrode measurements and radiation respons in C3H mouse tumors. *Radiat Res.* 1999;151:580-589.
- Rasey JS, Koh WJ, Evans ML, et al. Quantifying regional hypoxia in human tumors with positron emission tomography of [¹⁸F]fluoromisonidazole: a pretherapy study of 37 patients. *Int J Radiation Oncology Biol Phys.* 1996;36:417-428.
- Rasey JS, Hofstrand PD, Chin LK, et al. Characterization of [¹⁸F]Fluoroetanidazole, a new radiopharmaceutical for detecting tumor hypoxia. *J Nucl Med.* 1999;40:1072-1079.
- Rasey JS, Casciari JJ, Hofstrand PD, et al. Determining hypoxic fraction in a rat glioma by uptake of radiolabeled fluoromisonidazole. *Rad Res.* 2000;153:84-92.
- Reischl G, Dorow DS, Cullinane C, et al. Imaging of hypoxia with [¹²⁴I]IAZA in comparison with [¹⁸F]FMISO and [¹⁸F]FAZA – first small animal PET results. *J Pharm Pharmaceut Sci.* 2007;10:203-211.
- Riedl CC, Brader P, Zanzonico P, et al. Tumor hypoxia imaging in orthotopic liver tumors and peritoneal metastasis: a comparative study featuring dynamic ¹⁸F-MISO and ¹²⁴I-IAZG PET in the same study cohort. *Eur J Nucl Med Mol Imaging.* 2007;35:39-46.
- Riedl CC, Brader P, Zanzonico PB, et al. Imaging hypoxia in orthotopic rat liver tumors with iodine 124-labeled iodoazomycin galactopyranoside PET. *Radiology.* 2008;248:561-570.
- Rischin D, Hicks RJ, Fisher R, et al. Prognostic significance of [¹⁸F]-Misonidazole positron emission tomography-detected tumor hypoxia in patients with advanced head and neck cancer randomly assigned to chemoradiation with or without tirapazamine: a substudy of trans-tasman radiation oncology group study 98.02. *J Clin Oncol.* 2006;24:2098-2104.
- Rumsey WL, Kuczynski B, Patel B, et al. SPECT imaging of ischemic myocardium using a technetium-99m-nitroimidazole ligand. *J Nucl Med.* 1995;36:1445-1450.
- Russel J, Carlin S, Burke SA, et al. Immunohistochemical detection of changes in tumor hypoxia. *Radiation Oncology Biol Phys.* 2009;73:1177-1186.
- Saitoh JI, Sakurai H, Suzuki Y, et al. Correlations between in vivo tumor weight, oxygen pressure, ³¹P NMR spectroscopy, hypoxic microenvironment marking by β-D-iodinated

- azomycin galactopyranoside (β -D-IAZGP), and radiation sensitivity. *Int J Radiation Oncology Biol Phys.* 2002;54:903-909.
- Sakata K, Someya M, Nagakura H, et al. A clinical study of hypoxia using endogenous hypoxic markers and polarographic oxygen electrodes. *Strahlenther Onkol.* 2006;182:511-517.
- Semenza GL, Jiang BH, Leung SW, et al. Hypoxia response elements in the aldolase A, enolase 1, and lactate dehydrogenase A gene promoters contain essential binding sites for hypoxia-inducible factor 1. *J Biol Chem.* 1996;271:32529-32537.
- Semenza GL. HIF-1: Mediator of physiological and pathophysiological responses to hypoxia. *J Appl Physiol.* 2000;88:1474-1480.
- Scigliano S, Pinel S, Poussier S, et al. Measurement of hypoxia using invasive oxygen-sensitive electrode, pimonidazole binding and ^{18}F -FDG uptake in anaemic or erythropoietin-treated mice bearing human glioma xenografts. *Int J Oncol.* 2008;32:69-77.
- Semenza GL. Oxygen-dependent regulation of mitochondrial respiration by hypoxia-inducible factor 1. *Biochem J.* 2007;405:1-9.
- Shi CQX, Sinusas AJ, Dione DP, et al. Technetium-99m-nitrimidazole (BMS181321): a positive imaging agent for detecting myocardial ischemia. *J Nucl Med.* 1995;36:1078-1086.
- Shin KH, Diaz-Gonzalez JA, Russell J, et al. Detecting changes in tumor hypoxia with carbonic anhydrase IX and pimonidazole. *Cancer Biol Ther.* 2007;6:70-75.
- Siim BG, Laux WT, Rutland MD, et al. Scintigraphic imaging of the hypoxia marker $^{99\text{m}}\text{Tc}$ -labeled 2,2'-(1,4-diaminobutane)bis(2-methyl-3-butanone) dioxime ($^{99\text{m}}\text{Tc}$ -labeled HL-91; Prognox): noninvasive detection of tumor response to the antivascular agent 5,6-dimethylxanthenone-4-acetic acid. *Cancer Res.* 2000;60:4582-4588.
- Smith TAD. The rate-limiting step for tumor [^{18}F]fluor-2-deoxy-D-glucose (FDG) incorporation. *Nucl Med Biol.* 2001;28:1-4.
- Sorger D, Patt M, Kumar P, et al. [^{18}F]Fluoroazomycin-arabinofuranoside (^{18}F FAZA) and [^{18}F]Fluoromisonidazole (^{18}F FMISO): a comparative study of their selective uptake in hypoxic cells and PET imaging in experimental rat tumors. *Nucl Med Biol.* 2003;30:317-326.

- Souvatzoglou M, Grosu AL, Röper B, et al. Tumour hypoxia imaging with [¹⁸F]FAZA PET in head and neck cancer patients: a pilot study. *Eur J Nucl Med Mol Imaging*. 2007;34:1566-1575.
- Stainsby WN, Snyder B, Wech HG. A pictographic essay on blood and tissue oxygen transport. *Medicine and Science and Sports and Exercise*. 1988;20:213-221.
- Stypinski D, Wiebe LI, McEwan AJ, et al. Clinical pharmacokinetics of ¹²³I-IAZA in healthy volunteers. *Nucl Med Comm*. 1999;20:559-567.
- Stypinski D, McQuarrie SA, Wiebe LI, et al. Dosimetry estimations for ¹²³I-IAZA in healthy volunteers. *J Nucl Med*. 2001;42:1418-1423.
- Suzuki T, Nakamura K, Kawase T, et al. Biodistribution of hypoxic marker, ^{99m}Tc-HL91 (4,9-diaza-3,3,10,10-tetramethyldecane-2,11-dione dioxime). *Kaku Igaku*. 2001;38:333-341.
- Suzuki T, Nakamura K, Kawase T, et al. Monitoring of response to radiation therapy for human tumor xenografts using ^{99m}Tc-HL91 (4,9-diaza-3,3,10,10-tetramethyldecane-2,11-dione dioxime). *Ann Nucl Med*. 2003;17:131-138.
- Tanaka T, Furukawa T, Fujieda S, et al. Double-tracer autoradiography with Cu-ATSM/FDG and immunohistochemical interpretation in four different mouse implanted tumor models. *Nucl Med Biol*. 2006;33:743-750.
- Tatsumi M, Yutani K, Kusuoka H, et al. Technetium-99m HL91 uptake as a tumour hypoxia marker; relationship to tumour blood flow. *Eur J Nucl Med*. 1999;26:91-94.
- Teicher BA, Holden SA, Al-Achi A, et al. Classification of antineoplastic treatments by their differential toxicity toward putative oxygenated and hypoxic tumor subpopulations in vivo in the FSaIIc murine fibrosarcoma. *Cancer Res*. 1990;50:3339-3344.
- Thorwarth D, Eschmann SM, Holzner F, et al. Combined uptake of [¹⁸F]FDG and [¹⁸F]FMISO correlates with radiation therapy outcome in head-and-neck cancer patients. *Radiother Oncol*. 2006;80:151-156.
- Tolvanen T, Lehtiö K, Kulmala J, et al. ¹⁸F-Fluoroerythronitromodazole radiation dosimetry in cancer studies. *J Nucl Med*. 2002;43:1674-1680.
- Troost EGC, Laverman P, Kaanders JHAM, et al. Imaging hypoxia after oxygenation modification: comparing [¹⁸F]FMISO autoradiography with pimonidazole immunohistochemistry in human xenograft tumors. *Radiother Oncol*. 2006;80:157-164.
- Troost EGC, Laverman P, Philippens MEP, et al. Correlation of [¹⁸F]FMISO autoradiography and pimonidazole immunohistochemistry in human head and neck carcinoma xenografts. *Eur J Nucl Med Mol Imaging*. 2008;DOI 10.1007/s00259-008-0772-7.

- Urtasun RC, Parliament MB, McEwan AJ, et al. Measurement of hypoxia in human tumours by non-invasive spect imaging of iodoazomycin arabinoside. *Br J Cancer Suppl.* 1996;27:S209-S212.
- Valk PE, Mathis CA, Prados MD, et al. Hypoxia in human gliomas: demonstration by PET with fluorine-18-fluoromisonidazole. *J Nucl Med.* 1992;33:2133-2137.
- Van de Wiele C, Versijpt J, Dierckx RA, et al. ⁹⁹Tc(m) labelled HL91 versus computed tomography and biopsy for the visualization of tumour recurrence of squamous head and neck carcinoma. *Nucl Med Commun.* 2001;22:269-275.
- Van de Wiele Christophe (2006). PET and SPECT in IMRT: Future prospects. In: Bortfeld T, Schmidt-Ullrich R, De Neve W, Wazer DE (eds) Image-guided IMRT. Springer, Berlin, pp 171-175
- Vaupel P, Kallinowski F, Okunieff. Blood flow, oxygen and nutrient supply, and metabolic microenvironment of human tumors: a review. *Cancer Res.* 1989;49:6449-6465.
- Vaupel P. The role of hypoxia-induced factors in tumor progression. *Oncologist.* 2004;9:10-17.
- Vaupel P, Harrison L. Tumor hypoxia: causative factors, compensatory mechanisms, and cellular response. *Oncologist.* 2004;suppl 5:4-9.
- Vaupel P, Mayer A. Hypoxia in cancer: significance and impact on clinical outcome. *Cancer Metastasis Rev.* 2007;26:225-239
- Vavere AL, Lewis JS. Cu-ATSM: a radiopharmaceutical for the PET imaging of hypoxia. *Dalton Trans.* 2007;DOI: 10.1039/b705989b
- Vordermark D, Kaffer A, Riedl S, et al. Characterization of carbonic anhydrase IX (CA IX) as an endogenous marker of chronic hypoxia in live human tumor cells. *Int J Radiation Oncology Biol Phys.* 2005;61:1197-1207.
- Warburg O. On the origin of cancer cells. *Science.* 1956;123:309-314.
- Wyss MT, Honer M, Schubiger PA, et al. NanoPET imaging of [¹⁸F]fluoromisonidazole uptake in experimental mouse tumours. *Eur J Nucl Med Mol Imaging.* 2006;33:311-318.
- Yang DJ, Wallace S, Cherif A, et al. Development of F-18-labeled fluoroerythronitromidazole as a PET agent for imaging tumor hypoxia. *Radiology.* 1995;194:795-800.
- Yapp DTT, Woo J, Kartono A, et al. Non-invasive evaluation of tumour hypoxia in the Shionogi tumour model for prostate cancer with ¹⁸F-EF5 and positron emission tomography. *BJU Int.* 2007;99:1154-1160.

- Yuan H, Schroeder T, Bowsher JE, et al. Intertumoral differences in hypoxia selectivity of the PET imaging agent $^{64}\text{Cu}(\text{II})$ -diacetyl- bis(N^4 -methylthiosemicarbazone). *J Nucl Med*. 2006;47:989-998.
- Yutani K, Kusuoka H, Fukuchi K, et al. Applicability of $^{99\text{m}}\text{Tc}$ -HL91, a putative hypoxic tracer, to detection of tumor hypoxia. *J Nucl Med*. 1999;40:854-861.
- Zanzonico P, O'Donoghue J, Chapman JD, et al. Iodine-124-labeled iodo-azomycin-galactoside imaging of tumor hypoxia in mice with serial microPET scanning. *Eur J Nucl Med Mol Imaging*. 2004;31:117-128.
- Zanzonico P, Campa J, Polycarpe-Holman D, et al. Animal-specific positioning molds for registration of repeat imaging studies: comparative microPET imaging of F18-labeled fluoro-deoxyglucose and fluoro-misonidazole in rodent tumors. *Nucl Med Biol*. 2006;33:65-70.
- Zhang X, Melo T, Ballinger JR, et al. Studies of $^{99\text{m}}\text{Tc}$ -BnAO (HL-91): a non-nitroaromatic compound for hypoxic cell detection. *Int J Radiation Oncology Biol Phys*. 1998;42:737-740.
- Zhang X, Melo T, Rauth AM, et al. Cellular accumulation and retention of the technetium-99m-labelled hypoxia markers BRU59-21 and butylene amine oxime. *Nucl Med Biol*. 2001;28: 949-957.
- Zhao FQ, Keating AF. Functional properties and genomics of glucose transporters. *Curr Genomics*. 2007;8:113-128.
- Ziemer LS, Evans SM, Kachur AV, et al. Noninvasive imaging of tumour hypoxia in rats using the 2-nitroimidazole ^{18}F -EF5. *Eur J Nucl Med*. 2003;30:259-266.
- Zimny M, Gagel B, DiMartino E, et al. FDG—a marker of tumour hypoxia? A comparison with [^{18}F]fluoromisonidazole and pO_2 -polarography in metastatic head and neck cancer. *Eur J Nucl Med Mol Imaging*. 2006;33:1426-1431.

1.7 Outline and objectives

Given their close interaction, the objective of this work was to explore the relation between tumor oxygenation and tumor metabolism and evaluate the possible consequences and benefits of this relation for [^{18}F]FDG - PET imaging. Furthermore, a new radiotracer of tumor vasculature was evaluated.

Chapter 2 of this work focuses on the relation between tumor oxygenation and tumor metabolism and investigates whether or not this relation can be exploited in order to improve functional imaging using [^{18}F]FDG - PET. In partim 2.1, the effects of an increase in tumor oxygenation on tumor metabolism were studied by investigating changes in expression of proteins important for tumor metabolism, survival and spread in a rat colorectal xenograft after treatment with rhEPO. In partim 2.2, the effects of a decrease in tumor oxygenation or a direct HIF-1 activation on tumor metabolism were studied by investigating [^{18}F]FDG-uptake in an *in vitro* and *in vivo* model of human colorectal carcinoma. In partim 2.3, the distribution of the exogenous nitroimidazole hypoxia marker pimonidazole was compared with the expression of GLUT1 and 3, HK2 and CA IX in a spontaneous canine mammary gland tumor. In partim 2.4, the expression of the endogenous hypoxia marker CA IX was compared with [^{18}F]FDG-PET SUVmax and SUVmean values in patients suffering from NSCLC.

In Chapter 3 of this work a new radiotracer ($^{99\text{m}}\text{Tc}-(\text{CO})_3 \text{His-CNA35}$) that selectively binds tumor vasculature subendothelial collagen, was evaluated. As tumor vasculature and tumor hypoxia are highly interconnected, non-invasive imaging of tumor vasculature might provide insights into tumor hypoxia. In this manuscript, the synthesis, purification, biodistribution, dosimetry and *in vivo* imaging qualities of this new molecule are examined.

Chapter 2: Tumor Hypoxia and Glucose Metabolism

2.1 Research article: Combined effect of EPO and radiotherapy on the expression of endogenous molecular markers of tumour metabolism and metastasis.

Cancer Biother Radiopharm. 2009;24:565-572.

Combined effect of EPO and radiotherapy on the expression of endogenous molecular markers of tumour metabolism and metastasis.

Gilles Mees ¹, Philippe Fonteyne ¹, Wim Ceelen ², Tom Boterberg ³, Patrick Pauwels ⁴, Christel Vangestel ⁵, Nancy Van Damme ⁵, Marc Peeters ^{5,*}, Rudi Dierckx ^{1,6}, Christophe Van De Wiele ^{1,6}

¹ Department of Nuclear Medicine and Molecular Imaging, University Medical Center Groningen, University of Groningen, The Netherlands

² Department of Surgery, University Hospital Ghent, Belgium

³ Department of Radiotherapy, University Hospital Ghent, Belgium

⁴ Department of Pathology, University Hospital Ghent, Belgium

⁵ Department of Gastroenterology, University Hospital Ghent, Belgium

⁶ Departments of Nuclear Medicine, Experimental Cancerology and Radiotherapy, University Hospital Ghent, Belgium

* Senior Clinical Investigator, Research Foundation Flanders (FWO)

ABSTRACT

Erythropoietin has been used to correct cancer-related anaemia and to improve tumour hypoxia which both adversely affect the clinical condition of cancer patients and response to radiotherapy. Data available on the effects of erythropoietin treatment in cancer are, however, conflicting. Several clinical studies investigating the influence of erythropoietin treatment have given contradictory results as to whether or not this treatment positively influences survival. In the light of these conflicting results, we studied the effects of erythropoietin treatment either alone or in combination with radiotherapy on tumour oxygenation and on the expression pattern of several proteins related to tumour metabolism, survival and spread in a rat colorectal cancer model. We found a statistically significant upregulation of hexokinase I, N-cadherin, and glucose transporter 3 when erythropoietin treatment was combined with radiotherapy. Because these three proteins have distinct functions in protecting the cell in compromised conditions, these results indicate a detrimental role for the combination of

erythropoietin treatment and radiotherapy through the stimulation of tumour cell metabolism, inhibition of apoptosis and stimulation of tumour spread, and seem to indicate that rhEPO treatment negatively modulates RT efficacy.

KEYWORDS: EPO, radiotherapy, apoptosis, metastasis, glucose transporter

INTRODUCTION

Anaemia adversely affects the clinical condition of cancer patients and contributes to the development of tumour hypoxia which in turn adversely affects response to radiotherapy. Since erythropoietin (EPO) is a well recognized and effective treatment for anaemia, this pleiotropic cytokine, which is involved in the proliferation and differentiation of the erythroid lineage, has been used to correct cancer-related anaemia and improve tumour hypoxia (1-7). Data available on this subject are, however, conflicting. On the one hand, in various clinical trials conducted in diverse groups of cancer patients it was found that treatment with recombinant human EPO (rhEPO) significantly increased the quality of life and survival rate of cancer patients, respectively by increasing their haemoglobin levels and by reducing the need for potentially risky red blood cell transfusions (8,9). However, a recent meta-analysis of 57 of such trials performed, including 9353 patients, suggested that treatment of anaemia with rhEPO may have no impact on overall survival in patients with cancer (10). In addition, recent experimental findings have advocated a role for EPO as a strong anti-apoptotic agent in multiple non-erythroid tissues but also in neoplastic tissues. Also, the discovery of EPO receptors (EPO-R) on malignant cells, suggests that EPO may act as a tumour growth factor (1-3). Finally, contrary to initial findings, more recently, a number of randomized clinical trials, reported that rhEPO might actually adversely affect cancer survival rates of cancer patients treated by means of radiotherapy, mainly due to tumour progression (11,12). While strongly criticized for methodological pitfalls, these studies led the FDA to force a “black label” warning concerning the use of rhEPO in cancer patients.

In the light of these conflicting results, the influence of rhEPO either alone or in combination with radiotherapy on tumour oxygenation was studied in a rat colorectal cancer model given both treatment options may profoundly influence tumour oxygenation. Subsequently, the influence of rhEPO either alone or in combination with radiotherapy on the expression pattern

of several proteins related to tumour metabolism, survival and spread was studied in the same model.

MATERIALS AND METHODS

Animal and Tumour Model

Male Wag/Rij rats were bought from Harlan (Horst, The Netherlands). The CC531 cell line is a 1,2-dimethylhydrazine-induced, moderately differentiated, and weakly immunogenic colon adenocarcinoma, syngeneic with WAG/Rij rats. This cell line is well studied and has been proven to provide a tumour-host model similar to human colorectal carcinogenesis (13). Cells were grown in plastic culture flasks in RPMI 1640 medium, buffered with HEPES (20 mM) (Invitrogen Corporation, Gibco, Ghent, Belgium) additionally supplemented with 10 % fetal calf serum, 4 mM L-glutamine, 50 U/ml penicillin, and 50 µg/ml streptomycin at 37 °C in a humidified atmosphere with 5 % CO₂ in air. The cells were transferred at 95 % confluency. Two million cells suspended in 0,2 ml of saline were injected subcutaneously (s.c.) in the proximal hind leg. Tumours reached a size of 0,5 – 1 cm after a period of 4 weeks. All the experiments with rats were approved by the institutional ethical committee and animal handling was done according to institutional guidelines for animal care.

Experimental Therapy

Animals were randomly divided into two groups in which some of the animals received RT: a control group (n = 20) in which 11 animals received RT and a rhEPO group (n = 26) receiving rhEPO in which 16 animals received RT. rhEPO (Eprex, Janssen Cilag, Beerse, Belgium) was administered at a dose of 3 x 0,1 ml (286 IU) s.c. per week. The dosage was based on a dose-finding study during which five or eight rhEPO administrations weekly resulted in an excessive haematocrit rise and important mortality (data not shown). Recombinant human EPO has been shown to bind to the rodent EPO receptor (14). Rats were longitudinally studied during 3 weeks using the following timeframe: start of rhEPO administration (day 1); first oxygenation measurement (day 8); fractionated RT 5 x 5 Gy (day 13 – 17); second oxygenation measurement, and killing by anaesthesia overdose and excision of tumours for histology (all on day 22).

Radiotherapy

Rats were not sedated and the tumour-bearing hind leg was immobilised using a purpose-built Plexiglass holder, as described previously (15,16). Briefly, rats were placed in the holder in prone position. The hind legs were pulled through an opening in the holder and immobilised. Before each fraction, a radiation field was simulated encompassing the tumour with a margin of 1,5 cm. Photon irradiation was performed with a 5MV linear accelerator (Elekta, Crawley, UK). Five fractions of 5 Gy (total dose 25 Gy) were delivered on five consecutive days. As the tumours were inoculated s.c., they were covered with tissue-equivalent silicone bolus of 1cm to prevent the build-up effect under the skin. One single direct field at a fixed source-skin distance of 100 cm was used. The dose was calculated to the midpoint of the tumours according to their volume in each individual animal, as obtained during simulation.

Tissue pO₂-measurements

Tissue oxygenation was measured with a fibre-optic probe based on fluorescence quenching (OxyLite, Oxford Optronix, Oxford, UK) (17,18). A precalibrated fibreoptic probe was inserted 5 mm deep into the tumour using a Seldinger technique; the probe was then withdrawn in 40 steps of 100 mm each over a total distance of 4 mm using a micromanipulator (model MN151, Narishige International Ltd, London, UK). After each micromanipulator movement, measurements were started as soon as a stable reading was obtained. Tissue pO₂ was sampled every 2 s. Tissue pO₂ was expressed in mmHg. Oxygenation measurements were performed in the animals that received RT, 5 days before and 5 days after the completion of RT.

Immunohistochemistry

Formalin fixed, paraffin embedded tissue samples were used for immunohistochemistry with the appropriate antibodies. Sections of 4 µm thick were mounted on SuperFrost® microscope slides (Menzel-Glaser, Braunschweig, Germany), which were deparaffinized in xylene and rehydrated in a downgraded series of ethanol. After flushing in water, heat induced antigen retrieval was performed for 20 minutes with the appropriate buffer (EDTA pH = 8.0 or CIT pH = 6.0), after which the tissue slides were cooled down for 20 minutes and then flushed in water for 10 minutes. The endogenous peroxidase activity was blocked for 5 minutes with 0,3 % hydrogen peroxide (DAKO, Glostrup, Denmark) on each tissue slide. Primary antibodies were then incubated for 1 hour at room temperature; the appropriate antibodies with their corresponding dilution factors (primary antibody diluted in 1% BSA/PBS) are indicated in

Table 1 (see Table 1). After washing, the tissue sections were incubated for 30 minutes at room temperature with a labelled polymer-HRP anti-rabbit secondary antibody (DAKO, Glostrup, Denmark). The colour reaction was developed using the chromogen 3,3-diaminobenzidine+ (DAB) (DAKO, Glostrup, Denmark) for 10 minutes. After washing, the tissue sections were counterstained with Mayer's haematoxylin.

Phosphate-buffered saline with 1% BSA instead of the primary antibody was used as negative control on each slide in order to exclude false positive responses from non-specific binding of the secondary antibody. Prior to staining the specimens, an isotype control was performed to estimate the non-specific binding of target primary antibodies to cell surface antigens. Non-specific binding is due to Fc receptor binding or other protein-protein interactions.

Antibody	Company	Pretreatment	Dilution	+ control tissue
GLUT 1	ABCAM, ab15309	EDTA	1/100	internal RBC
GLUT 3	Santa Cruz Biotechnology, sc-30107	CIT	1/50	testis
GLUT 4	Santa Cruz Biotechnology, sc-7938	EDTA	1/100	placenta
GLUT 8	α -Diagnostics International, GT81-A	CIT	1/10	testis
GLUT 9	α -Diagnostics International, GT91-A	EDTA	1/25	pancreas ca
HK I	Santa Cruz Biotechnology, sc-28885	EDTA	1/500	liver
HK II	Santa Cruz Biotechnology, sc-28889	EDTA	1/100	liver
HK III	Santa Cruz Biotechnology, sc-28890	EDTA	1/400	liver
SGLT-1	Fitzgerald, 70R-SR005	CIT	1/20	kidney
N-CAD	ABCAM, ab12221	CIT	1/100	brain

TABLE 1. The different antibody dilutions and heat induced pre-treatment methods needed for the immunostainings. For each antibody the correct positive control tissues were used to optimize the immunostainings. (EDTA = ethylenediaminetetraacetic acid, CIT = citrate)

Immunohistochemical Analysis

The intensity and amount of positive tumour cells in the immuno-reaction were scored independently by two experienced observers, blinded to the clinical results. The percentage of tumour cells that were positive on the immuno-reaction were scored as follows : 0% (score 0), 0-20% (score 1), 20-40% (score 2), 40-60% (score 3), 60-80% (score 4) and 80-100% (score 5). Intensities of staining were categorized as absent (score 0), faint (score 1), average (score 2) or strong (score 3). Positive tumour cells were counted per high-power field (final magnification, 400 X). An estimation of intensity and % positive tumour cells was made after counting ten high-powerfields. A final histological score was calculated as following: Hscore

= $[(a_1 \times i_1) + (a_2 \times i_2)] / 2$, where i = the score of intensity, a = the score of amount tumour cells that stained positive and 1 and 2 refer to the scores of the two observers.

Statistical Analysis

SPPS for Windows, version 15.0 was used for statistical analysis. Differences between two groups of continuous data were analysed with the Student's t-test (two-tailed, paired or unpaired as appropriate). To assess differences between the four different experimental groups, one-way analysis of variance (ANOVA) was performed with post-hoc Fisher's protected least significant differences (FLSD) on each variable. P value < 0.05 was considered significant.

RESULTS

Effects of rhEPO Treatment and RT on Tumour pO_2

Mean pO_2 values in the tumour before and after RT in both groups are shown in Figure 1 (Fig. 1). Both before ($p = 0,007$) and after ($p = 0,015$) RT, pO_2 values were significantly higher in the rhEPO treated rats. In the control group, no significant difference in tumour oxygenation was observed after RT ($p = 0,201$). In the rhEPO group, on the contrary, RT induced a reoxygenation ($p = 0,019$).

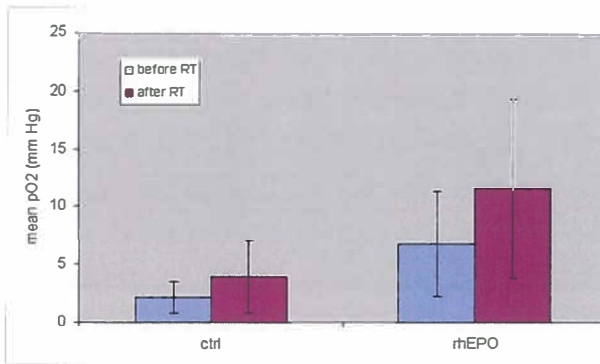


FIGURE 1. Mean pO_2 values in the control group before (2,1; sd 1,3) and after (3,9; sd 3,0) RT. Mean pO_2 values in the rhEPO group before (6,7; sd 4,5) and after (11,5; sd 7,7) RT. Both before ($p = 0,007$; Student's t-test) and after ($p = 0,015$; Student's t-test) RT, pO_2 values were significantly higher in the rhEPO treated rats. In the rhEPO group RT induced a reoxygenation ($p = 0,019$; Student's t-test).

Effects of rhEPO Treatment on Haematocrit

Data in this study were acquired from material which was part of larger set of data from another study.³⁸ In this study, haematocrit values were tested before starting the experiment and on day 8. In rhEPO-treated rats, mean haematocrit showed a 25% increase from $50,7 \pm 0,4\%$ before therapy to $62,6 \pm 0,4\%$ on day 8 ($p < 0,001$). In the control group, haematocrit values remained unchanged.

Effects of rhEPO Treatment and RT on Expression of GLUT1, GLUT3, GLUT4, GLUT8, GLUT9 and SGLT1

Mean Hscores for GLUT1 expression for the different experimental groups were respectively: ctrl: 7,9 (range 4,0 to 12,0; sd 2,4), rhEPO: 11,1 (range 1,5 to 15; sd 4,9), ctrl+RT: 9,0 (range 4,0 to 13,5; sd 3,1), rhEPO+RT: 9,0 (range 2,5 to 13,5; sd 3,0). Mean Hscores for GLUT3 expression for the different experimental groups were respectively: ctrl: 5,6 (range 1,5 to 9,0; sd 3,2), rhEPO: 4,7 (range 3,0 to 9,0; sd 1,9), ctrl+RT: 5,9 (range 1,5 to 13,5; sd 3,5), rhEPO+RT: 7,9 (range 2,5 to 12,0; sd 2,9) (Fig. 2). Mean Hscores for GLUT4 expression for the different experimental groups were respectively: ctrl: 3,9 (range 1,0 to 9,0; sd 2,7), rhEPO: 5,7 (1,5 to 10, 0; sd 2,9), ctrl+RT: 4,9 (range 2,5 to 8,0; sd 2,3), rhEPO+RT: 5,2 (range 2,5 to 10,0; sd 2,5). Mean Hscores for GLUT8 expression for the different experimental groups were respectively: ctrl: 7,3 (range 1,0 to 12,0; sd 3,1), rhEPO: 5,8 (range 1,5 to 12,0; sd 3,3), ctrl+RT: 7,7 (range 3,0 to 15,0; sd 4,1), rhEPO+RT: 7,7 (1,5 to 15,0; sd 3,6). Mean Hscores for GLUT9 expression for the different experimental groups were respectively: ctrl: 1,1 (range 0,5 to 2,5; sd 0,7), rhEPO: 2,2 (range 0,5 to 4,0; sd 1,1), ctrl+RT: 3,1 (range 0,5 to 10,0; sd 3,5), rhEPO+RT: 2,4 (range 0,5 to 7,0; sd 1,8). Mean Hscores for SGLT1 expression for the different experimental groups were respectively: ctrl: 12,3 (range 3,5 to 15,0; sd 3,7), rhEPO: 10,1 (range 0,5 to 15,0; sd 6,0), ctrl+RT: 9,3 (range 0,0 to 15,0; sd 5,1), rhEPO+RT: 11,9 (range 0,5 to 15,0; sd 5,1). Immunostaining of GLUT1 was mainly membranous and negative controls showed no staining. Immunostaining of GLUT3, GLUT4, GLUT8, GLUT9 and SGLT1 was cytoplasmic and negative controls showed no staining. A significant increase in GLUT3 expression was observed in the rhEPO group upon RT treatment ($p = 0,01$; ANOVA). (Fig. 2, Fig. 3)

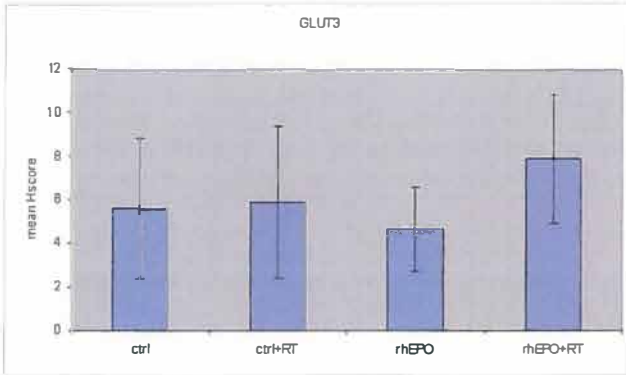


FIGURE 2. Mean Hscores for GLUT3 expression for the different experimental groups were respectively: ctrl: 5,6 (range 1,5 to 9,0; sd 3,2), rhEPO: 4,7 (range 3,0 to 9,0; sd 1,9), ctrl+RT: 5,9 (range 1,5 to 13,5; sd 3,5), rhEPO+RT: 7,9 (range 2,5 to 12,0; sd 2,9). A significant increase in GLUT3 expression was observed in the rhEPO group upon RT treatment ($p = 0,01$).

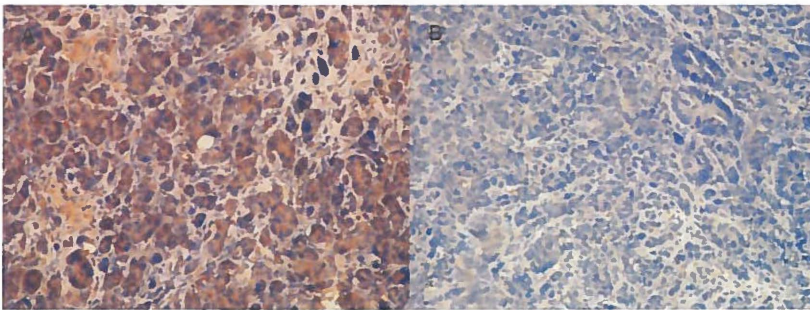


FIGURE 3. Immunohistochemical analysis of Glut3 expression: an example comparing a sample with a high Hscore and a sample with a low Hscore. Panel A: Sample of rat that received RT and rhEPO (Hscore 12,0) (200x). Panel B: Sample of rat that received no treatment (Hscore 2,5) (200x).

Effects of rhEPO Treatment and RT on Expression of HKI, HKII and HKIII

Mean Hscores for HKI expression for the different experimental groups were respectively: ctrl: 8,6 (range 3,5 to 10,0; sd 2,0), rhEPO: 8,0 (range 1,0 to 13,5; sd 3,3), ctrl+RT: 10,7 (range 7,0 to 15,0; sd 3,2), rhEPO+RT: 11,7 (range 8,0 to 15,0; sd 2,9) (Fig. 4). Mean Hscores for HKII expression for the different experimental groups were respectively: ctrl: 7,7 (range 2,5 to 13,5; sd 3,4), rhEPO: 7,1 (range 0,0 to 10,0; sd 3,2), ctrl+RT: 7,5 (range 0,0 to 13,5; sd 3,5), rhEPO+RT: 9,1 (range 0,0 to 13,5; sd 3,3). Mean Hscores for HKIII expression for the different experimental groups were respectively: ctrl: 0,9 (range 0,0 to 2,0; sd 0,6), rhEPO:

1,3 (range 0,0 to 2,5; sd 0,8), ctrl+RT: 0,9 (range 0,0 to 2,5; sd 0,7), rhEPO+RT: 1,0 (range 0,0 to 2,5; sd 0,6). Immunostaining of the hexokinases was cytoplasmatic and negative controls showed no staining.

A significant increase in HKI expression was observed in the rhEPO group upon RT treatment ($p = 0,003$; ANOVA). Additionally, HKI expression in the rhEPO group that received RT was significantly higher than in the control group that didn't receive RT ($p = 0,016$; ANOVA) and HKI expression in the control group that received RT was significantly higher than in the rhEPO group that didn't receive RT ($p = 0,034$; ANOVA). (Fig. 4, Fig. 5)

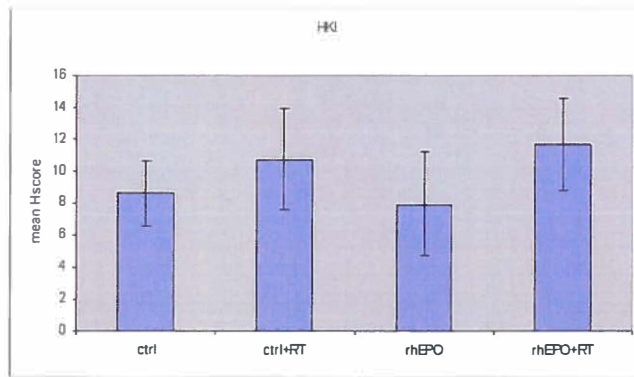


FIGURE 4. Mean Hscores for HKI expression for the different experimental groups were respectively: ctrl: 8,6 (range 3,5 to 10,0; sd 2,0), rhEPO: 8,0 (range 1,0 to 13,5; sd 3,3), ctrl+RT: 10,7 (range 7,0 to 15,0; sd 3,2), rhEPO+RT: 11,7 (range 8,0 to 15,0; sd 2,9). A significant increase in HKI expression was observed in the rhEPO group upon RT treatment ($p = 0,003$). Additionally, HKI expression in the rhEPO group that received RT was significantly higher than in the control group that didn't receive RT ($p = 0,02$) and HKI expression in the control group that received RT was significantly higher than in the rhEPO group that didn't receive RT ($p = 0,03$).

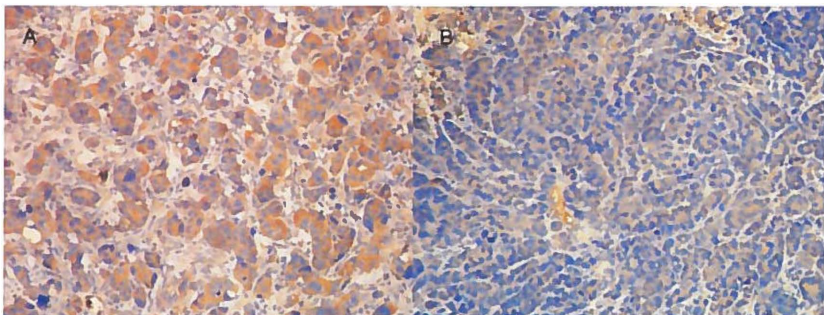


FIGURE 5. Immunohistochemical analysis of HKI expression: an example comparing a sample with a high Hscore and a sample with a low Hscore. Panel A: Sample of rat that

received RT and rhEPO (Hscore 15,0) (200x). Panel B: Sample of rat that received no treatment (Hscore 3,5) (200x).

Effects of rhEPO Treatment and RT on Expression of N-cadherin

Mean Hscores for N-CAD expression for the different experimental groups was respectively: ctrl: 6,6 (range 3,5 to 10,0; sd 2,4), rhEPO: 6,8 (range 3,5 to 10,0; sd 2,6), ctrl+RT: 9,6 (range 3,5 to 15,0; sd 4,5), rhEPO+RT: 9,9 (range 1,5 to 15,0; sd 3,9) (Fig. 6). Immunostaining of N-cadherin was mainly cytoplasmatic and negative controls showed no staining.

A significant increase in N-cadherin expression was observed in the rhEPO group upon RT treatment ($p = 0,037$; ANOVA). Additionally, N-cadherin expression in the rhEPO group that received RT was significantly higher than in the control group that didn't receive RT ($p = 0,030$; ANOVA). (Fig. 6, Fig. 7)

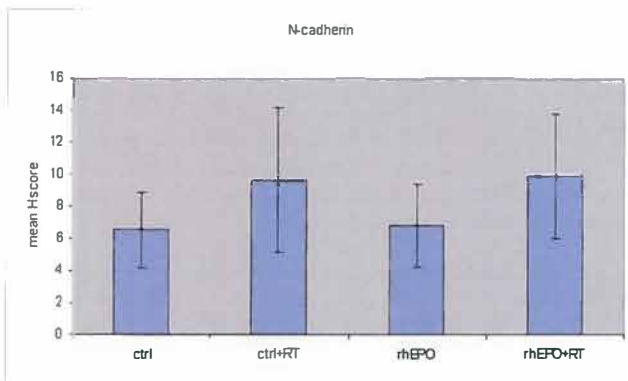


FIGURE 6. Mean Hscores for N-CAD expression for the different experimental groups was respectively: ctrl: 6,6 (range 3,5 to 10,0; sd 2,4), rhEPO: 6,8 (range 3,5 to 10,0; sd 2,6), ctrl+RT: 9,6 (range 3,5 to 15,0; sd 4,5), rhEPO+RT: 9,9 (range 1,5 to 15,0; sd 3,9). A significant increase in N-cadherin expression was observed in the rhEPO group upon RT treatment ($p = 0,04$). Additionally, N-cadherin expression in the rhEPO group that received RT was significantly higher than in the control group that didn't receive RT ($p = 0,03$).

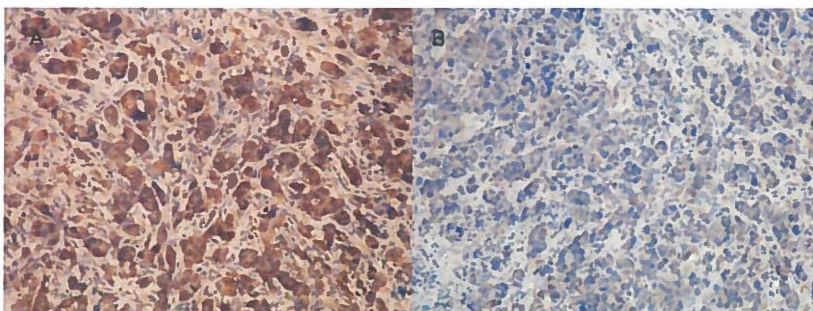


FIGURE 7. Immunohistochemical analysis of N-cadherin expression: an example comparing a sample with a high Hscore and a sample with a low Hscore. Panel A: Sample of rat that received RT and rhEPO (Hscore 15,0) (200x). Panel B: Sample of rat that received no treatment (Hscore 5,0) (200x).

	GLUT3	HKI	N-CAD
ANOVA	<u>0,05</u>	<u>0,01</u>	<u>0,05</u>
ctrl ↔ rhEPO	0,49	0,62	0,88
ctrl ↔ ctrl + RT	0,85	0,11	0,06
ctrl ↔ rhEPO + RT	0,07	<u>0,02</u>	<u>0,03</u>
rhEPO ↔ ctrl + RT	0,36	<u>0,03</u>	0,08
rhEPO ↔ rhEPO + RT	<u>0,01</u>	<u>0,003</u>	<u>0,04</u>
ctrl + RT ↔ rhEPO + RT	0,09	0,42	0,85

TABLE 2. Significant differences were found between the different experimental groups in the expression of GLUT3, HKI and N-CAD. Overview of the p-values of the different comparisons. No significant differences were found between the different experimental groups in the expression of GLUT1 ($p = 0,24$; ANOVA), GLUT4 ($p = 0,48$; ANOVA), GLUT8 ($p = 0,54$; ANOVA), GLUT9 ($p = 0,23$; ANOVA), SGLT1 ($p = 0,44$; ANOVA) HKII ($p = 0,45$; ANOVA) and HKIII ($p = 0,49$; ANOVA). P value $\leq 0,05$ was considered significant.

DISCUSSION

The aim of this study was to investigate the expression of several proteins related to tumour metabolism and invasion in a rat colorectal cancer model receiving RT in combination with rhEPO treatment. This was done to assess a possible influence of EPO and RT on tumour cell metabolism and invasion either through a direct effect on the tumour cells or by an indirect effect by changes in the oxygenation status of the tumour. A statistically significant upregulation of hexokinase I (HKI), N-cadherin, and glucose transporter 3 (GLUT3) was found when rhEPO treatment was combined with RT.

Our results first of all indicate that rhEPO treatment increases tumour oxygenation. To date, the mechanisms by which rhEPO improves tumour oxygenation remain unclear. Besides its effect on haemoglobin levels, several direct effects of rhEPO have been described by which rhEPO can influence tumour oxygenation. Blackwell et al. found that systemic rhEPO administration to non-anaemic rats bearing mammary adenocarcinoma flank tumours improved tumour oxygenation independent of the effects on haemoglobin levels (17). Tovari

et al. found that rhEPO had profound effects on tumoural blood vessels in human epidermoid and colorectal cancer xenograft models through changes in vascular endothelial growth factor (VEGF) expression and microvessel morphology (19). Although there are several reports that RT alone causes an increase in tumour oxygenation, our results did not indicate this (20,21). We did find however, that RT causes an increase in tumour oxygenation when rhEPO is administered, possibly indicating a synergistic effect of both treatments.

We further found a significant increase in GLUT3 glucose transporter expression in the rhEPO group upon RT treatment. Facilitative glucose transporters (GLUTs) mediate the transport of glucose and other monosaccharides across the plasma membrane of mammalian cells. The whole family of human GLUT proteins consists of 14 members with different substrate specificities, kinetic properties and tissue expression profiles. GLUT3 is a high affinity glucose transporter ($K_m = 10,6 \text{ mM}$) that is mainly expressed in the brain where it mediates glucose transport into neurons. As GLUT3 is believed to operate more efficiently at lower substrate concentrations than other isoforms, it is expected to supplement GLUT1 in tissues with a high energy demand (22). Besides glucose, GLUT3 also transports galactose, mannose, maltose, xylose or dehydroascorbic acid. Upregulation of GLUT3 has frequently been described in human tumours, where it is believed to be involved in fulfilling the high energy demand of the tumour (23,24). Because of its high affinity for glucose and its ability to transport other energy substrates besides glucose, it's tempting to view an upregulation of GLUT3 as a stress reaction of the tumour cell in an effort to absorb as much energy from its environment as possible. As such, an upregulation of GLUT3 may be seen as a survival benefit allowing the tumour cell to cope with its compromised situation more efficiently.

Our results also indicate a significant increase in HKI expression in the rhEPO group upon RT treatment. Additionally, HKI expression in the rhEPO group that received RT was significantly higher than in the control group that didn't receive RT and HK1 expression in the control group that received RT was significantly higher than in the rhEPO group that didn't receive RT. HKI is a metabolic enzyme belonging to the family of the hexokinases which comprises 4 members (HKI, HKII, HKIII, and HKIV or glucokinase). Hexokinases have a role in glucose metabolism, converting glucose to glucose-6-phosphate. Overexpression of HK is a common feature in cancer as it allows the tumour cell to maintain a high rate of glycolysis by maintaining the downhill concentration gradient necessary to move glucose into the cell through glucose transporters. The overexpressed form of HK is preferentially bound to the outer mitochondrial membrane. This interaction markedly reduces the enzyme's sensitivity to product inhibition by glucose-6-phosphate, provides preferred

access to mitochondrial generated ATP, and protects against proteolytic degradation (25-27). In addition to their role in glucose metabolism by augmenting cellular energy supply and levels of glucose-6-phosphate, HKI and HKII are also believed to play an active role in regulating cell death. *In vitro* and *in vivo* studies have shown that HKI and HKII play a role in protecting against mitochondrial regulated apoptosis through direct interaction with mitochondria and, more specifically, with the voltage-dependent anion channel (VDAC) through their N-terminal hydrophobic regions. A mechanism has been proposed in which binding of HK to VDAC induces channel closure leading to the prevention of cytochrome C release, which represents the mitochondrial phase of apoptosis (26,28-30). In this respect, HKI overexpression in U-937 cells protected against apoptotic cell death induced by staurosporine and HKI and II overexpression in HEK293 cells protected against apoptotic cell death induced by hydrogen peroxide (28,31). Again, the increase in HKI expression upon treatment with rhEPO and RT suggests activation of an anti-apoptotic mechanism in the remaining tumour cells allowing them to survive in compromised conditions.

Finally, our results indicate a significant increase in Neural (N) - cadherin expression in the rhEPO group upon RT treatment. Additionally, N-cadherin expression in the rhEPO group that received RT was significantly higher than in the control group that didn't receive RT. The cadherin family of adhesion molecules regulates cell-cell interactions during development and during normal tissue homeostasis. N-cadherin is a cell-adhesion molecule belonging to the family of the cadherins that is normally found in fibroblasts and neural cells and has a role in tumour cell invasion and metastasis. Metastasis is a complex multistep process involving a series of tumour-host interactions that finally result in colonization of distant tissue. While E-cadherin, which is responsible for maintaining interactions of epithelial cells, is frequently downregulated during tumour progression, N-cadherin is frequently upregulated during tumour progression and increases the invasiveness of tumour cells (32). This switch in cadherin expression, often referred to as the cadherin switch, can be the result of an epithelial to mesenchymal transformation (EMT) of tumour cells. EMT plays a critical role in the progression of tumours towards a more aggressive phenotype that is associated with increased motile and invasive capability (33). A number of studies described upregulation of N-cadherin expression in several invasive tumour cell lines and tumour tissues from different origins (34). Additionally, its exogenous expression in tumour cells induces a scattered morphology and heightened motility, invasion and metastasis (35-37). This N-cadherin upregulation provides tumour cells with a way to permeate local and distant tissues and facilitate its survival by interacting with N-cadherin expressing host cells of the stroma or the endothelium through a

homophillic interaction (32,34). Therefore, the increase in N-cadherin expression upon treatment with rhEPO and RT suggests that the remaining tumour cells are enhancing their metastatic capacities enabling them to spread from their primary site to one or more metastatic sites. Upon visual confirmation of this changing phenotype, we observed a shift towards a poorly differentiated form with highly anaplastic cells and an increase in abnormal mitotic figures.

The effects of rhEPO treatment on response to RT, chemotherapy or photodynamic therapy remain a matter of debate. Whereas some studies indicate that rhEPO treatment has beneficial effects on radiosensitivity (5-7) and leads to a survival benefit (8,9), other studies report on a diminished survival in case of rhEPO treatment (11,12). Although the latter studies were strongly criticized for study design, conduct and post-trial analysis, there are indeed increasing reports on the modulation of the effects of RT by rhEPO treatment. The mechanism by which this occurs remains unclear. In a recent study by Ceelen et al., an attempt was made to clarify these mechanisms. It was concluded that rhEPO treatment resulted in spatially heterogeneous modulation of RT effects on tumour microvessels. Treatment with rhEPO prevented RT-induced changes in microvascular permeability and tumour vascular volume, accompanied by a larger microvessel diameter and altered spatial complexity (38). The results seen in this study seem to confirm the unfavourable effects of rhEPO treatment on RT efficacy.

To conclude, our results indicate a detrimental role for the combination of rhEPO treatment and RT through the stimulation of tumour cell metabolism, inhibition of apoptosis and stimulation of tumour spread. A significant upregulation of HKI, N-cadherin and GLUT3 was observed after treatment with RT in combination with rhEPO treatment. These three proteins have distinct functions in protecting the cell in compromised conditions. As a consequence, these results seem to confirm the results of other groups whereby rhEPO treatment seemed to modulate the effects of RT on the tumour. The mechanism by which this occurs, remains largely unclear and needs further clarification.

REFERENCES

1. Hardee ME, Arcasoy MO, Blackwell KL, et al. Erythropoietin biology in cancer. *Clin Cancer Res.* 2006;12:332-339.

2. Sinclair AL, Todd MD, Forsythe K, et al. Expression and function of erythropoietin receptors in tumors. *Am Cancer Soc.* 2007;110:477-488.
3. Jelkmann W, Bohlius J, Hallek M, et al. The erythropoietin receptor in normal and cancer tissues. *Crit Rev Oncol Hemat.* 2008;67:39-61.
4. Varlotto J, Stevenson MA. Anemia, tumor hypoxia, and the cancer patient. *Int J Radiat Oncol.* 2005;63:25-36.
5. Stuben G, Pottgen C, Knuhmann K, et al. Erythropoietin restores the anemia-induced reduction in radiosensitivity of experimental human tumors in nude mice. *Int J Radiat Oncol.* 2003;55:1358-1362.
6. Pinel S, Barberi-Heyob M, Cohen-Jonathan E et al. Erythropoietin-induced reduction of hypoxia before and during fractionated irradiation contributes to improvement of radioresponse in human glioma xenografts. *Int J Radiat Oncol.* 2004;59:250-259.
7. Lövey J, Bereczky B, Gilly R, et al. Recombinant human erythropoietin alpha improves the efficacy of radiotherapy of a human tumor xenograft, affecting tumor cells and microvessels. *Strahlenther Onkol.* 2008;184:1-7.
8. Littlewood TJ, Bajetta E, Nortier JWR, et al. Effects of epoetin alfa on hematologic parameters and quality of life in cancer patients receiving nonplatinum chemotherapy: results of a randomized, double-blind, placebo-controlled trial. *J Clin Oncol.* 2001;19:2865-2874.
9. Bohlius J, Langensiepen S, Schwarzer G, et al. Recombinant human erythropoietin and overall survival in cancer patients: results of a comprehensive meta-analysis. *J Natl Cancer Inst.* 2006;97:489-498.
10. Bohlius J, Wilson J, Seidenfeld J, et al. Recombinant human erythropoietins and cancer patients: updates meta-analysis of 57 studies including 9353 patients. *J Natl Cancer Inst.* 2006;98:708-714.
11. Henke M, Laszig R, Rube C, et al. Erythropoietin to treat head and neck cancer patients with anaemia undergoing radiotherapy: randomised, double-blind, placebo-controlled trial. *Lancet.* 2003;362:1255-1260.
12. Leyland-Jones B, Semiglazov V, Pawlicki M, et al. Maintaining normal hemoglobin levels with epoetin alfa in mainly nonanemic patients with metastatic breast cancer receiving first-line chemotherapy: a survival study. *J Clin Oncol.* 2005;23:5960-5972.
13. Hagens M, Koelemij R, Ensink NG, et al. The development of novel mouse monoclonal antibodies against the CC531 rat colon adenocarcinoma. *Clin Exp Metastas.* 2000;18:281-289.

14. Okano M, Suga H, Masuda S, et al. Characterization of erythropoietin isolated from rat serum – biochemical comparison of rat and human erythropoietins. *Biosci Biotech Bioch.* 1993;57:1882-1885.
15. Ceelen W, El Malt M, Cardon A, et al. Influence of preoperative high-dose radiotherapy on postoperative outcome and colonic anastomotic healing – experimental study in the rat. *Dis Colon Rectum.* 2001;44:717-721.
16. El-Malt M, Ceelen W, De Meerleer G, et al. Influence of preoperative combined radiochemotherapy on surgical outcome and colonic anastomotic healing: experimental study in the rat. *Int J Radiat Oncol.* 2001;50:1073-1078.
17. Blackwell KL, Kirkpatrick JP, Snyder SA, et al. Human recombinant erythropoietin significantly improves tumor oxygenation independent of its effects on hemoglobin. *Cancer Res.* 2003;63:6162-6165.
18. Brurberg KG, Graff BA, Olsen DR, et al. Tumor-line specific pO₂ fluctuations in human melanoma xenografts. *Int J Radiat Oncol.* 2004;58:403-409.
19. Tovari J, Gilly R, Raso E, et al. Recombinant human erythropoietin alpha targets intratumoral blood vessels, improving chemotherapy in human xenograft models. *Cancer Res.* 2005;65:7186-7193.
20. Stüben G, Thews O, Pöttgen C, et al. Tumour oxygenation during fractionated radiotherapy. *Acta Oncol.* 1999;38:209-213.
21. Ljungkvist ASE, Bussink J, Kaanders JHAM, et al. Dynamics of hypoxia, proliferation and apoptosis after irradiation in a murine tumor model. *Radiat Res.* 2006;165:326-336.
22. Wood IS, Trayhurn P. Glucose transporters (GLUT and SGLT): expanded families of sugar transport proteins. *Brit J Nut.* 2003;89:3-9.
23. Macheda ML, Rogers S, Best JD. Molecular and cellular regulation of glucose transporter (GLUT) proteins in cancer. *J Cell Physiol.* 2005;202:654-662.
24. Medina RA, Owen GI. Glucose transporters: expression, regulation and cancer. *Biol Res.* 2002;35:9-26.
25. Wilson JE. Isozymes of mammalian hexokinase: structure, subcellular localization and metabolic function. *J Exp Bio.* 2003;206:2049-2057.
26. Pedersen PL, Mathupala S, Rempel A, et al. Mitochondrial bound type II hexokinase: a key player in the growth and survival of many cancers and an ideal prospect for therapeutic intervention. *Biochim Biophys Acta.* 2002;1555:14-20.
27. Mathupala SP, Rempel A, Pedersen PL. Aberrant glycolytic metabolism of cancer cells: a remarkable coordination of genetic, transcriptional, post-transcriptional, and

- mutational events that lead to a critical role for type II hexokinase. *J Bioenerg Biomembr.* 1997;29:339-343.
28. Azoulay-Zohar H, Israelson A, Abu-Hamad S, et al. In self-defence: hexokinase promotes voltage-dependent anion channel closure and prevents mitochondria-mediated apoptotic cell death. *Biochem J.* 2004;377:347-355.
 29. Pastorino JG, Shulga N, Hoek JB. Mitochondrial binding of hexokinase II inhibits Bax-induced cytochrome release and apoptosis. *J Biol Chem.* 2002;277:7610-7618.
 30. Abu-Hamad S, Zaid H, Israelson A, et al. Hexokinase-I protection against apoptotic cell death is mediated via interaction with the voltage-dependent anion channel-1. *J Biol Chem.* 2008;283:13482-13490.
 31. Sun L, Shukair S, Naik TJ, et al. Glucose phosphorylation and mitochondrial binding are required for the protective effects of hexokinases I and II. *Mol Cell Biol.* 2008;28:1007-1017.
 32. Agiostratidou G, Hulit J, Phillips GR, et al. Differential cadherin expression: potential markers for epithelial to mesenchymal transformation during tumor progression. *J Mammary Gland Biol.* 2007;12:127-133.
 33. Thiery JP. Epithelial-mesenchymal transitions in development and pathologies. *Curr Opin Cell Biol.* 2003;15:740-746.
 34. Hazan RB, Qiao R, Keren R, et al. Cadherin switch in tumour progression. *Ann NY Acad Sci.* 2004;1014:155-163.
 35. Nieman MT, Prudoff RS, Johnson KR, et al. N-cadherin promotes motility in human breast cancer cells regardless of their E-cadherin expression. *J Cell Biol.* 1999;147:631-644.
 36. Islam S, Carey TE, Wolf GT, et al. Expression of N-cadherin by human squamous carcinoma cells induces a scattered fibroblastic phenotype with disrupted cell-cell adhesion. *J Cell Biol.* 1996;135:1643-1654.
 37. Hazan RB, Phillips GR, Qiao RF, et al. Exogeneous expression of N-cadherin in breast cancer cells induces cell migration, invasion, and metastasis. *J Cell Biol.* 2000;148:779-790.
 38. Ceelen W, Boterberg T, Smeets P, et al. Recombinant human erythropoietin α modulates the effects of radiotherapy on colorectal cancer microvessels. *Br J Canc.* 2007;96:692-700.

2.2 Research article: Pharmacological activation of tumor hypoxia: a means to increase tumor [¹⁸F]FDG-uptake?

Accepted for publication
in
Molecular Imaging

Pharmacological activation of tumor hypoxia: a means to increase tumor [¹⁸F]FDG-uptake?

Gilles Mees¹, Rudi Dierckx^{1,2}, Christel Vangestel³, Debby Laukens³, Nancy Van Damme⁴, Christophe Van de Wiele^{1,2}

¹ Department of Nuclear Medicine and Molecular Imaging, University Medical Center Groningen, University of Groningen, The Netherlands

² Department of Nuclear Medicine, Ghent University Hospital, Belgium

³ Department of Gastroenterology, Ghent University Hospital, Belgium

⁴ Department of Surgery, Ghent University Hospital, Belgium

ABSTRACT

Introduction: Tumor hypoxia and tumor metabolism are linked through the activation of metabolic genes following HIF-1 activation. This raises the question whether this relation can be exploited to improve [¹⁸F]FDG-PET imaging. To do this, [¹⁸F]FDG-uptake was investigated after chemical induction of hypoxia and chemical activation of HIF-1 in an *in vitro* and *in vivo* model of a human colorectal carcinoma.

Methods: [¹⁸F]FDG-uptake, HIF-1 α protein levels and mRNA expression of GLUT1, HK2, HIF-1 α and CA IX were determined in HT29 cells after treatment with 200 μ M CoCl₂ and 500 μ M DMOG. In a HT29 xenograft, the distribution of endogenous and exogenous markers of hypoxia was investigated using immunohistochemistry and tumor [¹⁸F]FDG-uptake was determined after treatment with a single dose of 5 mg/kg hydralazine and 8 mg DMOG.

Results: Treatment of HT29 cells with CoCl₂ and DMOG induced functional HIF-1 and resulted in increased [¹⁸F]FDG-uptake. In a HT29 xenograft, a similar spatial distribution of pimonidazole, CA IX and GLUT1 was found and treatment with DMOG resulted in significant increases in SUV_{max} and SUV_{mean} using [¹⁸F]FDG-PET imaging.

Conclusion: Chemical activation of HIF-1 can increase *in vitro* and *in vivo* [¹⁸F]FDG-uptake. Imaging after pharmacological HIF-1 activation might possibly increase tumor [¹⁸F]FDG-uptake when using [¹⁸F]FDG-PET imaging.

Key words: [^{18}F]FDG, tumor hypoxia, DMOG, HIF-1, PHD

INTRODUCTION

2-Deoxy-2- [^{18}F]fluoro-D-glucose ([^{18}F]FDG) is the most widely used positron emission tomography (PET) radiotracer in oncology. This non-invasive imaging method, which is routinely used for cancer detection, staging and monitoring of response and recurrence in several tumor types, is based on the accumulation of a radiolabeled glucose analogue in tumor cells as a consequence of their enhanced glucose uptake and glycolysis. Although the precise determinant remains unclear, major factors considered to play a key role in the higher [^{18}F]FDG-uptake by malignant cells appear to be overexpression of different types of glucose transporters (GLUTs), a high hexokinase (HK) activity and a low glucose-6-phosphatase (G6P) activity (1,2). Despite its widespread use, a number of problems and limitations still exist. First of all, because glucose is used as an energy substrate throughout the body, [^{18}F]FDG-uptake in some benign tissues and certain physiological processes is common and complicates its oncological use: high uptake in normal brain tissue complicates brain tumor detection, aspecific bladder activity interferes with bladder and prostate cancer diagnosis, and inflammation and infection processes are known to be highly [^{18}F]FDG avid. Secondly, some tumors such as prostate carcinoma, mucinous carcinoma and hepatocellular carcinoma display low [^{18}F]FDG-uptake due to low metabolic rates or elevated G6P levels (3,4). In these patients, the lack of identification of sites of malignant invasion or underestimation of the disease may result in insufficient or lack of treatment, adversely affecting patient outcome.

It is becoming more and more clear that tumor hypoxia, a characteristic feature of locally advanced solid tumors, plays an important role in tumor metabolism and as a result in [^{18}F]FDG-PET imaging. As hypoxic conditions aggravate the already profound and inherent dependence of malignant cells on glycolysis (5) through the Pasteur effect, cancer cells adapt to these hypoxic conditions by the induction of target genes involved in glucose metabolism ensuring necessary energy supply. Many of these adaptations are coordinated by the transcription factor hypoxia-inducible factor (HIF) - 1, which has been verified as a master regulator of oxygen homeostasis under hypoxic conditions (6). HIF-1 is a heterodimer consisting of HIF-1 α and HIF-1 β , whose biological activity is determined by the expression and activity of HIF-1 α , which is constantly expressed and subsequently rapidly destroyed

under normal oxygen conditions. This involves a mechanism where posttranslational hydroxylation by specific prolyl hydroxylases (PHD) allows binding of the von Hippel-Lindau protein (VHL) tumor suppressor protein, which in turn leads to ubiquitination and proteasomal degradation. Under hypoxic conditions however, stabilization of HIF-1 α occurs through inactivation of the PHDs, allowing it to translocate to the nucleus where it can bind with the constitutively expressed HIF-1 β to form a functional transcription factor that will transactivate several target genes (7,8). As a number of these genes are involved in tumor glucose metabolism and consequently in the uptake and trapping of [^{18}F]FDG, tumor hypoxia and functional imaging using [^{18}F]FDG-PET are inherently linked. As a result, artificially induced tumor hypoxia or chemical HIF-1 activation might provide a means to increase tumor [^{18}F]FDG-uptake and improve tumor detection using [^{18}F]FDG-PET imaging. Several approaches exist to induce tumor hypoxia in an *in vitro* and an *in vivo* setting. *In vitro* approaches comprise either the use of hypoxic chambers or either a direct chemical activation of HIF-1 using hypoxia mimics like cobalt chloride or chemicals inhibiting PHDs like dimethylxalylglycine (DMOG) (9). A commonly used *in vivo* approach uses a peripheral vasodilator named hydralazine hydrochloride which, through indirect inhibition of tumor blood flow, causes tumor hypoxia (10).

In this manuscript we studied the relationship between tumor hypoxia and [^{18}F]FDG-uptake and investigated whether this relationship could be exploited to improve [^{18}F]FDG-PET imaging. To do this, [^{18}F]FDG-uptake was investigated after chemical induction of hypoxia and chemical activation of HIF-1 in an *in vitro* and *in vivo* model of human colorectal carcinoma.

MATERIALS AND METHODS

HT29 Cell Culture

HT29 human colorectal carcinoma cells (ACC 299, DSMZ, Braunschweig, Germany) were cultured in McCoy's 5A medium (Invitrogen Corporation, Gibco, Merelbeke, Belgium) supplemented with 10% fetal bovine serum (Invitrogen Corporation), 4 mM L-glutamine, 50 $\mu\text{l/ml}$ penicillin and 50 $\mu\text{g/ml}$ streptomycin (Invitrogen Corporation) and incubated at 37°C in a humidified atmosphere of 5% CO₂ in air. Cells were kept in exponential growth phase by

routine passage every 3-4 days (split ratio of 1/4 - 1/6). Glucose concentration of McCoy's 5A medium is 3000 mg/L (16.67 mM).

[¹⁸F]FDG Uptake Experiments

For radiotracer uptake experiments, 2.5×10^5 HT29 cells were seeded in a cavity of a 12-well plate (Multiwell™, BD Falcon®, Becton Dickinson, Franklin Lakes, NJ USA) and cultured in a humidified atmosphere of 5% CO₂ in air at 37°C in cell culture medium. Cells were incubated with 200 μM cobalt chloride (CoCl₂) (Merck, Darmstadt, Germany) and 500 μM dimethylxalylglycine (DMOG; Echelon Biosciences, Salt Lake City, UT USA) for 5, 12 and 24 hours. Phosphate buffered saline (PBS) was used to dissolve CoCl₂ and DMOG. Control samples were treated with vehicle alone (PBS) and comparisons were made to vehicle-treated controls at each time point. After incubation, 0.74 MBq [¹⁸F]FDG was added to each well. After a 60 minutes incubation period at 37°C and 5% CO₂, cells were washed three times with ice-cold PBS and lysed in 0.5 ml RIPA-buffer (Thermo Scientific, Rockford, IL USA). Cell lysates were counted using an automated gamma counter (Cobra II series, Canberra-Packard, Meriden, CT USA). Protein concentration of each sample was determined using the BCA protein assay kit (Pierce, Rockford, IL USA) according to the manufacturer's recommendations and bovine serum albumin was used as protein standard. Uptake/well was corrected for protein concentration.

Quantitative Real-Time PCR

After an identical experimental set-up like the [¹⁸F]FDG-uptake experiments, HT29 cells were lysed in RLT-buffer (Qiagen, Westburg BV, The Netherlands) and needle homogenization was performed. Total RNA was extracted using the RNeasy Mini Kit (Qiagen) according to manufacturer's instructions. One microgram of total RNA was converted to single strand complementary DNA (cDNA) by reverse transcription (Superscript, Invitrogen) with Oligo(dT) priming. cDNA was used in real-time quantification using the SYBR green kit (GC Biotech, Alphen aan den Rijn, The Netherlands) and 250 nM of each primer. A two-step program was run on the LightCycler 480 (Roche, Vilvoorde, Belgium). Cycling conditions were 95°C for 10 min, 40 cycles of 95°C for 15 s and 60°C for 1 min. Melting curve analysis confirmed primer specificities. All reactions were run in duplicate and normalized to the geometric mean of human HMBS and SDHA. The efficiency of each primer was calculated using a standard curve of reference genomic or cDNA (Roche). Amplification efficiency was

determined using the formula $10^{-1/\text{slope}}$. For the actual calculations, the base of the exponential amplification function was used. (e.g. 2.04 in case of 104% amplification efficiency). Forward and reverse sequences of all reference genes and target genes are shown in Table 1.

Gene symbol	Forward Primers (5' - 3')	Reverse Primers (5' - 3')
hHIF-1 α	TGCCAGCTCAAAGAAAACA	ACCAACAGGGTAGGCAGAAC
hCA IX	TGACTTCAGCCGCTACT	CAGCATCACTGTCTGGTTA
hGLUT1	AAATGCTTGTGGATTGAGGG	GTCGAAGTCTAAGCCGTTGC
hHK2	CCCTGCCACCAGACTAA	GGATCAGAGCCACAACG
SDHA	TGGGAACAAGAGGGCATCTG	CCACCACTGCATCAAATTCATG
HMBS	GGCAATGCGGCTGCAA	GGGTACCCACGCGAATCAC

TABLE 1. Sequences of used qRT-PCR primers. hHIF-1 α , human hypoxia inducible factor 1 α ; hCA IX, human carbonic anhydrase IX; hGLUT1, human glucose transporter 1; hHK2, human hexokinase 2; SDHA, succinate dehydrogenase complex subunit A; HMBS, hydroxymethylbilane synthase

Enzyme-Linked Immunosorbent Assay (ELISA)

After an identical experimental set-up like the [^{18}F]FDG-uptake experiments, HT29 cells were lysed using lysis buffer. Levels of HIF-1 α in HT29 cell lysates were measured using a human HIF-1 α ELISA kit (R&D Systems DYC1935, Minneapolis, MN, USA) according to manufacturer's instructions and normalized to total protein content of cell lysates.

Animal Model

Four-to-six week old Female CD-1[®] nude mice were purchased from Charles River (Brussels, Belgium) and housed in a standard facility at the Department of Animal Sciences, Ghent University Hospital. All procedures were carried out in accordance with the guidelines and regulations for use and care of animals and approved by the local ethical committee, Faculty of Medicine, Ghent University (EC nr. 08/40). One million cells suspended in 0.1 ml of PBS were injected subcutaneously (sc) in the proximal hind leg. Tumor growth curves were obtained using calliper measurement and the estimate volume formula $V = 1/2 (a^2b)$, where a and b represent the short and long axis of the tumor, respectively. Experiments were initiated when tumors had reached approximately 10 mm in diameter, generally 14 days after implantation. When used, pimonidazole hydrochloride (Hypoxyprobe[™]-1, Chemicon

International, Billerica, MA USA) was administered intraperitoneally (ip) to mice one hour before sacrifice at a dosage of 60 mg/kg according to the manufacturers' instructions.

Immunohistochemistry

After resection of the tumors, the specimens were routinely processed, formalin fixed and paraffin embedded. Tissue sections of 5 μ m thick were mounted on SuperFrost[®] microscope slides (Menzel-Glaser, Braunschweig, Germany), which were deparaffinized in xylene and rehydrated in a downgraded series of ethanol. After washing the slides in the appropriate buffer (tris-buffered saline (TBS) with 0.1% Tween 20), heat induced antigen retrieval was performed for 20 minutes with citrate buffer (pH = 6.0), after which the slides were cooled down for 20 minutes. The endogenous peroxidase activity was blocked for 5 minutes with 0.3 % hydrogen peroxide (Dako, Glostrup, Denmark). Slides were then incubated with primary antibodies diluted in PBS with 1% bovine serum albumin (BSA) for 1 hour at room temperature (GLUT1 ABCAM ab15309, 1/200; GLUT3 ABCAM ab15311, 1/50; HK2 Santa-Cruz sc-28889, 1/100; CAIX ABCAM ab15086, 1/1500; HIF-1 α ABCAM ab114977, 1/100). After washing, the tissue sections were incubated for 30 minutes at room temperature with a HRP-labeled anti-rabbit secondary antibody (Dako). The colour reaction was developed using the chromogen 3,3-diaminobenzidine⁺ (DAB) (Dako) for 30 seconds. The tissue sections were counterstained with Mayer's haematoxylin. In order to exclude false positive responses from non-specific binding of the secondary antibody, negative controls were incubated with 1% PBS-BSA instead of the primary antibody. Prior to staining the specimens, an isotype control was performed to estimate the non-specific binding of target primary antibodies to cell surface antigens.

Immunohistochemical Analysis

An Optronicscolor digital camera (Olympus Corporation, Tokyo, Japan) and specialized software (Cell D Olympus Imaging Solutions, Münster, Germany) was used to analyse immunohistochemical stainings. The intensity and percentage of positive tumor were scored independently by two experienced observers. The percentage of tumor cells that were positive were scored as follows : 0% (score 0), 0-20% (score 1), 20-40% (score 2), 40-60% (score 3), 60-80% (score 4) and 80-100% (score 5). Intensities of staining were categorized as absent (score 0), faint (score 1), moderate (score 2) or strong (score 3). An estimation of intensity and percentage of positive tumor cells was made after counting ten high-powerfields (200x).

A final histological score (Hscore) was calculated as following: $Hscore = [(a1 \times i1) + (a2 \times i2)] / 2$, where i = the score of intensity, a = the score of amount tumor cells that stained positive and 1 and 2 refer to the scores of the two observers. A previously described semiquantitative scoring system was used to score pimonidazole staining: absent (score 0), > 0 to 5% (score 1), > 5 to 15% (score 2), > 15 to 30% (score 3), >30% (score 4) (11).

pO₂-Measurements

Tumor oxygenation after hydralazine treatment was measured with a fibre-optic probe based on fluorescence quenching (OxyLite, Oxford Optronix, Oxford, UK) (12). After anaesthesia was initiated using a constant flow of 2% isoflurane, a precalibrated fibreoptic probe was inserted 5 mm deep into the tumor using a Seldinger technique and kept in that same position for the duration of the experiment using a micromanipulator (model MN151, Narishige International Ltd, London, UK). Animals were kept under anaesthesia for the duration of the experiment. Measurements were started and after approximately one hour to one hour and a half, a single dose of 5 mg/kg hydralazine hydrochloride (Sigma Aldrich, Schnellendorf, Germany) was injected ip. Tissue pO₂ was sampled every second. Tissue pO₂ was expressed in mmHg. After approximately three hours, measurements were stopped and animals were sacrificed.

[¹⁸F]FDG-PET Imaging

[¹⁸F]FDG-PET examinations were performed on 3 consecutive days (day 0, 1 and 2), using the first scan as a baseline scan before treatment. On day 1 and day 2 mice were treated with: a single ip dose of 5 mg/kg hydralazine 3h or 8h before [¹⁸F]FDG administration, a single ip dose of 8mg DMOG 8h before [¹⁸F]FDG administration, or a single ip dose of vehicle alone (PBS) 8h before [¹⁸F]FDG administration. Each experimental group consisted of 5 animals. Mice fasted for 6h before an intravenous (iv) injection with 3.7 MBq of in-house produced [¹⁸F]FDG. One and a half hour post-injection, mice were anaesthetized with a mixture of 100 mg/kg Ketamine and 10 mg/kg Xylazine. When mice were sedated, they were positioned side by side in the field of view (FOV) of a conventional PET camera (Allegra™, Philips Medical Systems, Eindhoven, The Netherlands). After a 5 min transmission scan, a 10 min one-bed position PET acquisition was obtained. Images were reconstructed by a 3D-RAMLA technique using blobs as basis functions and with a pixel size of 2x2x2 mm. Attenuation and

scatter correction were applied during reconstruction and images were transferred to a remote workstation for further image analysis.

Volumes of interest (VOI) were drawn around the tumor using PMOD 3.0 software (PMOD Technologies, Zurich, Switzerland) and SUVmax and SUVmean (Standardized Uptake Values) were calculated. VOIs from baseline scans were copied onto the treatment scans. [¹⁸F]FDG uptake was also determined in a reference tissue (brain) to ensure that changes in tumor SUV were not a consequence of differences in injection technique or due to varying systemic clearance of the radiotracer from the body. Brain was chosen as it allowed easy and reproducible placement of VOIs. Briefly, a spherical VOI (5mm diameter) was placed central in the brain using PMOD 3.0 software (PMOD Technologies) and SUVmax and SUVmean were calculated.

Statistical Analysis

All statistical analyses were performed using SPSS software (version 15.0; SPSS Inc., Chicago, IL, USA). Correlation analysis was performed using the Spearman rank test. Differences between three or more unmatched groups were analyzed using one-way analysis of variance (ANOVA). Differences between two paired groups were analyzed using a paired t-test. Differences between two unpaired groups were analyzed using an unpaired t-test. A P value < 0.05 was considered statistically significant.

RESULTS

CoCl₂ and DMOG Induce Functional HIF-1

HIF-1 α protein levels and mRNA expression levels of GLUT1, HK2, HIF-1 α and CA IX were determined after incubation of HT29 cells with 200 μ M CoCl₂ and 500 μ M DMOG for 5, 12 and 24h. Results are summarized in Figure 1 and 2. These results indicate that functional HIF-1 is induced through HIF-1 α protein stabilisation after treatment with CoCl₂ and DMOG resulting in increased transcription of GLUT1, HK2 and CA IX genes. As opposed to CoCl₂, DMOG does not increase HIF-1 α mRNA levels.

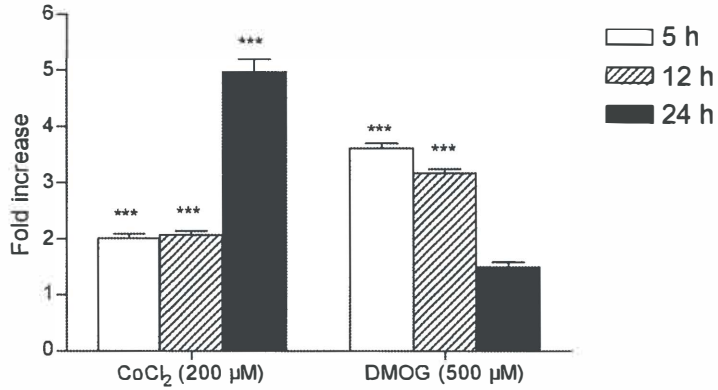


FIGURE 1. Protein expression levels of HIF-1 α in HT29-cells after treatment with 200 μ M CoCl₂ and 500 μ M DMOG for 5h (white bars), 12h (hatched bars) and 24h (black bars). Fold changes are shown as mean \pm SEM (n = 8) and are shown relative to control samples treated with vehicle (PBS) at each time point. *** p < 0.001

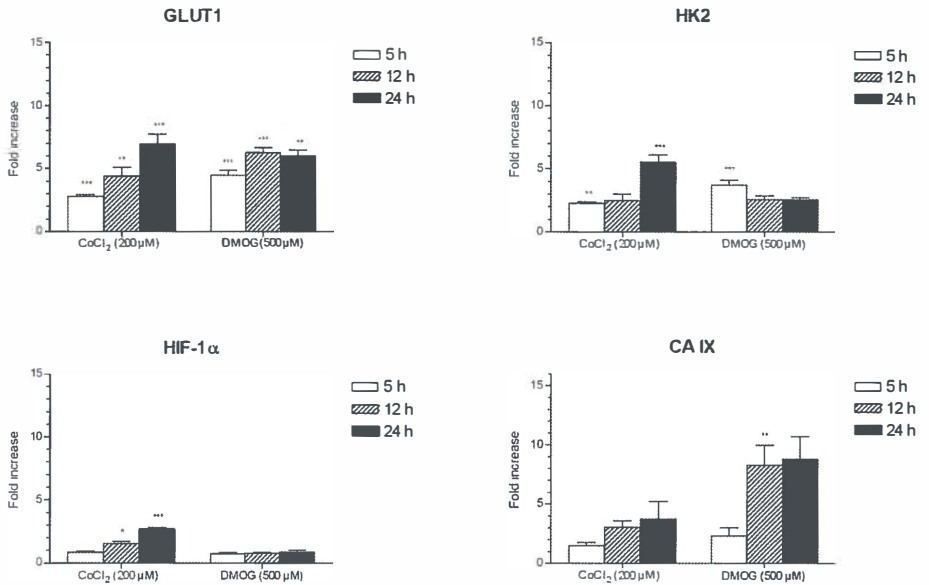


FIGURE 2. mRNA expression levels of GLUT1, HK2, HIF-1 α and CA IX genes in HT29-cells after treatment with 200 μ M CoCl₂ and 500 μ M DMOG for 5h (white bars), 12h (hatched bars) and 24h (black bars). Fold changes in transcription levels are determined by SYBR Green qPCR using the geometric mean of hHMBS and hSDHA as reference genes. Fold changes are shown as mean \pm SEM (n = 5) and are shown relative to control samples treated with vehicle (PBS) at each time point. * p < 0.05, ** p < 0.01, *** p < 0.001

Chemical Activation of HIF-1 Increases In Vitro [¹⁸F]FDG Uptake

[¹⁸F]FDG-uptake was determined after incubation of HT29 cells with 200 μ M CoCl₂ and 500 μ M DMOG for 5, 12 and 24h. Results are summarized in Figure 3. Treatment with 200 μ M CoCl₂ for 12h and 24h resulted in a significant increase in [¹⁸F]FDG-uptake ($p < 0.001$). Incubation for 5h had no effect. Treatment with 500 μ M DMOG for 5h, 12h and 24h resulted in a significant increase in [¹⁸F]FDG-uptake ($p < 0.001$). Treatment with 200 μ M CoCl₂ and 500 μ M DMOG for 5, 12 and 24h did not result in significant changes in protein concentration (data not shown).

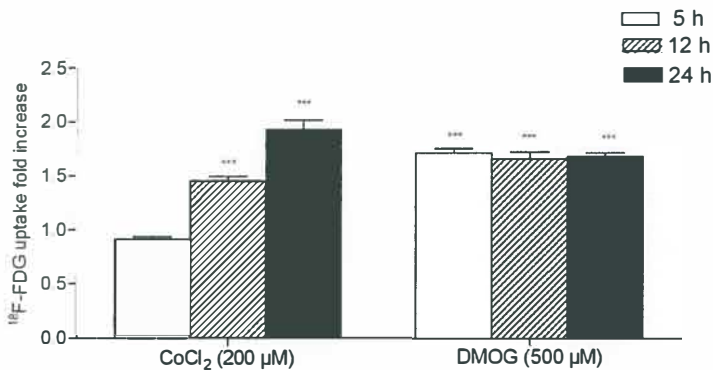


FIGURE 3. [¹⁸F]FDG-uptake in HT29-cells after treatment with 200 μ M CoCl₂ and 500 μ M DMOG for 5h (white bars), 12h (hatched bars) and 24h (black bars). Fold changes are shown as mean \pm SEM ($n = 9$) and are shown relative to control samples treated with vehicle (PBS) at each time point. *** $p < 0.001$

In Vivo Detection of Hypoxia in a HT29 Xenograft

We compared the distribution of the exogenous hypoxia marker pimonidazole with the expression of GLUT1, GLUT3, HK2, HIF-1 α and CA IX in a HT29 xenograft. A total number of 18 tumor specimens was investigated. Mean pimonidazole score was 1.9 ± 0.19 . Mean Hscore for GLUT1 expression was 7.3 ± 0.69 . Mean Hscore for GLUT3 expression was 8.6 ± 0.75 . Mean Hscore for CA IX expression was 6.3 ± 0.64 . Mean Hscore for HK2 expression was 1.6 ± 0.22 . Mean Hscore for HIF-1 α expression was 7.6 ± 0.82 . A low but significant correlation was found between pimonidazole staining and CA IX - Hscore ($R = 0.491$; $P = 0.038$). Further, a significant correlation was found between GLUT1 - Hscore and CA IX - Hscore ($R = 0.746$; $P = 0.001$). Expression of HK2 was cytoplasmic and low.

Expression of GLUT1, GLUT3 and CA IX was membranous. A uniform, low expression of GLUT3 in the entire tumor section was observed. HIF-1 α expression was cytoplasmic and more or less uniformly expressed throughout the entire tumor section with a number of hotspots. Pimonidazole staining and expression of CA IX were localized around areas of necrosis, although a more diffuse and patchy staining was observed in areas away from necrosis as well. GLUT1 expression was seen throughout the entire tumor section with the highest expression colocalizing with pimonidazole and CAIX. Overall, upon visual inspection we observed that although an absolute spatial colocalization was absent, pimonidazole staining and expression of GLUT1 and CA IX showed a strong overlap and a similar pattern (see Figure 4).

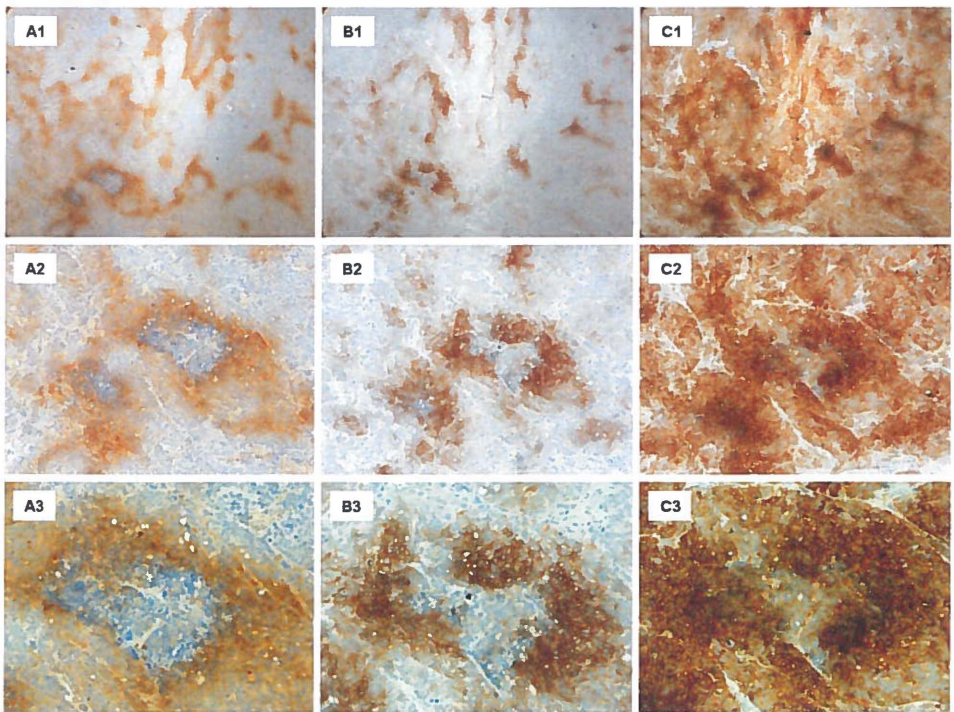


FIGURE 4. Immunohistochemical staining in HT29 xenograft: pimonidazole (A1 40x; A2 100x; A3 200x), CA IX (B1 40x; B2 100x; B3 200x), GLUT1 (C1 40x; C2 100x; C3 200x).

Chemical Activation of HIF-1 Increases In Vivo [^{18}F]FDG Uptake

Tumor [^{18}F]FDG-uptake was determined after treatment with 5 mg/kg hydralazine and 8 mg DMOG in a HT29 xenograft. Tumor pO₂-measurements were conducted in 3 animals after a

single dose of 5 mg/kg hydralazine hydrochloride to verify its mechanism of action. After insertion of the probe in the tumor, pO₂-values showed considerable variation. A steep drop in tumor pO₂-values was observed immediately after administration of a single dose of 5 mg/kg hydralazine (see Figure 5). In all three animals, tumor oxygenation levels were significantly lower after hydralazine treatment ($p < 0.001$). [¹⁸F]FDG-PET examinations were performed on 3 consecutive days (day 0, 1 and 2), using the first scan as a baseline scan before treatment. Results are summarized in Figure 6. Baseline tumor SUVmax and SUVmean (day 0) were not significantly different between the control and the treatment groups. No significant changes in tumor SUVmax and SUVmean were observed in the control group during the length of the experiment. Treatment with a single dose of hydralazine caused a minor decrease in tumor SUVmax and SUVmean. After treatment with a single dose of 8 mg/kg IP of DMOG, we observed an increase in tumor SUVmax and SUVmean which was statistically significant on day 1 ($p = 0.013$ and $p = 0.014$, respectively). Brain [¹⁸F]FDG-uptake was also determined. Baseline brain SUVmax and SUVmean (day 0) were not significantly different between the control and the treatment groups. No significant changes in brain SUVmax and SUVmean were observed in the control, DMOG and hydra 8h groups during the length of the experiment. A significant decrease in brain SUVmax was observed in the hydra 3h group ($p = 0.042$).

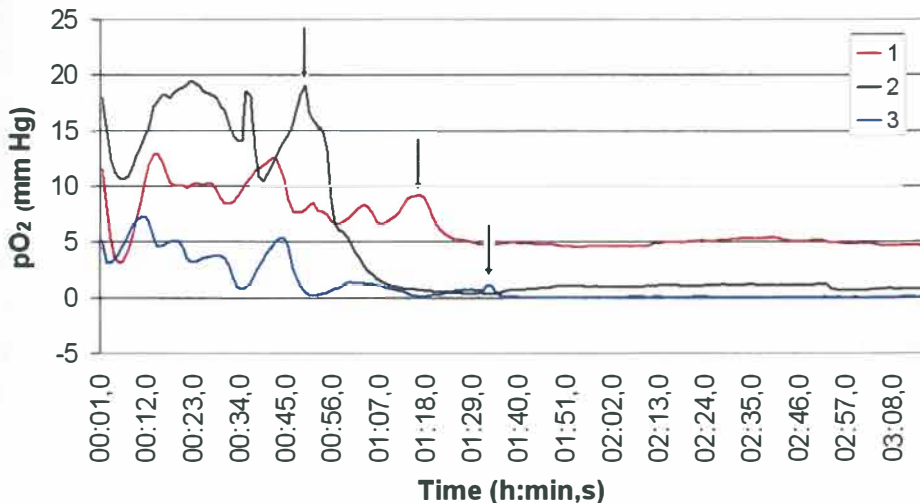


FIGURE 5. Tumor oxygenation values in three animals. Arrows indicate the moment when a single dose of 5mg/kg hydralazine ip was administered. In all three animals, tumor oxygenation levels were significantly lower after hydralazine treatment ($p < 0.001$). Mean

mmHg animal 1: pre-hydra: 8.78, post-hydra: 5.03; mean mmHg animal 2: pre-hydra: 15.57, post-hydra: 1.85; mean mmHg animal 3: pre-hydra: 2.37, post-hydra: 0.02.

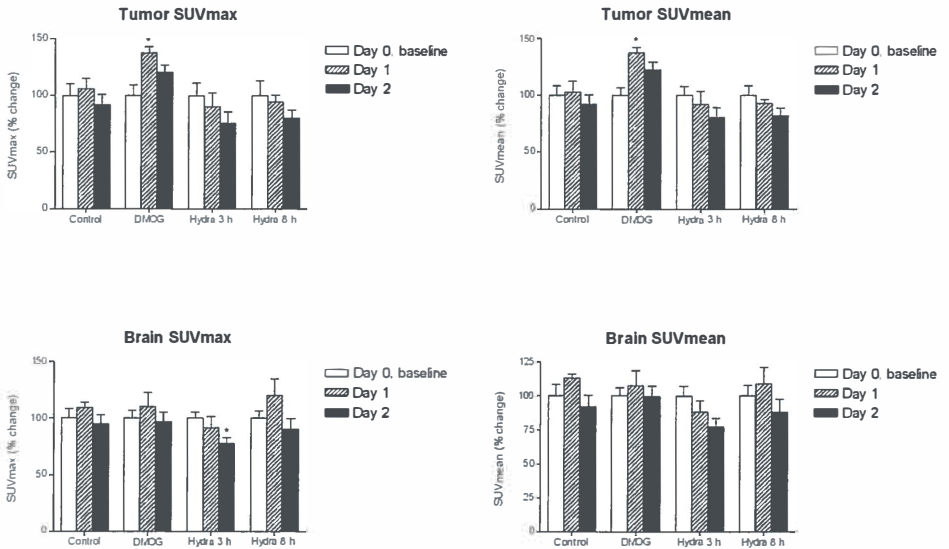


FIGURE 6. Tumor and brain SUVmax and SUVmean on day 0 (white bars), day 1 (hatched bars) and day 2 (black bars). Data are expressed as mean \pm SEM ($n = 5$) and as a percentage change compared to baseline scans. After treatment with a single dose of 8 mg/kg DMOG ip, we observed an increase in tumor SUVmax and SUVmean which was statistically significant on day 1 ($p = 0.013$ and $p = 0.014$ respectively). After treatment with a single dose of 5 mg/kg hydralazine ip 3h before [^{18}F]FDG administration, we observed an decrease in brain SUVmax which was significant on day 2 ($p = 0.042$). * $p < 0.05$

DISCUSSION

In this manuscript we studied the relationship between tumor hypoxia and [^{18}F]FDG-uptake and investigated whether this relationship could be exploited to improve [^{18}F]FDG-PET imaging. To do this, [^{18}F]FDG-uptake was determined after chemical induction of hypoxia and chemical activation of HIF-1 in an *in vitro* and *in vivo* model of a human colorectal carcinoma.

We first investigated whether chemical stabilization of HIF-1 α under normoxic conditions could increase [^{18}F]FDG-uptake *in vitro*. Treatment of HT29 cells with CoCl_2 and DMOG resulted in induction of HIF-1 through HIF-1 α protein stabilisation. This resulted in an

increased transcription of GLUT1, HK2 and CAIX genes. As opposed to CoCl₂, DMOG does not increase HIF-1 α mRNA levels, which is in line with its mechanism of action. Our results showed significant increases in [¹⁸F]FDG-uptake when HT29 colorectal carcinoma cells were treated with CoCl₂ and DMOG. CoCl₂ is a well known chemical inducer of hypoxia that has been successfully used in several studies. Its mechanism of action is not entirely clear and several hypotheses exist to explain its action (13-15). DMOG is a non-specific 2-oxoglutarate (OG) -dependent dioxygenase inhibitor. The 2-OG dioxygenase family includes PHD1-3 and factor inhibiting HIF-1 (FIH-1). Inhibition of these proteins results in stabilization of HIF-1 α and activation of HIF-1 (16). As confirmed in this study, both chemicals provide an easy platform to study the hypoxic response in an *in vitro* setting. Whereas CoCl₂-induced stimulation of [¹⁸F]FDG-uptake seems to increase as a function of time, the DMOG-induced stimulation appears to have an early set-on and remain constant throughout time. These results thus indicate a different mechanism of action of CoCl₂ and DMOG. Numerous *in vitro* studies in different types of cancer cell lines have reported an increase in [³H]FDG- or [¹⁸F]FDG-uptake after exposure to decreasing oxygen atmospheres (17-20). Some of these studies reported an increase in expression of GLUT1 and GLUT3 (17,19) while one study observed no changes in cellular levels of GLUT1, GLUT3, HK2, HIF1 α and attributed the increase in uptake to an increase in GLUT-activity (18). Studies reporting on glucose-uptake after a chemical induction of hypoxia are limited. Two studies in Clone 9 rat liver cells reported on an increase in 3-O-methyl D-glucose transport after treatment for 24h with 250 μ M CoCl₂ which was associated with an increase in GLUT1 mRNA and protein content (21,22). Similar results were obtained in BeWo choriocarcinoma cells and articular chondrocytes (23,24).

In a next step, we compared the distribution of endogenous and exogenous hypoxic markers in the tumors of non-treated HT29 xenografts. After injection, the exogenous hypoxia marker pimonidazole is reduced under hypoxic conditions and the resulting adducts are irreversibly bound to thiol-containing proteins in viable hypoxic cells ($pO_2 < 10$ mm Hg) (25). Pimonidazole staining and expression of CA IX were localized in perinecrotic areas and a more diffuse and patchy staining pattern was observed in areas away from necrosis as well. Both showed a strong colocalization and a weak, but significant correlation was found between pimonidazole staining and CA IX-Hscore, confirming the role of CA IX as one of the most reliable endogenous markers of tumor hypoxia. Given the timeframe of CAIX expression (26), this would confirm that CAIX as well as pimonidazole mainly demonstrate

chronic hypoxia. Two other studies previously reported a similar spatial distribution between pimonidazole staining and CA IX expression in a HT29 xenograft (27,28). GLUT1 was expressed throughout the entire tumor section with highest expression colocalizing with pimonidazole and CAIX. Although GLUT1 is also believed to be mainly a marker of chronic hypoxia (29), its expression might occur at higher oxygen levels than CA IX expression and pimonidazole reduction. HIF-1 α was more or less uniformly expressed throughout the whole tumour section with a number of hotspots independent of areas of necrosis. Taken together, these results confirm hypoxic activation of HIF-1 downstream proteins in our *in vivo* model.

To test whether or not artificial hypoxia or chemical activation of HIF-1 could induce an increase in [^{18}F]FDG-uptake in an *in vivo* situation, HT29 xenografts were treated with DMOG and hydralazine hydrochloride. Several studies reported that hydralazine causes tumor hypoxia through a process of preferential arterial vasodilation in normal versus tumor tissue concomitant with a reduction in blood pressure ('steal phenomenon') (10,30-32). In this study as well, a significant decrease in tumor pO $_2$ -values was observed in the HT29 xenograft after administration of a single dose of 5 mg/kg hydralazine. After treatment with a single dose of hydralazine we observed a minor decrease in tumor [^{18}F]FDG-uptake. Although one can hypothesize that this is the consequence of the decreased tumor perfusion that characterizes its mode of action, other studies do not indicate an effect on tracer delivery and subsequent binding as soon as thirty minutes after hydralazine treatment (30-32). These studies successfully used hydralazine to confirm the pO $_2$ dependence of several hypoxia-selective PET imaging agents. Possibly, the relative lack of selectivity that characterizes [^{18}F]FDG as compared to more selective tracers used in these studies, taken together with the peripheral vasodilatation after hydralazine treatment, may explain the results.

As opposed to hydralazine, DMOG has no direct effects on tumor oxygenation but directly stabilizes HIF-1 α through PHD inhibition. Systemic administration of DMOG has been described previously (33-35). After treatment with a single dose of DMOG we observed a significant increase in tumor [^{18}F]FDG-uptake. We hypothesize that this increase is the consequence of tumoral HIF-1 activation with an associated transcription of metabolic genes resulting in an increase in glucose/[^{18}F]FDG uptake. As proposed by Cummins et al., DMOG may be primarily active at the sites of acute insults. Indeed, they showed that systemic administration of DMOG did not alter basal myeloperoxidase activity and cytokine levels in normal colon tissue, but counteracted inflammation in colon subjected to inflammatory insults (33). Another study observed similar effects when systemic administration of DMOG induced

increased expression of HIF-1 α and downstream VEGF in muscle that was subjected to ischemic insult, but not in normal muscle (34). If this would be the case, tumor specific activation of HIF-1 can indeed be achieved with associated increase in glucose transport. We hereby propose a role for PHD-inhibitors as a potential tool to increase tumor [^{18}F]FDG-uptake in order to enhance sensitivity using [^{18}F]FDG-PET. Indeed, although [^{18}F]FDG-PET imaging is successful in detecting most types of cancer, there are a number of situations where [^{18}F]FDG-PET imaging is less successful due to low [^{18}F]FDG-avidity (e.g. hepatocellular carcinoma and prostate cancer) or a low or decreased tumor-to-background ratio (e.g. brain tumors due to high physiological glucose uptake in normal brain, bladder and prostate tumors due to [^{18}F]FDG excretion through the urinary system) (3,4). In these cases [^{18}F]FDG-PET imaging after a single treatment with PHD-inhibitors might possibly increase sensitivity. Whereas systemic use of DMOG in experimental animals to explore its effect in models of ischemic heart, renal and muscle disease and inflammatory bowel disease indicated no adverse effects (9,32-35), systemic use of DMOG in humans has not been reported. However, other prolyl hydroxylase domain-containing protein inhibitors are currently under development for the treatment of anaemic and ischemic conditions in humans (36,37). Although some of these compounds are currently undergoing phase I and phase II clinical trials, their oncological use has not been explored and deleterious effects on tumor progression thus need to be investigated as it is generally known that hypoxia impairs the effectiveness of therapy and negatively affects prognosis (38). Further studies thus will indicate whether the benefit of an increased detection is worth the transient activation of HIF-1.

CONCLUSION

We observed significant increases in [^{18}F]FDG-uptake following chemical activation of HIF-1 in an *in vitro* and *in vivo* model of a human colorectal carcinoma. In cases where [^{18}F]FDG-PET imaging is less successful, imaging after pharmacological HIF-1 activation might possibly increase sensitivity and provide a means to improve imaging.

REFERENCES

1. Smith TAD. The rate-limiting step for tumor [¹⁸F]fluor-2-deoxy-D-glucose (FDG) incorporation. *Nucl Med Biol.* 2001;28:1-4.
2. Ong LC, Jin Y, Song IC, et al. 2-[¹⁸F]-2-deoxy-D-glucose (FDG) uptake in human tumor cells is related to the expression of GLUT-1 and hexokinase II. *Acta Radiol.* 2008;49:1145-1153.
3. Kelloff GJ, Krohn KA, Larson SM, et al. The progress and promise of molecular imaging probes in oncologic drug development. *Clin Cancer Res.* 2005;11:7967-7985.
4. Endo K, Oriuchi N, Higuchi T, et al. PET and PET/CT using 18F-FDG in the diagnosis and management of cancer patients. *Int J Clin Onc.* 2006;11:286-296.
5. Warburg O. On the origin of cancer cells. *Science.* 1956;123:309-314.
6. Semenza GL. HIF-1: Mediator of physiological and pathophysiological responses to hypoxia. *J Appl Physiol.* 2000;88:1474-1480.
7. Vaupel P. The role of hypoxia-induced factors in tumor progression. *Oncologist.* 2004;9:10-17.
8. Kim JW, Gao P, Dang CV. Effects of hypoxia on tumor metabolism. *Cancer Metastasis Rev.* 2007;26:291-298.
9. Ockaili R, Natarajan R, Salloum F, et al. HIF-1 activation attenuates postischemic myocardial injury: role for heme oxygenase-1 in modulating microvascular chemokine generation. *Am J Physiol Heart Circ Physiol.* 2005;289:H542-H548.
10. Fisker RV, Horsman MR, Overgaard J. Hydralazine-induced changes in tissue perfusion and radiation response in a C3H mammary carcinoma and mouse normal tissues. *Acta Oncol.* 1991;30:641-647.
11. Raleigh JA, Chou SC, Bono EL, et al. Semiquantitative immunohistochemical analysis for hypoxia in human tumors. *Int J Rad Oncol Biol Phys.* 2001;49:569-574.
12. Brurberg KG, Graff BA, Rofstad EK. Temporal heterogeneity in oxygen tension in human melanoma xenografts. *Br J Cancer.* 2003;89:350-356.
13. Yuan Y, Hilliard G, Ferguson T, et al. Cobalt inhibits the interaction between hypoxia-inducible factor- α and von Hippel-Lindau protein by direct binding to hypoxia-inducible factor- α . *J Biol Chem.* 2003;278:15911-15916.
14. Hirsilä M, Koivunen P, Xu L, et al. Effect of desferrioxamine and metals on hydroxylases in the oxygen sensing pathway. *FASEB J.* 2005;19:1308-1310.
15. Torii S, Kurihara A, Li XY, et al. Inhibitory effect of extracellular histidine on cobalt-induced HIF-1 α expression. *J Biochem.* 2011;149:171-176.

16. Asikainen TM, Ahmad A, Schneider BK, et al. Stimulation of HIF-1alpha, HIF-2alpha, and VEGF by prolyl 4-hydroxylase inhibition in human lung endothelial and epithelial cells. *Free Radic Biol Med.* 2005;38:1002-1013.
17. Clavo AC, Brown RS, Wahl RL. Fluorodeoxyglucose uptake in human cancer cell lines is increased by hypoxia. *J Nucl Med.* 1995;36:1625-1632.
18. Burgman P, O'Donoghue JA, Humm JL, et al. Hypoxia-induced increase in FDG uptake in MCF7 cells. *J Nucl Med.* 2001;42:170-175.
19. Pedersen MWB, Holm S, Lund EL, et al. Coregulation of glucose uptake and vascular endothelial growth factor (VEGF) in two small-cell lung cancer (SCLC) sublines in vivo and in vitro. *Neoplasia.* 2001;3:80-87.
20. Oswald J, Treite F, Haase C, et al. Experimental hypoxia is a potent stimulus for radiotracer uptake in vitro: comparison of different tumor cells and primary endothelial cells. *Cancer Lett.* 2007;254:102-110.
21. Behrooz A, Ismail-Beigi F. Dual control of glut1 glucose transporter gene expression by hypoxia and by inhibition of oxidative phosphorylation. *J Biol Chem.* 1997;272:5555-5562.
22. Hwang DY, Ismail-Beigi F. Glucose uptake and lactate production in cells exposed to CoCl_2 and in cells overexpressing the glut-1 glucose transporter. *Arch Biochem Biophys.* 2002;399:206-211.
23. Baumann MU, Zamudio S, Illsley NP. Hypoxic upregulation of glucose transporters in BeWo choriocarcinoma cells is mediated by hypoxia-inducible factor-1. *Am J Physiol Cell Physiol.* 2007;293:C477-C485.
24. Peansukmanee S, Vaughan-Thomas A, Carter SD, et al. Effects of hypoxia on glucose transport in primary equine chondrocytes in vitro and evidence of reduced GLUT1 gene expression in pathologic cartilage in vivo. *J Orthopaedic Res.* 2008;27:529-535.
25. Gross MW, Karbach U, Groebe K, et al. Calibration of misonidazole labeling by simultaneous measurement of oxygen tension and labeling density in multicellular spheroids. *Int J Cancer.* 1995;61:567-573.
26. Vordermark D, Kaffer A, Riedl S, et al. Characterization of carbonic anhydrase IX (CA IX) as an endogenous marker of chronic hypoxia in live human tumor cells. *Int J Radiation Oncology Biol Phys.* 2005;61:1197-1207.
27. Shin KH, Diaz-Gonzalez JA, Russel J, et al. Detecting changes in tumor hypoxia with carbonic anhydrase and pimonidazole. *Cancer Biol Ther.* 2007;6:70-75.

28. Russel J, Carlin S, Burke SA, et al. Immunohistochemical detection of changes in tumor hypoxia. *Int J Radiat Oncol Biol Phys*. 2009;73:1177-1186.
29. Rafajova M, Zatovicova M, Kettman R, et al. Induction by hypoxia combined with low glucose or low bicarbonate and high posttranslational stability upon reoxygenation contribute to carbonic anhydrase IX expression in cancer cells. *Int J Oncol*. 2004;24:995-1004.
30. Lewis JS, Sharp TL, Laforest R, et al. Tumor uptake of copper-diacetyl-bis (N⁴-methylthiosemicarbazone): effect of changes in tissue oxygenation. *J Nucl Med*. 2001;42:655-661.
31. Kinuya S, Yokoyama K, Li XF, et al. Hypoxia-induced alteration of tracer accumulation in cultured cancer cells and xenografts in mice: implications for pre-therapeutic prediction of treatment outcomes with ^{99m}Tc-sestamibi, ²⁰¹Tl chloride and ^{99m}Tc-HL91. *Eur J Nucl Med*. 2002;29:1006-1011.
32. Lee BF, Chiu NT, Hsia CC, et al. Accumulation of Tc-99m HL91 in tumor hypoxia: in vitro cell culture and in vivo tumor model. *Kaohsiung J Med Sci*. 2008;24:461-471.
33. Cummins EP, Seeballuck F, Keely SJ, et al. The hydroxylase inhibitor dimethyloxalyglycine is protective in a murine model of colitis. *Gastroenterology*. 2008;134:156-165.
34. Milkiewicz M, Pugh CW, Egginton S. Inhibition of endogenous HIF inactivation induces angiogenesis in ischaemic skeletal muscles of mice. *J Physiol*. 2004;560:21-26.
35. Hill P, Shukla D, Tran MG, et al. Inhibition of hypoxia inducible factor hydroxylases protects against renal ischemia-reperfusion injury. *J Am Soc Nephrol*. 2008;19:39-46.
36. Yan L, Colandrea VJ, Hale JJ. Prolyl hydroxylase domain-containing protein inhibitors as stabilizers of hypoxia-inducible factor: small molecule-based therapeutics for anemia. *Expert Opin Ther Pat*. 2010;20:1219-1245.
37. Bernhardt WM, Wiesener MS, Scigalla P. Inhibition of prolyl hydroxylases increases erythropoietin production in ESRD. *J Am Soc Nephrol*. 2010;21:2151-2156.
38. Höckel M, Vaupel P. Tumor hypoxia: definitions and current clinical, biologic, and molecular aspects. *J Natl Cancer Inst*. 2001;93:266-276.

2.3 Research article: Metabolic correlates of tumour hypoxia in malignant canine mammary carcinoma.

Res Vet Sci. 2011;91:e125-128.

Metabolic correlates of tumour hypoxia in malignant canine mammary carcinoma.

Mees G ¹, Vangestel C ², Dierckx R ^{1,7}, Loomans S ³, Van Damme N ², Peremans K ⁴, De Rooster H ⁵, Van Goethem B ⁵, Pauwels P ⁶, Ducatelle R ³, Van de Wiele C ^{1,7}

- ¹ Department of Nuclear Medicine and Molecular Imaging, University Medical Center Groningen, University of Groningen, The Netherlands
- ² Department of Gastroenterology, Ghent University Hospital, Belgium
- ³ Department of Pathology, Faculty of Veterinary Medicine, Ghent, Belgium
- ⁴ Department of Medical Imaging, Faculty of Veterinary Medicine, Ghent, Belgium
- ⁵ Department of Small Animal Medicine and Clinical Biology, Faculty of Veterinary Medicine, Ghent, Belgium
- ⁶ Department of Pathology, Ghent University Hospital, Belgium
- ⁷ Department of Nuclear Medicine, Ghent University Hospital, Belgium

ABSTRACT

Given its importance in human and canine tumour biology, a profound understanding of tumour hypoxia is of paramount importance. Therefore, the aim of this work was to investigate the relationship between tumour hypoxia and the expression of a number of hypoxia-induced proteins that play a role in tumour metabolism. The hypoxia marker pimonidazole was administered to dogs affected by spontaneous mammary carcinoma and compared with immunohistochemical staining for GLUT1 and 3, HK 2 and CA IX. A statistically significant correlation was found between pimonidazole staining and GLUT1-expression ($R = 0.607$; $p = 0.001$). These results indicate a strong interaction between tumour hypoxia and tumour metabolism by the induction of proteins essential to maintain a stable tumour microenvironment.

Keywords: tumour hypoxia, pimonidazole, GLUT

The occurrence of heterogeneously distributed hypoxic and/or anoxic areas is a characteristic feature of locally advanced solid tumours and has been described in a wide range of human as well as canine malignancies (1). These areas of acute and chronic hypoxia are the result of an abnormal structure and function of the tumoural microvessels, increased diffusion distances between the nutritive blood vessels and the tumour cells, and disease- or treatment- related anaemia. Recent studies have demonstrated a clear relationship between this hypoxic microenvironment and tumour-associated metabolic alterations. In this respect, tumour hypoxia has been associated with an aggressive tumour phenotype, poor response to therapy, and worse prognosis in a wide range of human malignancies (2-4). Cancer cells adapt to hypoxic conditions by the induction of target genes involved in glucose metabolism, angiogenesis, erythropoiesis and apoptosis in an effort to overcome their compromised condition. Many of these adaptations are coordinated by the transcription factor hypoxia-inducible factor (HIF) - 1, which has been verified as a master regulator of oxygen homeostasis under hypoxic conditions (5). To compensate for the hypoxia-induced drop in mitochondrially produced ATP, cells will increase their glycolytic ATP-production (Pasteur effect) which is inherently inefficient when compared to aerobic degradation of glucose (Krebs cycle), leading to an increase in glucose transport and consumption. This is further enhanced by aerobic glycolysis (Warburg effect) (6). Several approaches, non-invasive and invasive, exist for the detection of tumour hypoxia (4). Numerous studies have investigated tumour hypoxia in a prospective and retrospective manner by studying the expression and localisation of endogenous and exogenous markers of hypoxia. Several different candidates have emerged as possible endogenous markers of hypoxia of which the most important are HIF-1 α , carbonic anhydrase IX (CA IX), glucose transporter (GLUT) 1 and 3. None of these have however, proven their selectivity for hypoxia as their expression is believed to be influenced by other parameters than merely hypoxia (7). The most relevant marker for qualitative and quantitative determination of tumour hypoxia in experimental and clinical circumstances is the exogenous hypoxia marker pimonidazole. This 2-nitroimidazole reagent is reduced under hypoxic conditions and the resulting adducts are irreversibly bound to thiol-containing proteins in viable hypoxic cells ($pO_2 < 10$ mm Hg) (8). Pimonidazole is a robust marker of hypoxia and its microregional distribution correlates with oxygen concentration at the cellular level (9,10). The objective of this study was to investigate the relationship between tumour hypoxia and the expression of a number of hypoxia-induced proteins that play a role in tumour metabolism in a spontaneous canine mammary carcinoma.

Privately owned dogs with a spontaneous mammary carcinoma and no other concurrent disease were eligible for the study at the Faculty of Veterinary Medicine, Ghent University. All dog owners signed an informed consent form and all procedures were approved by the local ethical committee. This spontaneous canine model was chosen because of its high incidence, easy resection and the common occurrence of multiple tumours. Pimonidazole hydrochloride (HCl) powder (HypoxyprobeTM-1, Chemicon International) was dissolved in 0.9% NaCl, filtered (0.2 µm) and given intravenously (i.v.) at a dosage of 0.28 g/m² as previously described (11). To decrease the amount of product needed in this study a weight limit for the dogs was set at 20kg. Tumours were resected 14 hours later (plasma half life of HypoxyprobeTM-1 in dogs is approximately 90 minutes). This timing was chosen for practical considerations to allow an overnight stay of the animals in the clinic after injection of pimonidazole HCl. This timing however, does not exceed the turnover rate of hypoxic cells, nor the stability of pimonidazole adducts in the tissue of interest (11,12). After resection of the tumours, the specimens were formalin fixed and paraffin embedded. Immunohistochemical staining of tissue sections was performed as previously described (13) with the appropriate primary and secondary antibodies (Table 1).

Antibody	Company	Dilution	Pos. Control Tissue	Isotype control	Secondary Reagent	Tertiary Reagent
Hypoxyprobe-1 Mab1	Chemicon International	1/50	tumour	Mouse IgG ₁ (Dako)	Biotin-conjugated F(ab) ₂ (Dako)	LSAB [®] 2 Streptavidin-HRP (Dako)
GLUT1	ABCAM, ab15309	1/200	brain (vascular)	Rabbit IgG (Dako)	Envision+ System-HRP (Dako)	/
GLUT3	ABCAM, ab15311	1/50	brain (neuronal)	Rabbit IgG (Dako)	Envision+ System-HRP (Dako)	/
HK2	Santa-Cruz, sc-28889	1/100	smooth muscle	Rabbit IgG (Dako)	Vectastain ABC system (Vector Labs)	/
CAIX	ABCAM, ab15096	1/100	tumour	Rabbit IgG (Dako)	Vectastain ABC system (Vector Labs)	/

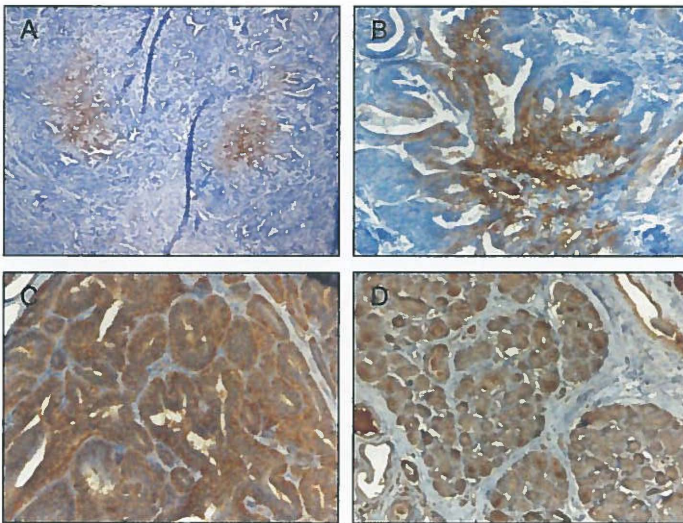
TABLE 1. The used primary and secondary antibodies with their corresponding dilution factors (primary antibody diluted in 1x PBS with 1% BSA). (Hypoxyprobe-1 Mab1: monoclonal antibody against pimonidazole, GLUT1: glucose transporter 1, GLUT3: glucose transporter 3, HK2 : hexokinase 2, CA IX : Carbonic anhydrase 9)

The intensity and percentage of positive tumour cells in the immuno-reaction were scored independently by two experienced observers. The percentage of tumour cells that were positive was scored as follows: 0% (score 0), 0-20% (score 1), 20-40% (score 2), 40-60% (score 3), 60-80% (score 4) and 80-100% (score 5). Intensities of staining were categorized as absent (score 0), faint (score 1), moderate (score 2) or strong (score 3). An estimation of intensity and percentage of positive tumour cells was made after counting ten high-powerfields. A final histological score (Hscore) was calculated as following: $Hscore = [(a1 \times i1) + (a2 \times i2)] / 2$, where i = the score of intensity, a = the score of amount tumour cells that stained positive and 1 and 2 refer to the scores of the two observers. A previously described semiquantitative scoring system was used to score pimonidazole staining: absent (score 0), >

0 to 5% (score 1), > 5 to 15% (score 2), > 15 to 30% (score 3), >30% (score 4) (14). SPSS for Windows, version 15.0 was used for statistical analysis. Data are expressed as mean \pm SEM (standard error of the mean). Correlation analysis was performed using the Spearman rank correlation test. Differences between two groups of paired data were analyzed using the Wilcoxon test. A p value < 0.05 was considered significant.

Ten female animals, weighing 3.5 kg to 13 kg participated in the study. All these animals had multiple tumour nodules. After unilateral mastectomy was performed, 36 mammary gland tumour specimens were harvested. After reviewing the specimens by a trained veterinary pathologist, 11 benign tumours (9 mammary adenomas, 1 lipoma and 1 leiomyoma) and 25 malignant tumours (11 mammary adenocarcinomas grade I, 1 mammary adenocarcinoma grade II and 13 mammary complex carcinomas grade I) were identified. Only the malignant tumours were included in this study.

Overall pimonidazole staining was modest and patchy (Fig. 1 - A) and mean score was 0.5 ± 0.15 . Immunostaining of GLUT1, GLUT3 and CA IX was membranous (Fig. 1 - B,C,E). Mean Hscore for GLUT1 expression was 1.5 ± 0.41 . Mean Hscore for GLUT3 expression was 6.1 ± 0.56 . Mean Hscore for CA IX expression was 8.4 ± 0.75 . Immunostaining of HK2 was cytoplasmic (Fig. 1 - D) and mean Hscore was 8.2 ± 0.40 . A significant correlation was found between pimonidazole staining and GLUT1-expression ($R = 0.607$; $p = 0.001$).



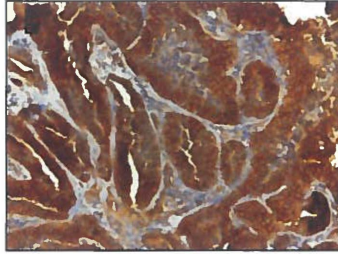


FIGURE 1. Immunohistochemical staining in canine specimens: pimonidazole (A, 100x), GLUT1 (B, 200x), GLUT3 (C, 200x), HK2 (D, 200x), CA IX (E, 200x).

Pimonidazole is widely accepted as a reliable marker of hypoxia and has been successfully used in several types of cancer (9,10). It provides hypoxia measurements with a high spatial resolution and as reduction only takes place in viable cells with functional nitro-reductase enzymes, dead cells do not generate a signal. After it has been reduced and bound in tumour tissue, loss of the marker mainly occurs through cell loss (12). It shows a steep increase in the amount of reduction below a pO_2 of 10 mmHg (8). This was confirmed in a study by Raleigh et al. in which pimonidazole binding was compared with micro-electrode pO_2 measurements (15). Other studies that compared pimonidazole binding with invasive oxygen measurements have given inconsistent results (16-18). Necrosis is thought to be the main confounding factor. To our knowledge, only two studies have previously investigated tumour hypoxia in canine tumours using pimonidazole. Azuma et al. quantified the longevity of pimonidazole adducts as an estimate of the lifetime of hypoxic cells and Kleiter et al. investigated the oral administration of pimonidazole as a means of minimizing invasiveness (11,19). Both studies illustrated the feasibility to demonstrate tumour hypoxia in spontaneous canine tumours using pimonidazole. In this study, a significant correlation was found between pimonidazole staining and GLUT1-expression ($p = 0.001$, Spearman rank). A similar correlation has been described previously in two studies that found a strong spatial colocalization and correlation between GLUT1-expression and pimonidazole staining, respectively in human bladder and cervical cancer (20,21). Contrary to these findings, studies trying to show a relationship between GLUT1-expression and invasive oxygen measurements have failed to demonstrate a strong correlation (22-24). Again, necrosis is thought to be a main confounding factor together with the influence of other microenvironmental parameters than merely hypoxia. While a significant correlation was found only between pimonidazole staining and GLUT1-expression, the histological scores of GLUT3 proved higher than those of GLUT1 ($p = 0.001$, Wilcoxon) indicating a possible higher impact of GLUT3 on tumour glucose metabolism

when compared to GLUT1 in this tumour type. Overexpression of GLUT3 has been reported in a variety of human cancers (25), confirming its importance for tumour metabolism.

To conclude, we found a significant correlation between pimonidazole staining and GLUT1-expression in a spontaneous canine mammary carcinoma. This indicates a strong interplay between tumour hypoxia and tumour metabolism by the hypoxia-driven induction of proteins essential to maintain a stable tumour microenvironment.

REFERENCES

1. Snyder SA, Dewhirst MW, Hauck ML. The role of hypoxia in canine cancer. *Vet Comp Oncol.* 2008;6:213-223.
2. Höckel M, Vaupel P. Tumor hypoxia: definitions and current clinical, biologic, and molecular aspects. *J Natl Cancer Inst.* 2001;93:266-276.
3. Vaupel P, Harrison L. Tumor hypoxia: causative factors, compensatory mechanisms, and cellular response. *Oncologist* 2004;9:4-9.
4. Vaupel P, Mayer A. Hypoxia in cancer: significance and impact on clinical outcome. *Cancer Metastasis Rev.* 2007;26:225-239.
5. Semenza GL. HIF-1: Mediator of physiological and pathophysiological responses to hypoxia. *J Appl Physiol.* 2000;88:1474-1480.
6. Warburg O. On the origin of cancer cells. *Science.* 1956;123:309-314.
7. Bussink J, Kaanders JHAM, van der Kogel AJ. Tumor hypoxia at the micro-regional level: clinical relevance and predictive value of exogenous and endogenous hypoxic cell markers. *Radiother Oncol.* 2003;67:3-15.
8. Gross MW, Karbach U, Groebe K, et al. Calibration of misonidazole labeling by simultaneous measurement of oxygen tension and labeling density in multicellular spheroids. *Int J Cancer.* 1995;61:567-573.
9. Raleigh JA, Calkins-Adams DP, Rinker LH, et al. Hypoxia and vascular endothelial growth factor expression in human squamous cell carcinomas using pimonidazole as a hypoxia marker. *Cancer Res.* 1998;58:3765-3768.
10. Ljungkvist ASE, Bussink J, Kaanders JHAM, et al. Dynamics of tumor hypoxia measured with bioreductive hypoxic cell markers. *Radiat Res.* 2007;167:127-145.

11. Azuma C, Raleigh JA, Thrall DE. Longevity of pimonidazole adducts in spontaneous canine tumors as an estimate of hypoxic cell lifetime. *Radiat Res.* 1997;148:35-42.
12. Ljuncqvist ASE, Bussink J, Kaanders JHAM, et al. Hypoxic cell turnover in different solid tumor lines. *Int J Radiat Oncol Biol Phys.* 2005;62:1157-1168.
13. Mees G, Vangestel C, Dierckx R, et al. Carbonic anhydrase IX expression correlates with FDG uptake by primary non-small cell lung cancer. *Cancer Biother Radiopharm.* 2010;25:149-154.
14. Raleigh JA, Chou SC, Bono EL, et al. Semiquantitative immunohistochemical analysis for hypoxia in human tumors. *Int J Radiat Oncol.* 2001;49:569-574.
15. Raleigh RA, Chou SC, Arteel GE, et al. Comparisons among pimonidazole binding, oxygen electrode measurements and radiation response in C3H mouse tumors. *Radiat Res.* 1999;151:580-589.
16. Bussink J, Kaanders JHAM, Strik AM, et al. Optical sensor-based oxygen tension measurements correspond with hypoxia marker binding in three human tumor xenograft lines. *Radiat Res.* 2000;154:547-555.
17. Olive PL, Banath JP, Aquino-Parsons C. Measuring hypoxia in solid tumours. Is there a gold standard? *Acta Oncol.* 2001;40:917-923.
18. Nordmark M, Loncaster J, Aquino-Parsons C, et al. Measurements of hypoxia using pimonidazole and polarographic oxygen-sensitive electrodes in human cervix carcinomas. *Radiother Oncol.* 2003;67:35-44.
19. Kleiter MM, Thrall DE, Malarkey DE, et al. A comparison of oral and intravenous pimonidazole in canine tumors using intravenous CCI-103F as a control hypoxia marker. *Int J Radiat Oncol.* 2006;64:592-602.
20. Airley RE, Loncaster J, Raleigh JA, et al. GLUT-1 and CAIX as intrinsic markers of hypoxia in carcinoma of the cervix: relationship to pimonidazole binding. *Int J Cancer.* 2003;104:85-91.
21. Hoskin PJ, Sibtain A, Daley FM, et al. GLUT1 and CAIX as intrinsic markers of hypoxia in bladder cancer: relationship with vascularity and proliferation as predictors of outcome of ARCON. *Br J Cancer.* 2003;89:1290-1297.
22. Airley R, Loncaster J, Davidson S, et al. Glucose transporter Glut-1 expression correlates with tumor hypoxia and predicts metastasis-free survival in advanced carcinoma of the cervix. *Clin Cancer Res.* 2001;7:928-934.

23. Mayer A, Hockel M, Wree A, et al. Microregional expression of glucose transporter-1 and oxygenation status: lack of correlation in locally advanced cervical cancers. *Clin Cancer Res.* 2005;11:2768–2773.
24. Sakata KI, Someya M, Nagakura H, et al. A clinical study of hypoxia using endogenous hypoxic markers and polarographic oxygen electrodes. *Strahlenther Onkol.* 2006;182:511–517.
25. Macheda ML, Rogers S, Best JD. Molecular and cellular regulation of glucose transporter (GLUT) proteins in cancer. *J Cell Physiol.* 2005;202:654–662.

2.4 Research article: CA-IX expression correlates with FDG-uptake by primary NSCLC.

Cancer Biother Radiopharm. 2010;25:149-154.

CA-IX expression correlates with FDG-uptake by primary NSCLC.

Gilles Mees ¹, Christel Vangestel ², Rudi Dierckx ^{1,5}, Patrick Pauwels ³, Jan Van Meerbeeck ⁴, Christophe Van de Wiele ^{1,5}

¹ Department of Nuclear Medicine and Molecular Imaging, University Medical Center Groningen, University of Groningen, The Netherlands

² Department of Gastroenterology, University Hospital Ghent, Belgium

³ Department of Pathology, University Hospital Ghent, Belgium

⁴ Department of Respiratory Medicine, University Hospital Ghent, Belgium

⁵ Departments of Nuclear Medicine, Experimental Cancerology and Radiotherapy, University Hospital Ghent, Belgium

ABSTRACT

Tumour cells are characterized by an increased rate of glucose consumption and glycolysis. This increased glucose consumption leads to tumour acidification, which represents a major obstacle for several therapeutic strategies. Tumour cells have adapted to this acidification by upregulation of several H⁺-extruding transporter systems and proteins to cope with this compromised situation. One of these proteins is carbonic anhydrase IX which catalyzes the reversible hydration of carbon dioxide to carbonic acid outside the cell, leading to an acidic extracellular pH and an physiological intracellular pH. The aim of this paper was to study semiquantitatively the expression of carbonic anhydrase IX in non-small cell lung cancer and to assess the existence of a possible relationship between carbonic anhydrase IX expression and tumour FDG-uptake, reflecting glucose metabolism. The levels and the extent of carbonic anhydrase IX expression were estimated in immunohistochemical stained formalin fixed, paraffin embedded tissue samples from 18 patients with non-small cell lung cancer and compared with FDG-uptake in FDG-PET imaging. We found a statistically significant correlation between carbonic anhydrase IX Hscores and SUV_{max} and SUV_{mean} values of the primary tumour. This relationship found provides indirect evidence for co-transcription of glucose transporters and hexokinases that drive tumour hyperglycolysis, and carbonic

anhydrase IX governed by HIF-1 and suggests that in the future it may be possible to identify non-small cell lung cancer patients that are most likely to benefit from carbonic anhydrase IX targeting therapy on the basis of FDG-PET imaging.

Keywords: CA IX, NSCLC, FDG-PET, pH

INTRODUCTION

As first described by Warburg more than 50 years ago, tumour cells utilize more glucose than normal cells and maintain a high glycolytic rate, even in conditions of adequate oxygen supply (aerobic glycolysis) (1). A major consequence of the Warburg effect and the accompanying aerobic glycolysis is tumour acidification because of the accumulation of lactic acid (2,3). Importantly, tumour acidification is associated with the acquisition of a metastatic phenotype and chemoresistance to weakly basic anticancer drugs such as vinca-alkaloids and anthracyclines (4). While the acidification process results in a drop of pH in the interstitial space, the intracellular pH in solid tumour cells remains close to the physiological value. This suggests that malignant cells extrude protons more avidly than their untransformed counterparts. Indeed, several H⁺-extruding transporter systems appear to be upregulated in cancer cells, respectively the monocarboxylate carrier which exports lactate and H⁺, the Na⁺-H⁺ antiporter and H⁺ channels (5).

In addition to an increased H⁺ efflux, a wide variety of tumour types, including non-small cell lung carcinoma, show increased expression of the transmembrane zinc metalloenzyme carbonic anhydrase IX (CA IX / CA 9). CA IX catalyzes the reversible hydration of carbon dioxide to carbonic acid outside the cell (6). Carbonic acid is subsequently transported inside the cell by HCO₃⁻ /Cl⁻ anion exchangers where it may buffer H⁺, while the H⁺ generated remains outside the cell contributing to the build up of the extracellular acid environment (5,7-9) Given the role of CA IX in the acidification of the extracellular tumour microenvironment and its neutralizing effect on the intracellular pH on the one hand and the association of tumour acidification with tumour invasion and chemoresistance, CA IX is an attractive target for cancer therapy.

Importantly, the genes encoding for the glucose transporter and hexokinases that drive tumour hyperglycolysis, and CA IX are both under the control of hypoxia-inducible factor-1 (HIF-1)

(10-12). Accordingly, the aim of this study was to study semiquantitatively the expression of CA IX in non-small cell lung cancer (NSCLC) and to assess the existence of a possible relationship between CA IX expression and tumour FDG-uptake, reflecting glucose metabolism by primary NSCLC. Such relationship, if existing, could provide a rationale for selection of those patients suffering from NSCLC whom may benefit from CA IX inhibition treatment, based on FDG-PET imaging.

MATERIALS AND METHODS

Patients

Eighteen patients in whom substantial biopsy material or a surgical resection specimen of a primary NSCLC was available and that had also undergone an FDG PET-CT scan one week before the intervention or biopsy-procedure were included. The diagnosis of NSCLC was histologically confirmed in all patients. CA IX expression was scored and related to FDG SUVmean and SUVmax of the primary tumour.

FDG-PET

Whole body FDG-PET scans were acquired on a dedicated PET-CT scanner (Gemini, Philips) from the neck to the pelvis. Patients were required to be fasting for a minimum of 4 hours prior to FDG injection. Blood glycaemia was monitored with a portable capillary glucometer. Patients received a dose of FDG based on their body weight using the following formula $((\text{body weight}/10)+1)*37$ MBq. The mean delay from FDG injection to imaging was 60 minutes, minimally 50 minutes. Images were acquired in a 3-dimensional mode and reconstructed with attenuation correction (CT-based) using OSEM (ordered subset expectation maximization). Data were processed using MIMVISTA software. Maximum FDG SUV was derived from a region of interest (ROI) drawn over the tumour lesion on the slice containing the most intense tumour signal, using CT as a reference. The mean tumour SUV value was defined using region growing using the voxel with the maximum value as seeding voxel and a threshold of 75% of the maximum value. The 75 % threshold was chosen in order to largely exclude regions of tumour necrosis that may significantly influence the mean SUV value.

Immunohistochemistry

Routinely processed, formalin fixed, paraffin embedded surgical pathology specimens were used for immunohistochemistry. Sections of 4 µm thick were mounted on SuperFrost® microscope slides (Menzel-Glaser, Braunschweig, Germany), which were deparaffinized in xylene and rehydrated in a downgraded series of ethanol. After flushing in water, heat induced antigen retrieval was performed for 20 minutes with the appropriate buffer (EDTA pH = 8.0), after which the tissue slides were cooled down for 20 minutes and then flushed in water for 10 minutes. The endogenous peroxidase activity was blocked for 5 minutes with 0,3 % hydrogen peroxide (DAKO , Glostrup, Denmark) on each tissue slide. Primary antibody (anti-CAIX, ABCAM ab15086, 1/2000 in 1% BSA/PBS) was then incubated for 1 hour at room temperature. After washing, the tissue sections were incubated for 30 minutes at room temperature with a labelled polymer-HRP anti-rabbit secondary antibody (DAKO , Glostrup, Denmark). The colour reaction was developed using the chromogen 3,3-diaminobenzidine+ (DAB) (DAKO , Glostrup, Denmark) for 10 minutes. After washing, the tissue sections were counterstained with Mayer's haematoxylin.

Phosphate-buffered saline with 1% BSA instead of the primary antibody was used as negative control on each slide in order to exclude false positive responses from non-specific binding of the secondary antibody. Prior to staining the specimens, an isotype control was performed to estimate the non-specific binding of target primary antibodies to cell surface antigens. Non-specific binding is due to Fc receptor binding or other protein-protein interactions.

Immunohistochemical analysis

The intensity and percentage of positive tumour cells in the immuno-reaction were scored independently by two experienced observers. Only membranous staining was scored (intensity and percentage of positive cells). The percentage of tumour cells that were positive on the immuno-reaction were scored as follows : 0% (score 0), 0-20% (score 1), 20-40% (score 2), 40-60% (score 3), 60-80% (score 4) and 80-100% (score 5). Intensities of staining were categorized as absent (score 0), faint (score 1), average (score 2) or strong (score 3). An estimation of intensity and percentage of positive tumour cells was made after counting ten high-powerfields. A final histological score was calculated as following: $Hscore = [(a1 \times i1) + (a2 \times i2)] / 2$, where i = the score of intensity, a = the score of amount tumour cells that stained positive and 1 and 2 refer to the scores of the two observers.

Statistical analysis.

SPSS for Windows, version 15.0 was used for statistical analysis. Correlation analysis was performed using the Spearman rank test (a P value < 0.05 was considered significant).

RESULTS

Patients

Patient results are shown in Table 1. There were 14 men and 4 women, mean age was 67 years, range: 52-82 years. Four patients presented with stage I disease, 3 presented with stage II disease, 7 patients with stage III disease and 4 patients suffered from stage IV disease. FDG-PET data: FDG SUVmax values of the primary tumour ranged from 0.7 to 22.1 (mean 10.0). FDG SUVmean values of the primary tumour ranged from 0.6 to 19 (mean 8.7).

Nb.	Gender	Age	T	TNM	FDG SUVmean	FDG SUVmax	CAIX Hscore
1	F	55	3	2	5.4	6.2	3
2	M	58	3	3	4.6	5.2	3
3	M	79	2	2	13.5	16.7	4.5
4	M	82	2	1	12.1	13.0	6
5	M	78	2	1	19	22.1	7.5
6	M	79	2	4	0.6	0.7	0.0
7	F	73	2	13	8.4	10.1	7.5
8	M	69	2	1	6.3	7.6	4.5
9	M	78	2	3	5.2	6.6	0.0
10	F	56	2	2	6.1	7.2	1.5
11	M	52	2	3	5.8	6.7	2.0
12	M	80	2	3	8.1	9.6	4.5
13	M	62	2	4	9.1	10.9	2.5
14	M	61	2	4	5.4	6.4	1.5
15	M	61	2	1	15.2	16.1	9.0
16	M	65	2	3	11.0	12.9	3.0
17	M	65	3	3	6.4	7.5	5.0
18	F	57	2	4	14.0	15.0	4.5

TABLE 1. T= T-stage, TNM= TNM stage

CA IX expression

Membranous tumour cell CA IX expression was detected in 16 (88 %) patients (see Figure 1). Mean Hscore for CA IX expression in the total group was 3,9 (range 0,0 to 9,0; sd 2,8). CA IX expression was not related to tumorsize (T-stage)

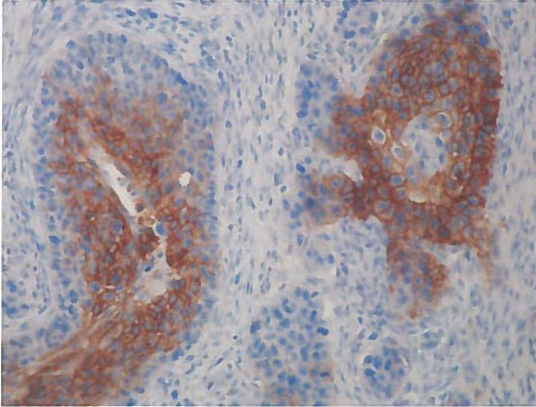


FIGURE 1. Immunohistochemical staining of CA IX (200 X). Staining was typically confined to the cell membrane and had a strong intensity.

Correlation Between CA IX Hscores and FDG SUVmax and SUVmean Values

A statistically significant correlation was observed when plotting CA IX Hscores against FDG SUVmax and FDG SUVmean values of the primary tumour, respectively $r = 0.716$ ($p = 0,001$) and $r = 0.758$ ($p = 0.0001$) (see Figures 2, 3, 4).



FIGURE 2. Shows high FDG uptake in the primary NSCLC of patient nb. 15 and corresponding intense CA IX staining on histology

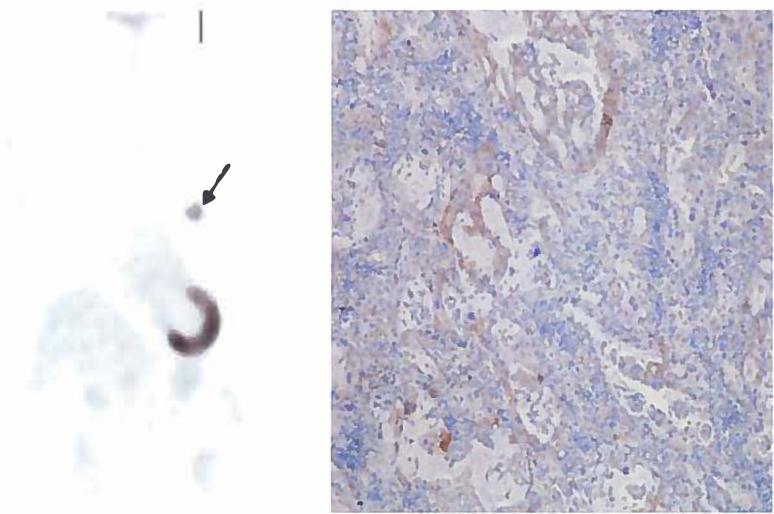


FIGURE 3. Shows moderate FDG uptake in the primary NSCLC of patient nb. 12 and corresponding moderate CA IX staining on histology

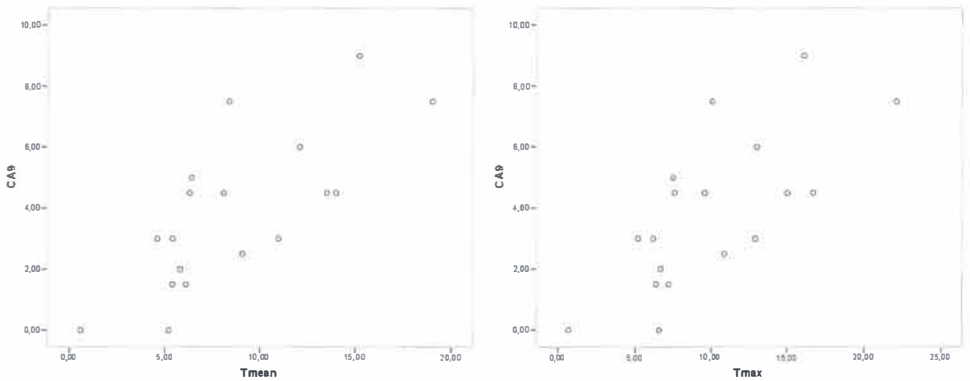


FIGURE 4. Scatterplot of the relationship between CA IX (CA9) Hscores and their corresponding FDG SUV mean values (Tmean) and FDG SUV max values (Tmax).

DISCUSSION

The aim of this study was to investigate the expression of CA IX in NSCLC and to determine a possible relationship with FDG-uptake in FDG-PET imaging.

In our series, 88 % of the tumours investigated showed positive membranous staining for CA IX. Other studies investigating CA IX expression in NSCLC yielded varying numbers of positive cases, respectively varying from 24,6 % to 81,8 % (13-17). In most of these studies,

however, a different scoring methodology was used. Vermynen et al. differentiated between cytoplasmic, cytoplasmic with membranous reinforcement or membranous only staining pattern and used a three-point scoring system for the intensity of staining. Immunostaining proved positive in 52 of 65 tumour samples with the percentage of stained cells in positive tumours being highly variable (13). Giatromanolaki et al. only made a distinction between negative, weak cytoplasmic and strong membrane/cytoplasmic staining. In their series, 39 out of 107 cases studied showed strong membrane/cytoplasmic expression of CA IX (14). Swinson et al. assessed the percentage of cells with membranous and cytoplasmic expression and divided CA IX expression into quartiles depending on the percentage of cells that stained positive (15). Kon-no et al. classified NSCLC tumours into CA IX positive or negative using a cut-off of 20 % of positive cancer cells showing an unequivocal strong membranous and/or cytoplasmic reaction; using this criterion, 33 out of 134 cases studied were CA IX positive (16). Finally, in the study by Kim et al. a similar scoring system to the one used in the study reported was used and a comparable percentage of patients, respectively 54 of 75 patients (72 %) showing CA IX expression, reported (17). Of interest, in four out of five studies the prognostic relevance of CA IX expression was studied (14-17). In three out of these four studies, respectively the studies by Giatromanolaki et al., Swinson et al. and Kim et al. CA IX expression was related to poor prognosis in both univariate analysis and multivariate analysis whereas in the study by Kon-no et al. CA IX expression was significantly associated with overall and disease-free survival in univariate analysis only (14-17).

In the series presented, a statistically significant correlation was observed between CA IX Hscores and SUV_{max} and SUV_{mean} values of the primary tumour. This relationship found provides indirect evidence for co-transcription of glucose transporter and hexokinases, that drive tumour hyperglycolysis, and CA IX governed by HIF-1 (10-12). To date, only one other study, respectively by van Baardewijk et al. reported simultaneously on FDG-uptake and CA IX expression in patients suffering from NSCLC. However, the purpose of this study was to address the prognostic value of FDG-PET imaging and several markers related to hypoxia (HIF-1 α and CA IX), proliferation (Ki-67) and glucose metabolism (GLUT1 and GLUT3). Accordingly, the scoring system used (a 4-point score system only taking into account the percentage of positive cells) was not optimized for correlation analysis and hence correlation analysis was not performed (18).

Chemotherapeutic drugs that are weakly ionized, e.g. vinca-alkaloids such as vinorelbine which is currently used in an adjuvant setting as well as in advanced NSCLC, will enter cells by passive diffusion in their non-ionized form. In this form, they will tend to partition

preferentially across the cell membrane into the compartment where their ionized form predominates. Accordingly, increasing the pH of tumours will enhance the uptake of such agents by the tumour cell, increasing their therapeutic potential. To date, many classes of highly effective in vitro CA IX inhibitors have been developed and the pharmacological evaluation of some of them has recently begun, e.g. the sulphonamide indisulam which is currently being tested in phase II clinical trials (4,19,20). The relationship found between CA IX expression and FDG-PET in this study suggest that in the future it may be possible to identify NSCLC patients that are most likely to benefit from CA IX targeting therapy on the basis of FDG-PET imaging.

In conclusion, our results show a statistically significant correlation between FDG-uptake in FDG-PET imaging and CA IX expression providing indirect evidence for co-transcription of glucose transporter and hexokinases, that drive tumour hyperglycolysis, and CA IX governed by HIF-1. Based on this finding, studies assessing the predictive value of FDG-PET imaging for CA IX therapy may prove worthwhile to pursue.

REFERENCES

1. Warburg O. On the origin of cancer cells. *Science*. 1956;123:309-314.
2. Gatenby RA, Gillies RJ. Glycolysis in cancer: a potential target for therapy. *Int J Biochem Cell Biol*. 2007;39:1358-1366.
3. Zhou J, Schmid T, Schnitzer S, et al. Tumor hypoxia and cancer progression. *Cancer Letters*. 2006;237:10-21.
4. Thiry A, Dogné JM, Masereel B, et al. Targeting tumor-associated carbonic anhydrase IX in cancer therapy. *Trends Pharmacol Sci*. 2006;27:566-573.
5. Swietach P, Vaughan-Jones RD, Harris AL. Regulation of tumor pH and the role of carbonic anhydrase 9. *Cancer Metastasis Rev*. 2007;26:299-310.
6. Potter C, Harris AL. Hypoxia inducible carbonic anhydrase IX, marker of tumor hypoxia, survival pathway and therapy target. *Cell Cycle*. 2004;3:164-167.
7. Robertson N, Potter C, Harris AL. Role of carbonic anhydrase IX in human tumor cell growth, survival and invasion. *Cancer Res*. 2004;64:6160-6165.
8. Svastova E, Hulikova A, Rafajova M, et al. Hypoxia activates the capacity of tumor-associated carbonic anhydrase IX to acidify extracellular pH. *FEBS Letters*. 2004;577:439-435.

9. Swietach P, Wigfield S, Cobden P, et al. Tumor-associated carbonic anhydrase 9 spatially coordinates intracellular pH in three dimensional multicellular growths. *J Biol Chem*. 2008;283:20473-20483.
10. Wykoff CC, Beasley NJP, Watson PH, et al. Hypoxia-inducible expression of tumor-associated carbonic anhydrases. *Cancer Research*. 2000;60:7075-7083.
11. Loncaster JA, Harris AL, Davidson SE, et al. Carbonic anhydrase (CA IX) expression, a potential new intrinsic marker of hypoxia: correlations with tumor oxygen measurements and prognosis in locally advanced carcinoma of the cervix. *Cancer Res*. 2001;61:6394-6399.
12. Olive PL, Aquino-Parsons C, Macphail SH, et al. Carbonic anhydrase 9 as an endogenous marker for hypoxic cells in cervical cancer. *Cancer Res*. 2001;61:8924-8929.
13. Vermylen P, Roufosse C, Burny A, et al. Carbonic anhydrase IX antigen differentiates between preneoplastic malignant lesions in non-small cell lung carcinoma. *Eur Respir J*. 1999;14:806-811.
14. Giatromanolaki A, Koukourakis MI, Sivridis E, et al. Expression of hypoxia-inducible carbonic anhydrase-9 relates to angiogenic pathways and independently to poor outcome in non-small cell lung cancer. *Cancer Res*. 2001;61:7992-7998.
15. Swinson DEB, Jones JL, Richardson D, et al. Carbonic anhydrase IX expression, a novel surrogate marker of tumour hypoxia, is associated with a poor prognosis in non-small cell lung cancer. *J Clin Oncol*. 2003;21:473-482.
16. Kon-no H, Ishii G, Nagai K, et al. Carbonic anhydrase IX expression is associated with tumor progression and a poor prognosis of lung adenocarcinoma. *Lung Cancer*. 2006;54:409-418.
17. Kim SJ, Rabbani ZN, Vollmer RT, et al. Carbonic anhydrase IX in early-stage non-small cell lung cancer. *Clin Cancer Res*. 2004;10:7925-7933.
18. van Baardwijk A, Dooms C, van Suylen RJ, et al. The maximum uptake of ¹⁸F-deoxyglucose on positron emission tomography scan correlates with survival, hypoxia inducible factor-1 α and GLUT-1 in non-small cell lung cancer. *Eur J Cancer*. 2007;43:1392-1398.
19. Morsy SMI, Badawi AM, Cecchi A, et al. Carbonic anhydrase inhibitors. Biphenylsulfonamides with inhibitory action towards the transmembrane, tumor-associated isozymes IX possess cytotoxic activity against human colon, lung and breast cancer cell lines. *J Enzyme Inhib Med Chem*. 2009;24:499-505.

20. Supuran CT, Scozzafava A. Carbonic anhydrase inhibitors: aromatic sulfonamides and disulfonamides act as efficient tumor growth inhibitors. *J Ezyme Inhib.* 2000;15:597-610.

Chapter 3: Tumor Hypoxia and Vasculature

Research article: ^{99m}Tc -labeled tricarbonyl His-CNA35 as an imaging agent for the detection of tumor vasculature.

J Nucl Med. 2012;53:464-471.

^{99m}Tc -labeled tricarbonyl His-CNA35 as an imaging agent for the detection of tumor vasculature.

Gilles Mees ¹, Rudi Dierckx ^{1,2}, Koen Mertens ², Simon Vermeire ³, Magali Van Steenkiste ⁴, Chris Reutelingsperger ⁵, Yves D'Asseler ², Kathelijne Peremans ³, Nancy Van Damme ⁶, Christophe Van de Wiele ^{1,2}

¹ Department of Nuclear Medicine and Molecular Imaging, University Medical Center Groningen, University of Groningen, The Netherlands

² Department of Nuclear Medicine, Ghent University Hospital, Belgium

³ Department of Medical Imaging, Faculty of Veterinary Medicine, Ghent University, Belgium

⁴ Laboratory of Radiopharmacy, Faculty of Pharmaceutical Sciences, Ghent University, Belgium

⁵ Department of Biochemistry, Cardiovascular Research Institute, University of Maastricht, The Netherlands

⁶ Department of Surgery, Ghent University Hospital, Belgium

ABSTRACT

Given its importance for a tumor's survival and growth, several therapeutic strategies rely on the selective inhibition of angiogenesis and the destruction of existing tumor vasculature. This raises the need for a non-invasive tool to evaluate tumor vasculature. We describe the radiosynthesis and evaluation of a novel imaging tracer that specifically binds tumor subendothelial collagen and thereby images tumor vasculature.

Methods: ^{99m}Tc -tricarbonyl was prepared and labeled with His-CNA35. After *in vitro* specificity testing, *in vivo* biodistribution and dosimetric studies were performed in healthy nude mice via planar imaging. $^{99m}\text{Tc}(\text{CO})_3$ His-CNA35 was evaluated for *in vivo* imaging of tumor vasculature in a HT29 colorectal carcinoma xenograft.

Results: The labeling procedure yielded a compound with 95-99% radiochemical purity and good *in vitro* stability. An *in vitro* binding test confirmed specificity and functionality. $^{99m}\text{Tc}(\text{CO})_3$ His-CNA35 rapidly cleared from the blood and predominantly accumulated in the

kidneys and liver. The effective dose for a proposed single-injection of 500 MBq $^{99m}\text{Tc}-(\text{CO})_3$ His-CNA35 is 3,70 mSv (per organ) or 2,01 mSv (per gram tissue). Tumors were successfully visualized and uptake correlated with *ex vivo* immunohistochemical staining of tumor vasculature.

Conclusion: $^{99m}\text{Tc}-(\text{CO})_3$ His-CNA35 may be a useful novel radioligand for the *in vivo* detection of tumor vasculature through subendothelial collagen binding. A non-invasive method of imaging tumor vasculature that could provide a reliable assessment of tumor vasculature would allow evaluation of the effectiveness of commonly used antiangiogenic therapies as well as determination of their optimal dosing and scheduling.

Key words: CNA35, tricarbonyl, tumor vasculature, HT29

As a tumor mass grows beyond the support capacity of the vasculature it relies on, the need for new blood vessels arises. This is achieved through the process of angiogenesis in which, through a multistep process that relies on the tumor-driven production of pro-angiogenic factors, new blood vessels are formed from existing ones. These resulting new blood vessels however, are structurally and functionally deficient when compared to normal ones. They are disorganized, tortuous and leaky which leads to heterogeneous blood flow, hypoxia, acidosis and elevated interstitial fluid pressure (IFP) with a disturbed tumor microenvironment as a result (1). Nevertheless, this neovascularization allows the tumor to grow and plays an important role in tumor invasiveness and metastasis. Given its importance, a number of therapeutic strategies rely on the selective inhibition of angiogenesis and destruction of tumor vasculature. In several types of cancer, antiangiogenic therapy alone or in combination with standard chemotherapeutic strategies have led to an improvement of survival (2,3). As the importance of these therapies increases, non-invasive methods are needed to provide a reliable assessment of tumor vasculature and thus provide a means for the management and planning of antiangiogenic therapy.

A possible mechanism to target tumor vasculature is based upon the selective exposure of collagen in these vessels due to their aberrant endothelial lining. Collagen-binding adhesion protein 35 (CNA35) is a 35 kDa collagen binding domain of specific bacterial adhesion proteins from *Staphylococcus aureus* where it participates in its infectious process. The collagen binding properties of these domains are well characterized and overexpression can be attained in *Escherichia Coli* in large quantities (4,5). CNA35 has previously been labeled

with a number of fluorophores in order to visualize collagen in tissues and life cell cultures and has a moderate affinity ($K_d \sim 0,5 \mu\text{M}$) for a variety of different collagen types (5-7). The proposed mechanism of binding involves the wrapping of the CNA35 protein around the triple helix of collagen (4). Collagens are an important component of the extracellular matrix (ECM), an interconnected molecular network providing mechanical support for cells and tissues and regulating certain biochemical and cellular processes. Up till now, 19 different collagens have been identified which are categorized into fibrillar and non-fibrillar collagens. Collagen IV is the major component of the vascular basement membrane, a specialized form of ECM that lines the blood vessels and separates epithelia from its underlying mesenchyme (8). In contrast to normal blood vessels, tumor vasculature displays an abnormal, incomplete endothelial lining that is characterized by large inter-endothelial junctions and an increased number of fenestrations (1). This allows CNA35 to penetrate the endothelial lining and bind the underlying collagen layer. In normal vessels these abnormalities do not exist in this degree, preventing major infiltration of the endothelial lining and subsequent binding of the underlying collagen layer. As a result, specific targeting of tumor vasculature is possible and non-invasive imaging of tumor vasculature is feasible when labeling CNA35 with a radioactive molecule.

The aim of this study was to radioactively label CNA35 and evaluate this marker of tumor vasculature in order to selectively image tumor vasculature non-invasively.

MATERIALS AND METHODS

$^{99\text{m}}\text{Tc}-(\text{CO})_3$ His-CNA35 Preparation

Preparation of the labeling precursor $^{99\text{m}}\text{Tc}$ -tricarbonyl ($[\text{}^{99\text{m}}\text{Tc}(\text{CO})_3(\text{OH}_2)_3]^+$) was performed according to manufacturer's instructions. One ml of eluted $^{99\text{m}}\text{TcO}_4^-$ (1480 - 2590 MBq) (GE Healthcare, Buckinghamshire, England) was added to the IsoLink™ vial (IsoLink™ kits were kindly provided by Mallinckrodt Medical B.V., The Netherlands) containing the following lyophilized products: 4.5 mg sodium boranocarbonate, 2.85 mg sodium tetraborate.10H₂O, 8.5 mg sodium tartrate.2H₂O. The vial was placed in a water bath for 30 minutes at 95 - 100°C after which the reaction vial was cooled down to room temperature. The precursor was brought at pH 7 by addition of 1M HCl. His-CNA35 (50 - 60 μg) (provided by Prof. Dr. C. Reutelingsperger, Department of Biochemistry, University Maastricht) was added to the precursor and incubated at 37°C for 1 to 1.5 hours while blown

dry with nitrogen (N₂) gas to reduce the reaction volume. Protein LoBind Tubes (Eppendorf, Hamburg, Germany) were used to prevent adhesion of the protein to the vial wall. The vial was washed with physiological saline (0.9% NaCl) and the reaction mixture was purified on a Sephadex™ G-25 medium PD-10 column (GE Healthcare Bio-Sciences AB, Uppsala, Sweden) which was activated with phosphate-buffered saline (PBS) containing 0.5% bovine serum albumin (BSA, Sigma-Aldrich-Fluka, Bornem, Belgium) and eluted with fractions of 500 µl PBS. The radioactivity of each fraction was measured in a dose calibrator (VIK-202, Veenstra, The Netherlands).

Radiochemical Analysis

The radiochemical purity of the ^{99m}Tc-(CO)₃ His-CNA35 was determined by instant thin-layer chromatography (ITLC) with silica gel-coated fiberglass sheets (Life Sciences, Pall Corporation, Zaventem, Belgium) using physiological saline as the mobile phase. Samples of radiolabeled His-CNA35 were tested for their *in vitro* stability at 4h and 24h after preparation at 4°C and 37°C in: PBS, McCoy's 5A cell medium supplemented with 10% fetal bovine serum (FBS) and human blood serum. Fifty microliter of ^{99m}Tc-(CO)₃ His-CNA35 was mixed with 50 µl PBS, cell medium or serum and ITLC was carried out to assess the radiochemical purity. At both time points, 5 µl of the samples were spotted on ITLC strips and radioactivity was counted using an automated gamma counter (Cobra II series, Canberra Packard, Meriden CT USA). High-pressure liquid chromatography (HPLC) was performed to analyze the integrity and radiochemical purity of the radiolabeled CNA35 with a size exclusion Shodex KW 802.5 column (7.8x 300 mm; Thomsom Instrument Company, Oceanside, CA USA) connected to a UV-VIS spectrometer λ 280 nm (SPD-6AV, Shimadzu, Deurne, Belgium) and a NaI γ counter (Model 2200, Ludlum, Sweetwater, TX USA). Elution was performed at a flow rate of 0.8 ml/min with a 0.1 M Potassium Phosphate buffer pH 7 and a Waters 510 dual head pump. The purity of the unlabeled and labeled compound was further analyzed with SDS-PAGE performed according to the method of Laemmli (9). The labeled (0.04 MBq) ^{99m}Tc-(CO)₃ His-CNA35 and unlabeled (5µg) His-CNA35 were mixed with an equal volume of Laemmli sample buffer (2x) and loaded on to a 15% SDS-PAGE gel. Ten µl of a protein ladder (10-250 kDa) from Biolabs was treated the same way. Electrophoresis was performed at 200V (Protean III system, Bio-Rad, Nazareth Eke, Belgium) until the dye front reached the bottom of the gel. Visualization of the separated proteins was done either with Coomassie Brilliant Blue R-250 staining (Bio-rad) or either by exposure of a superresolution film for 1

min to the radioactive gel after which visualization of the radioactive protein was effected with Cyclone Storage Phosphor equipment (PerkinElmer, Boston, USA).

In Vitro Solid-Phase Binding Assay

Collagen I -, collagen IV -, laminin - and fibronectin - coated multiwell plates (BD, Franklin Lakes NJ, USA) were blocked with 3% PBS/BSA for 3h at 37 °C, aspirated and washed three times with PBS. Afterwards, increasing concentrations of $^{99m}\text{Tc}-(\text{CO})_3$ His-CNA35 were added to each well and incubated for 3h at 37 °C. Supernatant was removed and wells were washed 2 times with PBS. Supernatant was measured using an automated gamma counter (Cobra II series, Canberra Packard) and uptake was calculated. To assess non-specific binding, uptake was measured in a noncoated multiwell plate (BD, Franklin Lakes NJ, USA) as well. All assays were done in triplicate.

HT29 Cell Culture

HT29 human colorectal carcinoma cells (ACC 299, DSMZ, Braunschweig, Germany) were cultured in McCoy's 5A medium (Invitrogen Corporation, Gibco, Merelbeke, Belgium) supplemented with 10% fetal bovine serum (Invitrogen Corporation), 4 mM L-glutamine, 50 µl/ml penicillin and 50 µg/ml streptomycin (Invitrogen Corporation) and incubated at 37°C in a humidified atmosphere of 5% CO₂ in air. Cells were kept in exponential growth phase by routine passage every 3-4 days (split ratio of 1/4 - 1/6).

Animal Model

Four-to-six week old female CD-1[®] nude mice were purchased from Charles River (Brussels, Belgium) and housed in a standard facility at the Department of Animal Sciences, Ghent University Hospital. All procedures were carried out in accordance to the guidelines and regulations for use and care of animals and approved by the local ethical committee, Faculty of Medicine, Ghent University (EC nr. 09/14). One million ($1 \cdot 10^6$) HT29 human colorectal carcinoma cells suspended in 0.1 ml of PBS were injected subcutaneously (sc) in the proximal right hind leg. Tumor growth curves were obtained using calliper measurement and the estimate volume formula (mm^3) = 1/2 (a²b), where a and b are the short and long axis of the tumor respectively. Experiments were initiated when tumors reached approximately 10 mm in diameter, generally 14 days after implantation.

Biodistribution and Dosimetry of Radiolabeled CNA35

For biodistribution and dosimetry studies, 4 healthy nude mice were positioned on the gammacamera and were maintained under isoflurane anaesthesia (2%) for the duration of the experimental procedure while body temperature was maintained. Following bolus tail-vein administration of 37 MBq (approximately 4 μ g) $^{99m}\text{Tc}-(\text{CO})_3$ His-CNA35 in 150 μ l, mice were imaged during the first 100 minutes (dynamic study, one hundred frames of one minute) followed by planar images of ten minutes at 4, 8 and 23 h after injection of the radiotracer for evaluation of the biodistribution of $^{99m}\text{Tc}-(\text{CO})_3$ His-CNA35 *in vivo*. Mice were imaged using a conventional triple-head gamma camera (Triad, Trionix, Twinsburg, OH USA) operated in planar mode with the animals positioned on one of the three detectors. Regions of interest (ROI) were drawn over the total body, liver, right kidney, left kidney, heart and part of the left hind leg (= background) using PMOD 3.0 software (PMOD Technologies, Zurich, Switzerland). ROI's were drawn on early images and the shape and size (number of pixels) were kept constant over all subsequent images per mouse. Total body retention was estimated using the no-excretion approach, that is total counts collected during the first minute of the dynamic study were assumed to correspond to the total injected dose (ID). Total counts from a later whole-body scan at time t_i were used to estimate percentage ID: %ID = (counts t_i / counts (first frame) x 100%). Following correction for background radiation, decay correction and, when needed, correction for residual activity in the tail, uptake in the organs was expressed as percentage of the injected dose.

Based upon quantification of whole body images (0-100 minutes, 4 h, 8 h, and 23 h) from the biodistribution studies, dosimetry of $^{99m}\text{Tc}-(\text{CO})_3$ His-CNA35 was estimated using MIRDose 3.1. Organ residence time was obtained by integrating the organ activity curve that was normalised with the injected activity, but not corrected for physical decay. For liver, right kidney, left kidney and the remainder of the body, time-activity curves (TAC) were constructed from the dynamic (first 100 min) and static planar scans at later time points. The TAC's were fitted to bi-exponential functions and residence times were calculated. Based on these, organ dose and effective dose were calculated with MIRDose 3.1. Data obtained from mice were converted to a 68-kg human reference adult, both using an activity per organ and an activity per mass approach.

In Vivo Imaging of Tumor Vasculature in a Human HT29 Colorectal Tumor Xenograft Model

For *in vivo* imaging of tumor vasculature, 10 HT29 colorectal carcinoma xenografts were injected intravenously (iv) with 18.5 MBq (approximately 2 μ g) $^{99m}\text{Tc}-(\text{CO})_3$ His-CNA35 in 150 μ l. Three hours post-injection (pi), mice were brought under isoflurane anaesthesia (2%) for the duration of scan while body temperature was maintained. A planar, static scan of 20 minutes was performed using a conventional triple-head gammacamera (Triad, Trionix, Twinsburg, OH USA) with the animals positioned on one of the three detectors. A syringe with a known amount of radioactivity was scanned along with the mice to allow semiquantification of the results using ROI analysis. ROIs were copied from the tumor-containing right hind leg to the left hind leg and data were expressed as tumor-to-background ratio's (T/B ratios) using the left hind leg as background. Directly after the scan, the animals were killed by cervical dislocation, tumors were removed, formalin fixed and paraffin embedded.

Detection of Tumor Vasculature by Immunohistochemistry

Tumor vasculature was evaluated using immunohistochemical markers for endothelial cells (CD105/Endoglin, R&D AF1320, 1/50), blood vessel basement membrane (collagen IV, Abcam ab6586, 1/500), and mural cells, i.e., pericytes and vascular smooth muscle cells (alpha smooth muscle actin, Abcam ab5694, 1/200). Tissue sections of 5 μ m thick were mounted on SuperFrost[®] microscope slides (Menzel-Glaser, Braunschweig, Germany), which were deparaffinized in xylene and rehydrated in a downgraded series of ethanol. After washing the slides in the appropriate buffer (tris-buffered saline (TBS) with 0.1% Tween 20), heat induced antigen retrieval was performed for 20 minutes in citrate buffer (pH = 6.0), after which the slides were cooled down for 15 minutes. The endogenous peroxidase activity was blocked for 5 minutes with 0.3 % hydrogen peroxide (Dako, Glostrup, Denmark). Slides were then incubated with the primary antibody overnight (CD105) or for 1 hour (collagen IV and α SMA) at room temperature (primary antibody diluted in PBS with 1% BSA). After washing, the tissue sections were incubated for 30 minutes at room temperature with a HRP-labeled anti-rabbit secondary antibody (Dako) or the combination of a biotinylated link and streptavidin-HRP (Dako). The colour reaction was developed using the chromogen 3,3-diaminobenzidine (DAB) (Dako) for 30 seconds. After washing, the tissue sections were counterstained with Mayer's haematoxylin. In order to exclude false positive responses from non-specific binding of the secondary antibody, negative controls were tested with 1% PBS-BSA instead of the primary antibody. Prior to staining the specimens, an isotype control was

performed to estimate the non-specific binding of target primary antibodies to cell surface antigens.

Immunohistochemical Analysis

An Optronicscolor digital camera (Olympus Corporation, Tokyo, Japan) and specialized software (Cell D Olympus Imaging Solutions, Münster, Germany) was used to analyse immunohistochemical stainings. MVD was assessed in sections stained for CD105 using the criteria of Weidner et al. (10). Briefly, the entire tumor section was scanned at low power (magnification x40) to identify vascular hot spots, which are the areas of highest vascularisation. Individual microvessels were then counted under high power (magnification x200) to obtain a vessel count in a defined area, and the average vessel count in five hot spots was taken as the MVD. Any brown stained endothelial cell or endothelial cell cluster that was clearly separated from adjacent microvessels, tumor cells, and other connective tissue elements was considered a single, countable microvessel. The same hotspots were used to count α -SMA and collagen IV positive vessels using the same procedure. A ratio of α -SMA to CD105 was used to calculate the vessel maturity index (VMI) which provided a percentage of mature vessels (11).

Statistical Analysis

All statistical analysis was performed using SPSS software (version 15.0; SPSS Inc., Chicago, IL, USA). Spearman correlation test was used to calculate correlations between $^{99m}\text{Tc}-(\text{CO})_3$ His-CNA35 tumor uptake and immunohistochemical stainings in the tumor. Data were considered statistically significant when a two-tailed p-value of < 0.05 was reached.

RESULTS

Radiochemical Profile of $^{99m}\text{Tc}-(\text{CO})_3$ -His CNA35

His-tagged CNA35, with a N-terminal extension containing six histidine residues, was successfully labeled with $^{99m}\text{Tc}-(\text{CO})_3$. Incubation of the His-CNA35 with the $^{99m}\text{Tc}-(\text{CO})_3$ occurred at physiological pH (pH = 7) and at a temperature of 37°C for about 1 - 1.5 hours. Although specialized vials were used to prevent adhesion of the protein to the vial wall, considerable residual activity was noted in the reaction vial. Radiochemical yields of 40-50% and specific radioactivities of approximately 8.9 - 10.4 MBq/ μg protein were obtained. ^{99m}Tc -

(CO)₃ His-CNA35 was purified on a calibrated PD-10 gel permeation column using PBS as eluent. The radiochemical purity of the labeled CNA35 was evaluated by ITLC with physiological saline as mobile phase. Radiochemical purities of 95 - 99% were obtained with the remainder being free ^{99m}Tc pertechnetate (1 - 4%). HPLC was performed to characterize the radiolabeled His-CNA35. ^{99m}Tc-(CO)₃ His-CNA35 was eluted at a retention time of 9.8 min. The SDS-PAGE showed a band of 36 kDa representing the radiolabeled His-CNA35. No other small molecules were identified. *In vitro*, no significant degradation of the product was noted for up to 24 hours, at 4°C and 37°C in: PBS, cell medium supplemented with 10% FBS or human blood serum. The stability tests thus demonstrated that ^{99m}Tc-(CO)₃ His-CNA35 has good thermodynamic stability in PBS, cell medium and human blood serum.

In Vitro Solid-Phase Binding Assay

Binding of ^{99m}Tc-(CO)₃ His-CNA35 to collagen I-, collagen IV-, laminin- and fibronectin-coated multiwell plates was studied in order to confirm the specificity and functionality of the labeled molecule. Results are summarized in Figure 1. Binding of ^{99m}Tc-(CO)₃ His-CNA35 to collagen I and IV was observed. Negligible binding was observed to laminin-, fibronectin- and noncoated surfaces which might be the result of non-specific adhesion to the plastic of the multiwell plates.

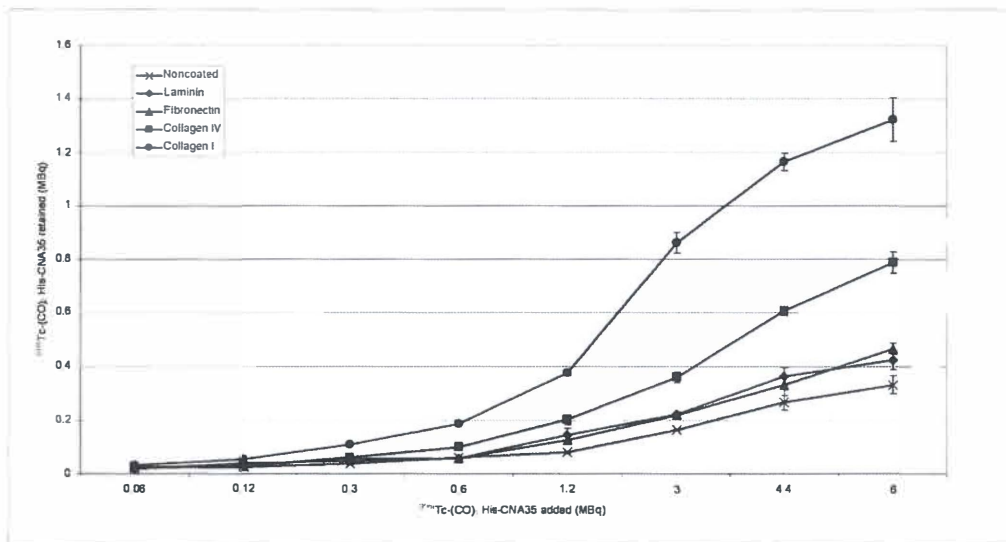


FIGURE 1. Binding of ^{99m}Tc-(CO)₃ His-CNA35 to collagen I-, collagen IV-, laminin-, fibronectin- and noncoated multiwell plates. Data are expressed as mean ± SEM (n = 3).

Biodistribution

Following bolus tail-vein administration of 37 MBq $^{99m}\text{Tc}(\text{CO})_3$ His-CNA35, mice were imaged during the first 100 minutes (dynamic study, one hundred frames of one minute) followed by planar images of ten minutes at 4, 8 and 23 h after injection of the radiotracer. The biodistribution of $^{99m}\text{Tc}(\text{CO})_3$ His-CNA35 in four healthy nude mice is summarized in Table 1 and Figure 2. Following intravenous injection $^{99m}\text{Tc}(\text{CO})_3$ His-CNA35, the radiotracer was rapidly cleared from the blood ($6,54 \pm 1,47$ %ID during the first minute and at 1 hour pi only $1,86 \pm 0,14$ %ID remained in the blood). Liver and kidneys showed the highest radiotracer uptake throughout the biodistribution experiment (see Table 1, Figure 2 and 3). At all time points, the right kidney showed a higher uptake when compared to the left kidney. Thus, renal excretion appears to be the main route of radiotracer clearance.

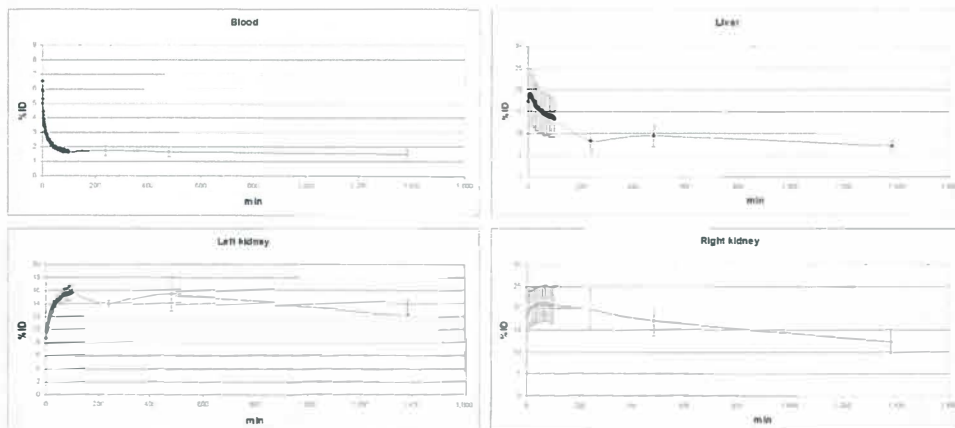


FIGURE 2. Decay-corrected $^{99m}\text{Tc}(\text{CO})_3$ His-CNA35 uptake vs time curves for bloodpool, liver, right kidney and left kidney. Planar scans were made from 0-100 min (dynamic study, 100 frames of 1 min) and at 4 h, 8 h and 23h pi (static study, 10 min). Kidneys show the highest radiotracer uptake (right kidney more than left), followed by the liver. A rapid clearance of the tracer from the blood was observed.

Time pi (min)	Blood (%ID ± SD)	Liver (%ID ± SD)	Right kidney (%ID ± SD)	Left kidney (%ID ± SD)
1	6.54 ± 1.47	17.30 ± 7.01	18.10 ± 4.32	8.79 ± 0.97
10	3.41 ± 0.35	18.47 ± 6.52	19.73 ± 4.20	11.06 ± 0.65
20	2.66 ± 0.19	17.41 ± 5.97	20.17 ± 4.06	12.71 ± 0.64
30	2.33 ± 0.23	16.10 ± 5.37	20.58 ± 4.02	13.64 ± 0.82
40	2.12 ± 0.22	15.47 ± 5.30	20.99 ± 4.15	14.27 ± 0.92
50	1.95 ± 0.16	15.05 ± 4.99	21.00 ± 4.12	14.64 ± 0.80
60	1.86 ± 0.14	14.55 ± 4.90	20.91 ± 4.09	14.87 ± 0.90
70	1.79 ± 0.15	14.19 ± 4.70	21.18 ± 4.12	15.19 ± 1.04
80	1.72 ± 0.20	13.89 ± 4.74	21.05 ± 3.96	15.38 ± 0.96
90	1.72 ± 0.13	13.66 ± 4.41	20.73 ± 4.04	15.48 ± 1.15
100	1.69 ± 0.15	13.30 ± 4.32	20.73 ± 4.10	15.72 ± 1.18
240	1.73 ± 0.34	8.23 ± 2.74	19.85 ± 4.20	13.96 ± 0.53
480	1.67 ± 0.33	9.34 ± 2.31	17.07 ± 3.24	15.40 ± 2.71
1380	1.49 ± 0.25	7.14 ± 1.12	12.23 ± 2.83	12.06 ± 2.36

TABLE 1. Biodistribution (%ID) of $^{99m}\text{Tc}-(\text{CO})_3$ His-CNA35 in nude mice ($n = 4$) at different time points post-injection. Pi, post-injection; ID, injected dose; SD, standard deviation

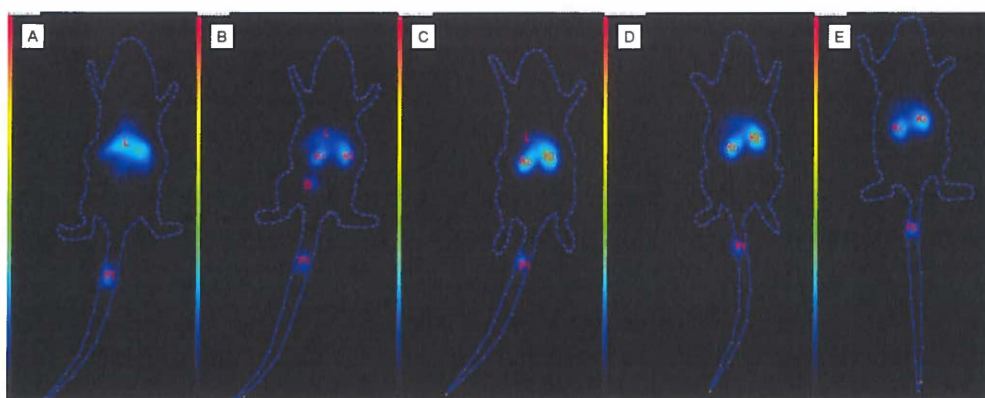


FIGURE 3. Posterior view of planar images showing *in vivo* biodistribution of $^{99m}\text{Tc}-(\text{CO})_3$ His-CNA35 in a healthy mouse (37 MBq $^{99m}\text{Tc}-(\text{CO})_3$ His-CNA35 injected), during first minute (A) and 100 minutes (B) after injection of the radiotracer (acquisition time of 1 minute); and 4h (C), 8h (D) and 23h (E) after injection of the radiotracer (acquisition time of

10 minutes). Liver and kidneys show the highest radiotracer uptake. L = liver, Kr = right kidney, Kl = left kidney, B = bladder, PI = place of injection

Dosimetry

To translate the mice biodistribution data into estimates of patient dose, the organ values were extrapolated from the data derived from the biodistribution data to a 68-kg man using the standard Medical Internal Radiation Dose (MIRD) scheme and S-tables. A summary of dosimetric parameters for the main excretory organs and total body is given in Table 2. Kidneys clearly had the highest absorbed dose, followed by the liver. The effective dose equivalent (EDE) and the effective dose (ED), when calculations were done per organ, were 0.0129 mSv/MBq and 0.00739 mSv/MBq, respectively. The EDE and the ED, when calculations were made per gram tissue, were 0.00612 mSv/MBq and 0.00402 mSv/MBq, respectively. The total ED for a proposed single-injection of dosage of 500 MBq $^{99m}\text{Tc}-(\text{CO})_3$ His-CNA35 will be 3,70 mSv (ED per organ) or 2,01 mSv (ED per gram tissue). MIRDose 3.1 also gives estimates of the dose in other organs, for example absorbed dose (per organ) for the lungs, ovaries, testes and uterus (radiation-sensitive organs) are 0.00317, 0.00294, 0.00156 and 0.00289 mGy/MBq, respectively.

Site	Per organ		Per gram tissue	
	Residence Time (h)	Absorbed Dose (mGy/MBq)	Residence Time (h)	Absorbed Dose (mGy/MBq)
Kidneys	2.74	0.138	1.05	0.0538
Liver	0.91	0.0145	0.33	0.00593
Total Body	7.56	0.00378	7.56	0.00252

TABLE 2. Dosimetric data for intravenously administered $^{99m}\text{Tc}-(\text{CO})_3$ His-CNA35.

In Vivo Imaging of Tumor Vasculature in a Human HT29 Colorectal Tumor Xenograft Model

Three hours after intravenous injection of $^{99m}\text{Tc}-(\text{CO})_3$ His-CNA35, a planar, static scan was made. Radiotracer uptake in the tumors was calculated by ROI-analysis and expressed as T/B ratios. In all 10 HT29 human colorectal carcinoma xenografts, tumors were visually determinable and showed a heterogeneous uptake of the radiotracer (see Figure 4). T/B ratios varied considerably among the different animals (mean 3.03 ± 0.88). $^{99m}\text{Tc}-(\text{CO})_3$ His-CNA35

uptake was correlated with MVD ($R = 0.733$, $p = 0.016$) and blood vessel-associated collagen IV ($R = 0.758$, $p = 0.011$) as determined by immunohistochemistry (see Figure 5). Additionally, we found a significant inverse correlation between $^{99m}\text{Tc}-(\text{CO})_3$ His-CNA35 uptake and the VMI ($R = -0.709$, $p = 0.022$) (see Figure 5).



FIGURE 4. *In vivo* imaging of tumor vasculature in 2 HT29 human colorectal carcinoma bearing mice (right hind leg) showing respectively a mouse (left) with high tumor uptake (T/B ratio 3.94) and a mouse (right) with low tumor uptake (T/B ratio 2.63).

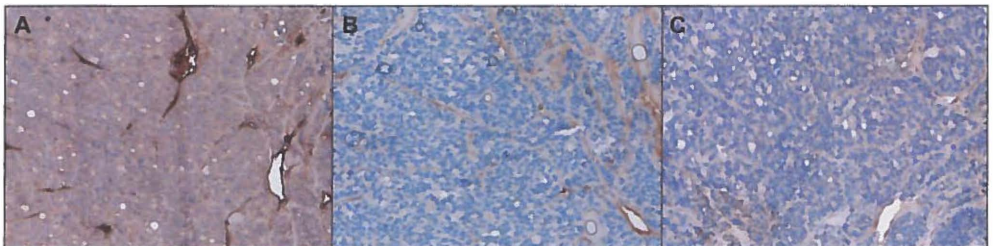


FIGURE 5. Immunohistochemical staining of CD105/Endoglin (A, 200x), Collagen IV (B, 200x), and α -SMA (C, 200x) in HT29 tumors.

DISCUSSION

In this manuscript, the successful radioactive labeling and validation of a new marker of tumor vasculature is described. This marker is based upon binding of tumor subendothelial collagen due to the structural deficits that characterize tumor vasculature.

This is the first report of the successful radioactive labeling of CNA35 to detect tumor vasculature non-invasively. Several studies have labeled CNA35 with fluorophores in order to detect collagen in an *in vitro* setting. Krahn et al. investigated the binding properties of CNA35-OG488 and confirmed binding to collagen types I-VI with various affinities and no binding to other ECM proteins (5). In the following *in vitro* study, collagen formation around HVS cells was successfully demonstrated (5). Using the same molecule, Boerboom et al. successfully obtained high resolution images of collagen in samples of HVS myofibroblast cell cultures, mouse carotid artery vessels and engineered cardiovascular constructs (6). The only *in vivo* study to our knowledge successfully performed fluorescent collagen labeling after intravenous injection of CNA35-OG488 (7).

In our study, labeling yields of approximately 40-50% and high radiochemical purities ($\geq 95\%$) were obtained. The incubation of CNA35 with the ^{99m}Tc -tricarbonyl took place at a temperature of 37°C at physiological pH and the radiotracer remained stable for up to 24h, at 4°C and 37°C , in physiological solution, cell medium and human blood serum. Overall, preparation of $^{99m}\text{Tc}(\text{CO})_3$ His-CNA35 was straightforward and resulted in a pure product with a good stability. The functionality and specificity of the labelled molecule were confirmed in an *in vitro* solid phase binding assay where binding of $^{99m}\text{Tc}(\text{CO})_3$ His-CNA35 to collagen I and IV was observed with negligible binding to fibronectin and laminin. These results confirm those obtained in a previous study (5).

The biodistribution study performed in 4 healthy nude mice revealed that the radiotracer rapidly cleared from the blood following iv injection and was predominantly retained in the liver and the kidneys indicating a urinary excretory pathway. Uptake in the right kidney was higher than in the left kidney at all time points. This may be explained by a partial overlap of the right kidney with the liver, or due to the position of the right kidney in relation to the camera. The high uptake in the liver and the kidneys may be due to the nature of the endothelial lining in these organs. Unlike in other organs, the blood vessels in the liver have a discontinuous endothelial coverage and the blood vessels of the kidneys have a fenestrated endothelium (12,13). As a result, labeling of collagen in the subendothelial layers of these blood vessels can occur. Megens et al. described a similar phenomenon when they studied the

uptake of a fluorescently labeled variant of CNA35 in healthy and atherosclerotic arteries of mice after both *ex vivo* and *in vivo* administration (7). Administration of $^{99m}\text{Tc}-(\text{CO})_3$ His-CNA35 to patients would cause an effective dose of 0.00739 mSv/MBq corresponding to a total effective dose of 3.70 mSv (ED per organ) for a patient dose of 500 MBq. These numbers are in the low range when compared to other tracers used in a clinical setting (14). However, allometric scaling from laboratory animals to humans was performed on the basis of body/organ weight which assumes that the biokinetics of compounds depends primarily on the metabolic rate of the animal which in turn is a function of the body weight or body surface area. The effective doses obtained in this study merely give an estimation of the effective dose that would be obtained in human patients. A detailed study in humans for a reliable estimation of the effective dose is still recommended.

To image tumor vasculature *in vivo*, human colorectal carcinoma xenografts were imaged 3 hours after injection of $^{99m}\text{Tc}-(\text{CO})_3$ His-CNA35 to allow sufficient bloodpool clearance. A heterogeneous uptake of the radiotracer was seen in all tumors. A significant correlation between $^{99m}\text{Tc}-(\text{CO})_3$ His-CNA35 uptake and MVD was demonstrated. Further we found a significant correlation between $^{99m}\text{Tc}-(\text{CO})_3$ His-CNA35 uptake and collagen IV that was associated with blood vessels. Additionally, we found a significant inverse correlation between $^{99m}\text{Tc}-(\text{CO})_3$ His-CNA35 uptake and the VMI. This VMI gives an estimate of the percentage of vessels that is associated with mural cells and thus an estimate of the maturity of the vessels. These results indicate that imaging using CNA35 gives a reliable estimate of existing tumour vasculature and confirm the proposed mechanism of binding in which the characteristic leakiness and immaturity of tumor blood vessels allows binding of subendothelial collagen IV and selective imaging of tumor vasculature. A limitation to our approach is the existence of capillaries with a fenestrated and/or discontinuous endothelium in a number of tissues like kidneys, endocrine glands, gastrointestinal tract and liver (12,13). Although biodistribution studies did not indicate much binding of our molecule to other organs except kidneys and liver and all tumors were visually determinable, future studies will have to assess the extent of non-specific binding in these organs. Discontinuous endothelium (or sinusoids) that can be found in the liver usually have an incomplete or absent basement membrane, which would prevent major binding (12,13).

Besides histological and circulating markers of tumor angiogenesis, a number of non-invasive markers of tumor vasculature and angiogenesis have been reported that use different imaging modalities. Compounds that specifically target VEGF (vascular endothelial growth factor) and its receptors together with compounds that target integrins are the best studied candidates to

image tumor vascularisation. Although several of these tracers have been tested in a pre-clinical and clinical setting where they successfully visualized several types of tumors and their metastases (15,16), none of these are routinely used in clinic and few have been used to detect antiangiogenic therapy response. In two studies, response to antiangiogenic therapy was successfully detected using ^{99m}Tc -HYNIC-VEGF and ^{89}Zr -ranibizumab (17,18). However, due to the long biological half-life of VEGF, labeling of VEGF or VEGF-targeting molecules with long-lived isotopes like ^{89}Zr or ^{111}In is needed (18,19), resulting in high radiation exposures. Using RGD (asparagine-glycine-aspartic acid) - peptide based tracers, several studies also successfully evaluated treatment response to antiangiogenic therapy (20-22). However, as integrins are expressed not only on endothelial cells but on tumor cells as well (20,23), and are minimally expressed on normal quiescent endothelial cells (24), RGD-peptide based tracers might not be truly representative of existing tumor vasculature. Furthermore, high uptake of ^{18}F -galacto-RGD in inflammatory lesions has been reported (25). In future studies, we will assess the potential of $^{99m}\text{Tc}(\text{CO})_3$ His-CNA35 to evaluate the effectiveness of commonly used antiangiogenic drugs. Additionally, we will attempt to label CNA35 with PET labels such as Gallium-68 (^{68}Ga), which has the advantage of a generator-based production and a convenient half-life (68min). Given its mechanism of action we further propose a role for radiolabeled CNA35 in evaluating the vascular normalisation window which follows antiangiogenic therapy (26). Non-invasive evaluation of the time frame of this normalisation window would allow selection of the appropriate timing to administer chemotherapy.

CONCLUSION

His-tagged CNA35 was successfully labeled with $^{99m}\text{Tc}(\text{CO})_3$ and this resulted in a pure, functional product with a good stability. The biodistribution study demonstrated a rapid blood clearance and a predominantly renal excretion. Tumors were successfully visualized and uptake correlated with *ex vivo* immunohistochemical staining of blood vessels and basement membrane and was inversely correlated with vessel maturity. Further research will determine whether or not $^{99m}\text{Tc}(\text{CO})_3$ His-CNA35 can provide a reliable tool for the management and planning of antiangiogenic therapy.

ACKNOWLEDGEMENTS

CNA35-cDNA was a kind gift of Dr. Maarten Merkx, TU/e Eindhoven, the Netherlands. Part of this work was financially supported by the European Union through the grant Euregional PACT II by the Interreg IV program of Grensregio Vlaanderen-Nederland (IVAVLANED-1.20)

REFERENCES

1. Fukumura D, Jain RK. Tumor microvasculature and microenvironment: targets for anti-angiogenesis and normalization. *Microvas Res.* 2007;74:72-84.
2. Homsí J, Daud AI. Spectrum of activity and mechanism of action of VEGF/PDGF inhibitors. *Cancer Control.* 2007;14:285-294.
3. Mia J, Waxman DJ. Combination of antiangiogenesis with chemotherapy for more effective cancer treatment. *Mol Cancer Ther.* 2008;7:3670-3684.
4. Zong Y, Xu Y, Liang X, et al. A 'collagen hug' model for Staphylococcus aureus CNA binding to collagen. *EMBO J.* 2005;24:4224-4236.
5. Krahn KN, Bouten CVC, van Tuijl S, et al. Fluorescently labeled collagen binding proteins allow specific visualization of collagen in tissues and live cell culture. *Anal Biochem.* 2006;350:177-185.
6. Boerboom RA, Krahn KN, Megens RTA, et al. High resolution imaging of collagen organisation and synthesis using a versatile collagen specific probe. *J Struct Biol.* 2007;159:392-399.
7. Megens RTA, oude Egbrink MGA, Cleutjens JPM, et al. Imaging collagen in intact viable healthy and atherosclerotic arteries using fluorescently labeled CNA35 and two-photon laser scanning microscopy. *Mol Imaging.* 2007;6:247-260.
8. LeBleu VS, MacDonald B, Kalluri R. Structure and function of basement membranes. *Exp Biol Med (Maywood).* 2007;232:1121-1129.
9. Laemli UK. Cleavage of structural proteins during the assembly of the head of bacteriophage T4. *Nature.* 1970;227:680-685.
10. Weidner N, Semple JP, Welch WR, et al. Tumor angiogenesis and metastasis - correlation in invasive breast-carcinoma. *N Engl J Med.* 1991;324:1- 8.

11. Spurbek WW, Ng CY, Vanin EF, et al. Retroviral vector-producer cell-mediated in vivo gene transfer of TIMP-3 restricts angiogenesis and neuroblastoma growth in mice. *Cancer Gene Ther.* 2003;10:161-167.
12. Young B, Heath JW. *Wheater's Functional Histology*. Edinburgh, Churchill Livingstone; 2000:274-309
13. Aird WC. Phenotypic heterogeneity of the endothelium. *Circ Res.* 2007;100:158-190.
14. ICRP. Radiation Dose to Patients from Radiopharmaceuticals - Addendum 3 to ICRP Publication 53. ICRP Publication 106. *Ann ICRP.* 2008; 38:1-198.
15. Cai W, Chen X. Multimodality molecular imaging of tumor angiogenesis. *J Nucl Med.* 2008;49:113S-128S.
16. Dijkgraaf I, Boerman OC. Radionuclide imaging of tumor angiogenesis. *Cancer Biother Radiopharm.* 2009;24:637-647.
17. Blankenberg FG, Backer MV, Levashova Z, et al. In vivo tumor angiogenesis imaging with site-specific labeled (99m)Tc-HYNIC-VEGF. *Eur J Nucl Med Mol Imaging* 2006;33:841-848.
18. Nagengast WB, Lub-de Hooge MN, Oosting SF, et al. VEGF-PET imaging is a noninvasive biomarker showing differential changes in the tumor during sunitinib treatment. *Cancer Res.* 2011;71:143-153.
19. Nagengast WB, Lub-de Hooge MN, van Straten EME, et al. VEGF-SPECT with ¹¹¹In-bevacizumab in stage III/IV melanoma patients. *Eur J Cancer.* 2011;47:1595-1602.
20. Jung KH, Lee KH, Paik JY, et al. Favorable biokinetic and tumor-targeting properties of ^{99m}Tc-labeled glucosamino RGD and effect of paclitaxel therapy. *J Nucl Med.* 2006;47:2000-2007.
21. Morrison MS, Ricketts SA, Barnett J, et al. Use of a novel Arg-Gly-Asp radioligand ¹⁸F-AH111585, to determine changes in tumor vascularity after antitumor therapy. *J Nucl Med.* 2009;50:116-122.
22. Battle MR, Goggi JL, Allen L, et al. Monitoring tumor response to antiangiogenic sunitinib therapy with ¹⁸F-fluciclatide, an ¹⁸F-labeled $\alpha_v\beta_3$ -integrin and $\alpha_v\beta_5$ -integrin imaging agent. *J Nucl Med.* 2011;52:424-430.
23. Beer AJ, Haubner R, Sarbia M, et al. Positron emission tomography using [¹⁸F] galacto-RGD identifies the level of integrin $\alpha_v\beta_3$ expression in man. *Clin Cancer Res.* 2006;12:3942-3949.

24. Brooks PC, Montgomery AM, Rosenfeld M, et al. Integrin $\alpha_v\beta_3$ antagonists promote tumor regression by inducing apoptosis of angiogenic blood vessels. *Cell*. 1994;79:1157-1164.
25. Haubner R, Weber WA, Beer AJ, et al. Noninvasive visualization of the activated alphavbeta3 integrin in cancer patients by positron emission tomography and [^{18}F] galacto-RGD. *PLoS Med*. 2005;2:e70.
26. Goel S, Duda DG, Xu L, et al. Normalization of the vasculature for treatment of cancer and other diseases. *Physiol Rev*. 2011;91:1071-1121.

Chapter 4: General Discussion

As the proteins responsible for [^{18}F]FDG-uptake are under control of HIF-1, the master regulator of the hypoxic response, the degree of [^{18}F]FDG-uptake might indirectly reflect the degree of tumor hypoxia and vice versa. Therefore, in this work we explored the relation between tumor oxygenation and tumor metabolism, and evaluated the possible consequences and benefits of this relation for functional imaging using [^{18}F]FDG - PET. In a second part of this work a new radiotracer of tumor vasculature was evaluated. As tumor vasculature and tumor hypoxia are highly interconnected, non-invasive imaging of tumor vasculature might provide insights into tumor hypoxia.

In Chapter 2, partim 2.1, the effects of an increase in tumor oxygenation on tumor metabolism were studied by investigating changes in expression of proteins important for tumor metabolism, survival and spread in a rat colorectal xenograft after treatment with rhEPO. Tumor pO_2 -measurements confirmed that pO_2 -values were significantly higher after treatment with rhEPO. To date, the mechanisms by which rhEPO improves tumor oxygenation remain unclear. Several direct effects of rhEPO have been described by which rhEPO can influence tumor oxygenation independent of the effects on hemoglobin levels or through changes in vascular endothelial growth factor (VEGF) expression and microvessel morphology (Blackwell et al. 2003, Tovari et al. 2005). Although rhEPO-treatment increased tumor oxygenation, we did not find significant differences in the expression of GLUT1, GLUT3, GLUT4, GLUT8, GLUT9, SGLT1, HKI, HKII, HKIII and N-cadherin between experimental groups receiving rhEPO and experimental groups that didn't. We did on the other hand, find significant increases in the expression of GLUT3, HKI and N-cadherin when rhEPO was combined with radiotherapy. As these proteins have distinct anti-apoptotic and pro-metastatic functions by increasing energy supply, preventing cytochrome C release and increasing tumor invasiveness, these findings substantiate results of earlier studies that reported that rhEPO might actually adversely affect survival rates of cancer patients treated by radiotherapy (Henke et al. 2003, Leyland-Jones et al. 2005) by acting as an anti-apoptotic agent and a growth factor not only on endothelial cells but on tumor cells as well (Hardee et al. 2006, Sinclair et al. 2007, Jelkmann et al. 2008). The mechanism by which this occurs remains largely unclear and needs further clarification.

In Chapter 2, partim 2.2, the effects of a decrease in tumor oxygenation or a direct HIF-1 activation on tumor metabolism were studied by investigating [^{18}F]FDG-uptake in an *in vitro* and *in vivo* model of human colorectal carcinoma. We first investigated the effects of

chemical activation of HIF-1 on [¹⁸F]FDG-uptake in human HT29 colorectal carcinoma cells. Treatment of HT29 colorectal carcinoma cells with the hypoxia mimicking chemicals CoCl₂ and DMOG resulted in induction of HIF-1 through HIF-1 α protein stabilization which resulted in increased transcription of GLUT1, HK2 and CA IX genes. As opposed to CoCl₂, DMOG did not increase HIF-1 α mRNA levels, which is in line with its mechanism of action where DMOG inhibits breakdown of HIF-1 α protein. Treatment of HT29 colorectal carcinoma cells with the hypoxia mimicking chemicals CoCl₂ and DMOG resulted in significant increases in [¹⁸F]FDG-uptake. Both chemicals are hypoxia mimics that, as confirmed in this study, provide an easy platform to activate HIF-1 and investigate the hypoxic response in an *in vitro* setting. Whereas CoCl₂-induced stimulation of [¹⁸F]FDG-uptake seems to increase as a function of time, the DMOG-induced stimulation appears to have an early set-on and remain constant throughout time. These results thus indicate a different mechanism of action of CoCl₂ and DMOG. Although numerous *in vitro* studies in different types of cancer cell lines have reported on an increase in [³H]-FDG or [¹⁸F]-FDG uptake after exposure to decreasing oxygen atmospheres (Clavo et al. 1995, Burgman et al. 2001, Pedersen et al. 2001, Oswald et al. 2007), studies reporting on glucose-uptake after a chemical induction of hypoxia are limited. Two studies in Clone 9 rat liver cells reported on an increase in 3-O-methyl D-glucose transport after treatment for 24h with CoCl₂ which was associated with an increase in GLUT1 mRNA and protein content (Behrooz et al. 1997, Hwang et al. 2002). Similar results were obtained in BeWo choriocarcinoma cells and articular chondrocytes (Baumann et al. 2007, Peansukmanee et al. 2008).

In a next step, we investigated [¹⁸F]FDG-uptake after induction of artificial hypoxia and chemical activation of HIF-1 in an *in vivo* xenograft model of human colorectal carcinoma. Comparison of endogenous and exogenous hypoxic markers in control animals showed a significant correlation between pimonidazole staining and CA IX expression, confirming the role of CA IX as one of the most reliable endogenous markers of tumor hypoxia. Given the timeframe of CA IX expression (Vordermark et al. 2005), this would confirm that CA IX as well as pimonidazole mainly demonstrate chronic hypoxia. Upon visual inspection we observed that, although an absolute spatial colocalization was absent, expression of CA IX and GLUT1 showed a strong overlap with pimonidazole staining and a similar staining pattern. To create artificial hypoxia in our *in vivo* tumor model, we used the peripheral vasodilator hydralazine hydrochloride which, through indirect inhibition of tumor blood flow ('steal phenomenon'), causes tumor hypoxia (Fisker et al. 1991). In this study as well, a

significant decrease in tumor pO_2 -values was observed in the HT29 xenograft after administration of a single dose of hydralazine. There have been several attempts to modulate tumor oxygenation in order to overcome RT resistance and improve response. Only a few studies have looked at the effects of this modulation on [^{18}F]FDG-PET imaging. In a study by Chan et al., a significant increase in [^{18}F]FDG-uptake was found in SCCVII tumor bearing mice breathing normal air when compared to carbogen, only when the highest uptake regions of the tumor were considered (Chan et al. 2006). Comparable results were obtained by Bentzen et al. (Bentzen et al. 2000). Another study by de Geus-Oei et al. found that [^{18}F]FDG-PET with hyperoxygenation in 22 patients suffering from head-and-neck cancer induced a profound, but variable metabolic change (de Geus-Oei et al. 2006). To our knowledge, only one study evaluated ^{14}C -2-deoxyglucose uptake in an hypoxic tumor model created by use of a tourniquet and observed a decrease in uptake as compared to the control tumor on the other thigh (Kubota et al. 1999). In our study, treatment with a single dose of hydralazine caused a minor decrease in SUV_{max} and SUV_{mean}. Perhaps the lack of effect that is seen after treatment with hydralazine is the consequence of the decreased tumor perfusion that characterizes its mode of action. Other studies, that successfully used hydralazine to confirm the pO_2 dependence of several hypoxia-selective PET imaging agents did not indicate an effect on tracer delivery and subsequent binding as soon as thirty minutes after hydralazine treatment (Lewis et al. 2001, Kinuya et al. 2002, Lee et al. 2008). Another possibility is an incorrect timing of hydralazine administration. The timing used in this study was based on work by Fisker et al., where an almost 90% reduction in tumor levels of 86-RbCl was observed within 15min following a single dose of 5 mg/kg hydralazine i.v. before slowly returning to control levels after about 8h (Fisker et al. 1991). We assumed that the ideal moment to inject [^{18}F]FDG would be the moment were a partial or complete recovery of tumor blood flow was present. In other words, it was our intention to find the time point where the effects of reduction of blood flow would not hamper tracer delivery but at the same time would ensure the hypoxic effects that would be necessary to activate the HIF-1 system and induce downstream gene expression of glucose transporters, hexokinases, We therefore chose to determine [^{18}F]FDG-uptake 3 hours and 8 hours after hydralazine treatment. To chemically activate HIF-1 in our *in vivo* tumor model, we used DMOG, which has no direct effects on tumor oxygenation but stabilizes and activates HIF-1 through PHD-inhibition. Systemic administration of DMOG has been described previously without adverse effects (Cummins et al. 2008, Milkiewicz et al. 2004, Hill et al. 2008). In our study, we observed an increase in SUV_{max} and SUV_{mean} after treatment with a single dose of DMOG

which was statistically significant on day 1. We hypothesize that the increase in tumor [¹⁸F]FDG-uptake after treatment with a single dose of DMOG is the consequence of tumoral HIF-1 activation with an associated transcription of metabolic genes resulting in an increase in glucose/[¹⁸F]FDG uptake. As proposed by Cummins et al., DMOG may be primarily active at the sites of acute insults. Indeed, they showed that DMOG did not alter basal myeloperoxidase activity and cytokine levels in normal colon tissue, but counteracted inflammation in colon subjected to inflammatory insults (Cummins et al. 2008). Another study observed similar effects when DMOG induced increased expression of HIF-1 α and downstream VEGF in muscle that was subjected to ischemic insult, but not in normal muscle (Milkiewicz et al. 2004). If this would be the case, tumor specific activation of HIF-1 can indeed be achieved with associated increase in glucose transport.

In Chapter 2, partim 2.3, the distribution of the exogenous hypoxia marker pimonidazole was compared with the expression of GLUT1 and 3, HK2 and CA IX in a spontaneous canine mammary gland carcinoma. This spontaneous canine tumor model was chosen because of its high incidence, easy resection and the common occurrence of multiple tumors. As described in Chapter 1, the exogenous hypoxia marker pimonidazole is the most relevant marker for qualitative and quantitative determination of tumor hypoxia in experimental and clinical circumstances. In this study a statistically significant correlation was found between pimonidazole staining and GLUT1 expression confirming the strong interplay between tumor hypoxia and tumor metabolism.

In Chapter 2, partim 2.4, the expression of CA IX was compared with [¹⁸F]FDG-PET SUVmax and SUVmean values in patients suffering from NSCLC. The transmembrane zinc metalloenzyme carbonic anhydrase IX (CA IX) catalyzes the reversible hydration of carbon dioxide to carbonic acid outside the cell and is involved in respiration and acid-base balance (Potter et al. 2004). As the gene for CA IX has been shown to be one of the most strongly hypoxia-inducible ones (Lal et al. 2001), it has emerged as one of the most reliable and frequently used endogenous hypoxia markers. In this study, a statistically significant correlation was found between CA IX expression and [¹⁸F]FDG SUVmax and SUVmean values of the primary tumor. Besides further confirming the strong interplay between tumor hypoxia and tumor metabolism, these results also suggest that in the future it may be possible to identify NSCLC patients that are most likely to benefit from CA IX targeting therapy on the basis of [¹⁸F]FDG-PET imaging.

In Chapter 3, a new radiotracer to detect tumor vasculature was evaluated. The radiolabeling of His-CNA35 with [^{99m}Tc] via tricarbonyl is described and its use in the detection of tumor vasculature is investigated. Overall preparation of $^{99m}\text{Tc}-(\text{CO})_3$ His-CNA35 was straightforward and resulted in a pure product with a good stability. An *in vitro* solid-phase binding assay confirmed the functionality and specificity of the labeled molecule. This assay confirmed binding of the molecule to collagen I and IV while negligible binding was observed to fibronectin-, laminin- and non-coated surfaces. These results confirm earlier results obtained in binding experiments performed with a fluorescently labeled variant of the CNA35 molecule (CNA35-OG488) where a strong affinity of CNA35 for collagen I and IV and a lack of major binding to other extracellular matrix proteins besides collagens, was described (Krahn et al. 2006). Biodistribution studies indicated a rapid clearance from the blood and a predominantly urinary excretory pathway. Mice biodistribution data were translated into estimates of patient dose and effective doses are in the low range when compared to other tracers used in a clinical setting (ICRP 2008). The effective dose numbers obtained in this study however, merely give an estimate of the actual patient dose and therefore, a detailed study in humans is still recommended. After injection of $^{99m}\text{Tc}-(\text{CO})_3$ His-CNA35 in untreated HT29 human colorectal carcinoma bearing mice, all tumors were visually determinable and showed a heterogeneous uptake of the radiotracer. Similar to biodistribution experiments, high uptake was seen in liver and kidneys which can be the result of the nature of the endothelial lining in these organs. Unlike in other organs, the blood vessels in the liver have a discontinuous endothelial coverage and the blood vessels of the kidneys have a fenestrated endothelium (Young et al. 2000, Aird et al. 2007). As a result, labeling of collagen in the subendothelial layers of these blood vessels can occur. In a study by Megens et al. that performed collagen imaging of a fluorescently labelled variant of CNA35 (CNA35-OG488) in normal wild-type mice and Apo E^{-/-} mice with induced atherosclerotic plaques after both *ex vivo* and *in vivo* administration, a similar phenomenon was described (Megens et al. 2007). To confirm uptake specificity, immunohistochemistry was performed on these animals and these results showed a significant correlation between T/B ratios and MVD (CD105/Endoglin) and blood vessel associated collagen IV. Further, an inverse correlation was found between T/B ratios and vessel maturity (VMI; αSMA). These results indicate that imaging using CNA35 gives a reliable estimate of existing tumor vasculature and confirm the proposed mechanism of binding in which the characteristic leakiness and immaturity of tumor blood vessels allows binding of subendothelial collagen IV and selective imaging of tumor vasculature.

Chapter 5: Conclusions and Future Perspectives

Several *in vitro* studies suggested that [¹⁸F]FDG-uptake is increased under hypoxic conditions (Clavo et al. 1995, Burgman et al. 2001, Pedersen et al. 2001, Oswald et al. 2007) and several studies performed in different xenograft models have described a correlation between [¹⁸F]FDG-uptake and pimonidazole staining (Scigliano et al. 2008, Dearling et al. 2004, Pugachev et al. 2005). Likewise, our results suggest a strong interplay between tumor hypoxia and tumor metabolism. More specifically, we found a significant correlation between pimonidazole staining and CA IX expression in a colorectal carcinoma mouse xenograft, a significant correlation between pimonidazole staining and GLUT1 expression in a spontaneous canine mammary gland carcinoma and a significant correlation between CA IX expression and [¹⁸F]FDG SUVmax and SUVmean values of the primary tumor of patients suffering from NSCLC. Whereas our results suggest that [¹⁸F]FDG-uptake might reflect tumor hypoxia, comparison of the distribution of [¹⁸F]FDG with more specialized hypoxia tracers has yielded mixed results (see Chapter 1). It appears that in those tumors where HIF-1 activation is mainly hypoxia-driven, the degree of [¹⁸F]FDG uptake may be a surrogate marker of tumor hypoxia. Therefore, it seems questionable that [¹⁸F]FDG can act as a reliable non-invasive marker of tumor hypoxia as several other hypoxia-independent microenvironmental parameters such as differentiation, pH, glucose availability, oncogene activation, ...affect the activation of HIF-1 and/or the expression of proteins downstream of HIF-1 that are involved in glucose metabolism. However, insight into the relationship between tumor hypoxia and tumor metabolism can create opportunities to increase [¹⁸F]FDG-uptake in situations where diagnostic accuracy is suboptimal: (i) tumors with a high differentiation and a low growth rate (prostate carcinoma, hepatocellular carcinoma and neuroendocrine tumors) often fail to take up [¹⁸F]FDG; (ii) the inability of [¹⁸F]FDG to evaluate lesions either in or adjacent to tissues with a high metabolic activity (brain) or physiological accumulation (urinary bladder); and (iii) the reduced specificity of [¹⁸F]FDG in the differentiation of malignant from an infective or inflammatory process (Kellof et al. 2005, Endo et al. 2006). In this work, [¹⁸F]FDG-uptake was increased in an *in vitro* and *in vivo* model of human colorectal carcinoma after chemical activation of HIF-1 using a PHD-inhibitor. Possibly, in situations where [¹⁸F]FDG-PET imaging is less successful, imaging after a single treatment with PHD-inhibitors might increase sensitivity. Several of these prolyl hydroxylase domain-containing protein inhibitors are currently under development for the treatment of anaemic and ischemic conditions in humans (Yan et al. 2010, Bernhardt et al. 2010). Although some of these compounds are currently undergoing phase I and phase II clinical trials, their oncological use has not been explored and deleterious effects on tumor

progression thus need to be investigated. Future studies will try to confirm the results obtained in the HT29 colorectal carcinoma xenograft using PHD-inhibitors in the spontaneous canine mammary carcinoma tumor model.

In a second part of this thesis a new radiotracer of tumor vasculature was evaluated. The successful labeling and *in vivo* imaging properties are described. However, a limitation to our approach is the existence of capillaries with a fenestrated and/or discontinuous endothelium in a number of tissues like kidneys, endocrine glands, gastrointestinal tract and liver (Young et al. 2000, Aird et al. 2007). Although biodistribution studies did not indicate much binding of our molecule to other organs except kidneys and liver and all tumors were visually determinable, future studies will have to assess the extent of non-specific binding in these organs.

Imaging of tumor vasculature is interesting for a number of reasons. *Firstly*, as the importance of anti-angiogenic chemotherapy increases, methods are needed to provide a reliable assessment of tumor vasculature and thus provide a means for the management and planning of anti-angiogenic therapy. Given the difficulties associated with invasive methods, a non-invasive method is of major clinical interest. Several candidate markers have been labeled with PET and SPECT labels to image tumor vasculature of which compounds that specifically target VEGF (vascular endothelial growth factor) and its receptors together with compounds that target integrins are the best studied. Although several of these tracers have been tested in a pre-clinical and clinical setting where they successfully visualized several types of tumors and their metastases (Cai et al. 2008, Dijkgraaf et al. 2009), none of these are routinely used in clinic and few have been used to detect antiangiogenic therapy response. In one study by Blankenberg et al., ^{99m}Tc -HYNIC-VEGF was successfully used to detect response to low-dose metronomic (antiangiogenic) and high-dose (tumoricidal) cyclophosphamide treatment in mice with 4T1 tumors (Blankenberg et al. 2006). Further, a recent study by Nagengast et al. successfully evaluated ^{89}Zr -ranibizumab as a biomarker of dynamic angiogenic changes in tumors after treatment with sunitinib (Nagengast et al. 2011). However, due to the long biological half-life of VEGF, labeling of VEGF or VEGF-targeting molecules with long-lived isotopes like ^{89}Zr or ^{111}In is needed (Nagengast et al. 2011, Nagengast et al. 2011), resulting in high radiation exposures. Using RGD (asparagine-glycine-aspartic acid) - peptide based tracers, several studies also successfully evaluated treatment response to antiangiogenic therapy (Jung et al. 2006, Morrison et al. 2009, Battle et al. 2011). However, as integrins are expressed not only on endothelial cells but on tumor cells as well (Jung et al. 2006, Beer et al.

2006), and are minimally expressed on normal quiescent endothelial cells (Brooks et al. 1994), RGD-peptide based tracers might not be truly representative of existing tumor vasculature. Furthermore, high uptake of ^{18}F -galacto-RGD in inflammatory lesions has been reported (Haubner et al. 2005). $^{99\text{m}}\text{Tc}(\text{CO})_3$ His-CNA35 provides a new means to target tumor vasculature and thereby image it. In future studies, the potential of this tracer to provide a reliable assessment of the efficiency of anti-angiogenic chemotherapy and thus a means for its management and planning, will be evaluated. Additionally, we will attempt to label CNA35 with PET labels such as Gallium-68 (^{68}Ga). Whereas SPECT imaging with $^{99\text{m}}\text{Tc}$ offers the advantage of ready availability at a low cost and versatile chemistry, PET ensures a superior spatial resolution and more accurate quantification. *Secondly*, given its characteristic mechanism of action, CNA35 might also be a valuable tool to evaluate the vascular 'normalisation window' that follows anti-angiogenic chemotherapy. This phenomenon states that careful application of antiangiogenic therapy can 'normalize' the abnormal tumor vasculature, resulting in more efficient delivery of drugs and oxygen to the targeted tumor cells and thereby enhancing RT and chemotherapy efficiency (Jain et al. 2005). Indeed, administration of antiangiogenic drugs as a single agent yielded only modest objective responses and no long term survival benefits in clinical trials. In contrast, when given in combination with chemotherapy, increases in survival were observed (Mia et al. 2008). It appears that antiangiogenic therapy can restore the imbalance between pro- and anti-angiogenic factors and thereby partially restore the structural and functional deficiencies that characterize tumor blood vessels. These deficiencies, as mentioned in Chapter 1, lead to heterogeneous blood flow, hypoxia, acidosis and elevated interstitial fluid pressure (IFP) with a disturbed tumor microenvironment as a result. Because tumor vasculature labeling with CNA35 is based upon these abnormalities, restoration of a normal tumor vessel wall would inhibit binding of the molecule. As a consequence, imaging using CNA35 would allow evaluation of the 'normalisation state' of tumor blood vessels. As suggested by Jain, it is crucial to identify the time window during which the vessels initially become normalized, as well as an understanding of how long they remain in that state (Jain 2005). Given its mechanism of binding, CNA35 might be an ideal candidate to identify the time frame of this 'normalisation window' and therefore the ideal moment to administer chemotherapy. *Finally*, as tumor vasculature and tumor hypoxia are highly interconnected, non-invasive imaging of tumor vasculature might provide insights into tumor hypoxia and allow estimation of the degree of tumor hypoxia. Few studies have reported on a comparison between tumor vasculature imaging agents and tumor hypoxia imaging agents. In one study by Picchio et al.,

a substantial discordance was found between the tumor distribution of [^{18}F]FAZA and [^{25}I]-Gluco-RGD in EMT6 tumor xenografts (Picchio et al. 2008). In several studies performed by the group from Nijmegen, the spatial distribution of exogenous markers of tumor hypoxia was compared with immunohistochemical markers of tumor vasculature. Whereas one study found only a weak and non-significant inverse correlation between hypoxic fraction and vascular density (Wijfels et al. 2000), another study found a significant inverse correlation between the hypoxic fraction and the density of perfused vessels (Rijken et al. 2000). Future studies will compare $^{99\text{m}}\text{Tc}$ -(CO) $_3$ His-CNA35 uptake with uptake of a specialized hypoxia tracer.

References

- Aird WC. Phenotypic heterogeneity of the endothelium. *Circ Res.* 2007;100:158-190.
- Asikainen TM, Ahmad A, Schneider BK, et al. Stimulation of HIF-1alpha, HIF-2alpha, and VEGF by prolyl 4-hydroxylase inhibition in human lung endothelial and epithelial cells. *Free Radic Biol Med.* 2005;38:1002-1013.
- Battle MR, Goggi JL, Allen L, et al. Monitoring tumor response to antiangiogenic sunitinib therapy with ¹⁸F-fluciclatide, an ¹⁸F-labeled $\alpha_v\beta_3$ -integrin and $\alpha_v\beta_5$ -integrin imaging agent. *J Nucl Med.* 2011;52:424-430.
- Baumann MU, Zamudio S, Illsley NP. Hypoxic upregulation of glucose transporters in BeWo choriocarcinoma cells is mediated by hypoxia-inducible factor-1. *Am J Physiol Cell Physiol.* 2007;293:C477-C485.
- Beer AJ, Haubner R, Sarbia M, et al. Positron emission tomography using [¹⁸F] galacto-RGD identifies the level of integrin $\alpha_v\beta_3$ expression in man. *Clin Cancer Res.* 2006;12:3942-3949.
- Behrooz A, Ismail-Beigi F. Dual control of glut1 glucose transporter gene expression by hypoxia and by inhibition of oxidative phosphorylation. *J Biol Chem.* 1997;272:5555-5562.
- Bentzen L, Keiding S, Horsman MR, et al. Feasibility of detecting hypoxia in experimental mouse tumours with 18F-fluorinated tracers and positron emission tomography--a study evaluating [¹⁸F]Fluoro-2-deoxy-D-glucose. *Acta Oncol.* 2000;39:629-637.
- Bernhardt WM, Wiesener MS, Scigalla P. Inhibition of prolyl hydroxylases increases erythropoietin production in ESRD. *J Am Soc Nephrol.* 2010;21:2151-2156.
- Blackwell KL, Kirkpatrick JP, Snyder SA, et al. Human recombinant erythropoietin significantly improves tumor oxygenation independent of its effects on hemoglobin. *Cancer Res.* 2003;63:6162-6165.
- Blankenberg FG, Backer MV, Levashova Z, Patel V, Backer JM. *In vivo* tumor angiogenesis imaging with site-specific labeled (99m)Tc-HYNIC-VEGF. *Eur J Nucl Med Mol Imaging.* 2006;33:841-848.
- Brooks PC, Montgomery AM, Rosenfeld M, et al. Integrin $\alpha_v\beta_3$ antagonists promote tumor regression by inducing apoptosis of angiogenic blood vessels. *Cell.* 1994;79:1157-1164.
- Burgman P, O'Donoghue JA, Humm JL, et al. Hypoxia-induced increase in FDG uptake in MCF7 cells. *J Nucl Med.* 2001;42:170-175.

- Cai W, Chen X. Multimodality molecular imaging of tumor angiogenesis. *J Nucl Med.* 2008;49:113S-128S.
- Chan LW, Hapdey S, English S, et al. The influence of tumor oxygenation on (18)F-FDG (fluorine-18 deoxyglucose) uptake: a mouse study using positron emission tomography (PET). *Radiat Oncol.* 2006;1:3 doi:10.1186/1748-717X-1-3
- Clavo AC, Brown RS, Wahl RL. Fluorodeoxyglucose uptake in human cancer cell lines is increased by hypoxia. *J Nucl Med.* 1995;36:1625-1632.
- Cummins EP, Seeballuck F, Keely SJ, et al. The hydroxylase inhibitor dimethylxalylglycine is protective in a murine model of colitis. *Gastroenterology.* 2008;134:156-165.
- Dearling JL, Flynn AA, Sutcliffe-Goulden J, et al. Analysis of the regional uptake of radiolabeled deoxyglucose analogs in human tumor xenografts. *J Nucl Med.* 2004;45:101-107.
- Dijkgraaf I, Boerman OC. Radionuclide imaging of tumor angiogenesis. *Cancer Biother Radiopharm.* 2009;24:637-647.
- Endo K, Oriuchi N, Higuchi T, et al. PET and PET/CT using 18F-FDG in the diagnosis and management of cancer patients. *Int J Clin Onc.* 2006;11:286-296.
- Fisker RV, Horsman MR, Overgaard J. Hydralazine-induced changes in tissue perfusion and radiation response in a C3H mammary carcinoma and mouse normal tissues. *Acta Oncol.* 1991;30:641-647.
- de Geus-Oei LF, Kaanders JH, Pop LA, et al. Effects of hyperoxygenation on FDG-uptake in head-and-neck cancer. *Radiother Oncol.* 2006;80:51-56.
- Hardee ME, Arcasoy MO, Blackwell KL, et al. Erythropoietin biology in cancer. *Clin Cancer Res.* 2006;12:332-339.
- Haubner R, Weber WA, Beer AJ, et al. Noninvasive visualization of the activated alphavbeta3 integrin in cancer patients by positron emission tomography and [¹⁸F] galacto-RGD. *PLoS Med.* 2005;2:e70.
- Hazan RB, Phillips GR, Qiao RF, et al. Exogenous expression of N-cadherin in breast cancer cells induces cell migration, invasion, and metastasis. *J Cell Biol.* 2000;148:779-790.
- Henke M, Laszig R, Rube C, et al. Erythropoietin to treat head and neck cancer patients with anaemia undergoing radiotherapy: randomised, double-blind, placebo-controlled trial. *Lancet.* 2003;362:1255-1260.
- Hill P, Shukla D, Tran MG, et al. Inhibition of hypoxia inducible factor hydroxylases protects against renal ischemia-reperfusion injury. *J Am Soc Nephrol.* 2008;19:39-46.

- Hirsilä M, Koivunen P, Xu L, et al. Effect of desferrioxamine and metals on hydroxylases in the oxygen sensing pathway. *FASEB J*. 2005;19:1308-1310.
- Hwang DY, Ismail-Beigi F. Glucose uptake and lactate production in cells exposed to CoCl₂ and in cells overexpressing the glut-1 glucose transporter. *Arch Biochem Biophys*. 2002;399:206-211.
- ICRP. Radiation Dose to Patients from Radiopharmaceuticals - Addendum 3 to ICRP Publication 53. ICRP Publication 106. *Ann ICRP*. 2008; 38:1-198.
- Jain RK. Normalization of tumor vasculature: an emerging concept in antiangiogenic therapy. *Science*. 2005;307:58-62.
- Jelkmann W, Bohlius J, Hallek M, et al. The erythropoietin receptor in normal and cancer tissues. *Crit Rev Oncol Hemat*. 2008;67:39-61.
- Jewell UR, Kvietikova I, Scheid A, et al. Induction of HIF-1 α in response to hypoxia is instantaneous. *FASEB J*. 2001;15:1312-1314.
- Jung KH, Lee KH, Paik JY, et al. Favorable biokinetic and tumor-targeting properties of ^{99m}Tc-labeled glucosamino RGD and effect of paclitaxel therapy. *J Nucl Med*. 2006;47:2000-2007.
- Kelloff GJ, Krohn KA, Larson SM, et al. The progress and promise of molecular imaging probes in oncologic drug development. *Clin Cancer Res*. 2005;11:7967-7985.
- Kinuya S, Yokoyama K, Li XF, et al. Hypoxia-induced alteration of tracer accumulation in cultured cancer cells and xenografts in mice: implications for pre-therapeutic prediction of treatment outcomes with ^{99m}Tc-sestamibi, ²⁰¹Tl chloride and ^{99m}Tc-HL91. *Eur J Nucl Med*. 2002;29:1006-1011.
- Krahn KN, Bouten CVC, van Tuijl S, et al. Fluorescently labeled collagen binding proteins allow specific visualization of collagen in tissues and live cell culture. *Anal Biochem*. 2006;350:177-185.
- Kubota K, Tada M, Yamada S, et al. Fukuda H, Ido T. Comparison of the distribution of fluorine-18 fluoromisonidazole, deoxyglucose and methionine in tumour tissue. *Eur J Nucl Med*. 1999;26:750-757.
- Lal A, Peters H, St Croix B, et al. Transcriptional response to hypoxia in human tumors. *J Natl Cancer Inst*. 2001;93:1337-1343.
- Lee BF, Chiu NT, Hsia CC, et al. Accumulation of Tc-99m HL91 in tumor hypoxia: in vitro cell culture and in vivo tumor model. *Kaohsiung J Med Sci*. 2008;24:461-471.

- Lewis JS, Sharp TL, Laforest R, et al. Tumor uptake of copper-diacetyl-bis (N⁴-methylthiosemicarbazone): effect of changes in tissue oxygenation. *J Nucl Med.* 2001;42:655-661.
- Leyland-Jones B, Semiglazov V, Pawlicki M, et al. Maintaining normal hemoglobin levels with epoetin alfa in mainly nonanemic patients with metastatic breast cancer receiving first-line chemotherapy: a survival study. *J Clin Oncol.* 2005;23:5960-5972.
- Megens RTA, oude Egbrink MGA, Cleutjens JPM, et al. Imaging collagen in intact viable healthy and atherosclerotic arteries using fluorescently labelled CNA35 and two-photon laser scanning microscopy. *Mol Imaging.* 2007;6:247-260.
- Mia J, Waxaman DJ. Combination of antiangiogenesis with chemotherapy for more effective cancer treatment. *Mol Cancer Ther.* 2008;7:3670-3684.
- Milkiewicz M, Pugh CW, Egginton S. Inhibition of endogenous HIF inactivation induces angiogenesis in ischaemic skeletal muscles of mice. *J Physiol.* 2004;560:21-26.
- Morrison MS, Ricketts SA, Barnett J, et al. Use of a novel Arg-Gly-Asp radioligand ¹⁸F-AH111585, to determine changes in tumor vascularity after antitumor therapy. *J Nucl Med.* 2009;50:116-122.
- Nagengast WB, Lub-de Hooge MN, Oosting SF, et al. VEGF-PET imaging is a noninvasive biomarker showing differential changes in the tumor during sunitinib treatment. *Cancer Res.* 2011;71:143-153.
- Nagengast WB, Lub-de Hooge MN, van Straten EME, et al. VEGF-SPECT with ¹¹In-bevacizumab in stage III/IV melanoma patients. *Eur J Cancer.* 2011;47:1595-1602.
- Ong LC, Jin Y, Song IC, et al. 2-[¹⁸F]-2-deoxy-D-glucose (FDG) uptake in human tumor cells is related to the expression of GLUT-1 and hexokinase II. *Acta Radiol.* 2008;49:1145-1153.
- Oswald J, Treite F, Haase C, et al. Experimental hypoxia is a potent stimulus for radiotracer uptake in vitro: comparison of different tumor cells and primary endothelial cells. *Cancer Lett.* 2007;254:102-110.
- Peansukmanee S, Vaughan-Thomas A, Carter SD, et al. Effects of hypoxia on glucose transport in primary equine chondrocytes in vitro and evidence of reduced GLUT1 gene expression in pathologic cartilage in vivo. *J Orthopaedic Res.* 2008;27:529-535.
- Pedersen MWB, Holm S, Lund EL, et al. Coregulation of glucose uptake and vascular endothelial growth factor (VEGF) in two small-cell lung cancer (SCLC) sublines in vivo and in vitro. *Neoplasia.* 2001;3:80-87.

- Potter C, Harris AL. Hypoxia inducible carbonic anhydrase IX, marker of tumor hypoxia, survival pathway and therapy target. *Cell Cycle*. 2004;3:164.
- Pugachev A, Ruan S, Carlin S, et al. Dependence of FDG uptake on tumor microenvironment. *Int J Radiat Oncol Biol Phys*. 2005;62:545-553.
- Rijken PFJW, Bernsen HJJA, Peters JPW, et al. Spatial relationship between hypoxia and the (perfused) vascular network in a human glioma xenograft: a quantitative multi-parameter analysis. *Int J Radiation Oncology Biol Phys*. 2000;48:571-582.
- Scigliano S, Pinel S, Poussier S, et al. Measurement of hypoxia using invasive oxygen-sensitive electrode, pimonidazole binding and 18F-FDG uptake in anaemic or erythropoietin-treated mice bearing human glioma xenografts. *Int J Oncol*. 2008;32:69-77.
- Sinclair AL, Todd MD, Forsythe K, et al. Expression and function of erythropoietin receptors in tumors. *Am Cancer Soc*. 2007;110:477-488.
- Smith TAD. The rate-limiting step for tumor [¹⁸F]fluor-2-deoxy-D-glucose (FDG) incorporation. *Nucl Med Biol*. 2001;28:1-4.
- Torii S, Kurihara A, Li XY, et al. Inhibitory effect of extracellular histidine on cobalt-induced HIF-1 α expression. *J Biochem*. 2011;149:171-176.
- Tovari J, Gilly R, Raso E, et al. Recombinant human erythropoietin alpha targets intratumoral blood vessels, improving chemotherapy in human xenograft models. *Cancer Res*. 2005;65:7186-7193.
- van Waarde A, Elsinga PH. Proliferation markers for the differential diagnosis of tumor and inflammation. *Curr Pharm Des*. 2008;14:3326-3339.
- Vordermark D, Kaffer A, Riedl S, et al. Characterization of carbonic anhydrase IX (CA IX as an endogenous marker of chronic hypoxia in live human tumor cells. *Int J Radiation Oncol Biol Phys*. 2005;61:1197-1207.
- Wijffels KIEM, Kaanders JHAM, Rijken PFJW, et al. Vascular architecture and hypoxic profiles in human head and neck squamous cell carcinomas. *Br J Cancer*. 2000;85:674-683.
- Yan L, Colandrea VJ, Hale JJ. Prolyl hydroxylase domain-containing protein inhibitors as stabilizers of hypoxia-inducible factor: small molecule-based therapeutics for anemia. *Expert Opin Ther Pat*. 2010;20:1219-1245.
- Young B, Heath JW. *Wheater's Functional Histology*. Edinburgh, Churchill Livingstone; 2000:274-309

Yuan Y, Hilliard G, Ferguson T, et al. Cobalt inhibits the interaction between hypoxia-inducible factor- α and von Hippel-Lindau protein by direct binding to hypoxia-inducible factor- α . *J Biol Chem*. 2003;278:15911-15916.



Curriculum Vitae

Personal

Name : Gilles Mees
Address : Kortrijkstraat 206
9700 Oudenaarde
Belgium
Telephone: 0032 – (0)473444249
E-mail: gillesmees@hotmail.com
Born: Ghent, 26/04/1984
Nationality: Belgian

Education

2002-2006: Master in Biomedical Sciences
Ghent University, Belgium

2006-2007: Master in Molecular Biotechnology
Ghent University, Belgium

2008-today: PhD in Medical Sciences
University of Groningen, the Netherlands

2008-2009 Degree C in Laboratory Animal Science, Ghent
University, Belgium

Scientific publications

Mees G, Fonteyne P, Ceelen W, Boterberg T, Pauwels P, Vangestel C, Van Damme N, Peeters M, Dierckx R, Van De Wiele C. Combined effect of EPO and radiotherapy on the expression of endogenous molecular markers of tumor metabolism and metastasis. *Cancer Biother Radiopharm.* 2009;24:565-572.

Mees G, Dierckx R, Vangestel C, Van de Wiele C. Molecular imaging of hypoxia with radiolabelled agents. *Eur J Nucl Med Mol Imaging.* 2009;36:1674-1686.

Vangestel C, Van de Wiele C, Mees G, Peeters M. Forcing cancer cells to commit suicide. *Cancer Biother Radiopharm.* 2009;24:395-407.

Mees G, Vangestel C, Dierckx R, Pauwels P, Van Meerbeeck J, Van de Wiele C. Carbonic anhydrase IX expression correlates with FDG uptake by primary non-small cell lung cancer. *Cancer Biother Radiopharm.* 2010;25:149-154.

Mees G, Vangestel C, Dierckx R, Loomans S, Van Damme N, Peremans K, De Rooster H, Van Goethem B, Pauwels P, Ducatelle R, Van de Wiele C. Metabolic correlates of tumour hypoxia in malignant canine mammary carcinoma. *Res Vet Sci.* 2011;91:e125-128.

Vangestel C, Peeters M, Mees G, Oltenfreiter R, Boersma HH, Elsinga Ph, Reutelingsperger C, N Van Damme, De Spiegeleer B, Van de Wiele C. Imaging of apoptosis in oncology: an update. *Mol Imaging.* 2011;10:340-358.

Philippe Deron, Hubert Vermeersch, Gilles Mees, Christel Vangestel, Patrick Pauwels, Christophe Van de Wiele. Expression and prognostic value of glucose transporters and hexokinases in tonsil and mobile tongue squamous cell carcinoma. *Histol Histopathol.* 2011;26:1165-1172.

Vangestel C, Van de Wiele C, Mees G, Mertens K, Staelens S, Reutelingsperger C et al. SPECT imaging of the early time course of therapy-induced cell death using ^{99m}Tc- (CO)₃ His-annexinA5 in a colorectal cancer xenograft model. *Mol Imaging.* 2012;11:135-147.

Mertens K, Mees G, Lambert B, Van de Wiele C, Goethals I. In-vitro FDG-uptake experiments: practical considerations. *Cancer Biother Radiopharm.* 2012;27:183-188.

Mees G, Dierckx R, Mertens K, Vermeire S, Van Steenkiste M, Reutelingsperger C, Peremans K, D'Asseler Y, Van Damme N, Van de Wiele C. ^{99m}Tc-labelled tricarbonyl His-CNA35 as an imaging agent for the detection of tumour vasculature. *J Nucl Med.* 2012;53:464-471.

Gilles Mees, Rudi Dierckx, Christel Vangestel, Debby Laukens, Nancy Van Damme, Christophe Van de Wiele. Pharmacological activation of tumor hypoxia: a means to increase tumor [¹⁸F]FDG-uptake? *Mol Imaging.* 2012 [Accepted for publication].

Gilles Mees, Christophe Van de Wiele. Radiolabelled probes targeting tumor hypoxia for personalized medicine. *Curr Pharm Des.* [Accepted for publication]

Christophe Van de Wiele, Alex Maes, Eddy Brugman, Yves D'Asseler, Bart De Spiegeleer, Gilles Mees, Karin Stellamans. SIRT in livermetastases: physiological and pathophysiological considerations. *Eur J Nucl Med Mol Imaging.* [Accepted for publication]

Gilles Mees, Alex Maes, Karin Stellamans, Eddy Brugman, Yves D'Asseler, Christophe Van de Wiele. Voxelwise correlation analysis of ^{99m}Tc-MAA and ⁹⁰Y-teraspher count distribution in VOI's encompassing large liver metastases. *Clin Nucl Med.* [Submitted]

Christophe Van de Wiele, Karin Stellamans, Eddy Brugman, Gilles Mees, Bart De Spiegeleer, Yves D'Asseler, Alex Maes. Pretreatment quantitative ^{99m}Tc-MAA SPECT/CT and FDG PET/CT VOI analysis of liver metastases: relationship with treatment response to SIRT. *Nuklearmedizin.* [Submitted]

Abstracts at international congresses

Gilles Mees, Rudi Dierckx, Christel Vangestel, Nancy Van Damme, Kathelijne Peremans, Hilde De Rooster, Patrick Pauwels, Richard Ducatel, Christophe Van de Wiele. Metabolic correlates of tumour hypoxia in a spontaneous canine mammary gland tumour and a human colorectal xenograft. 20th IRIST Congress – Groningen. April 7-10, 2010. Poster.

Gilles Mees, Christel Vangestel, Rudi Dierckx, Patrick Pauwels, Jan Van Meerbeeck, Christophe Van de Wiele. CA-IX expression correlates with FDG-uptake by primary NSCLC. 20th IRIST Congress – Groningen. April 7-10, 2010. Poster.

Mees G, Dierckx R, Mertens K, Vermeire S, Van Steenkiste M, Reutelingsperger C, Peremans K, D'Asseler Y, Van Damme N, Van de Wiele C. ^{99m}Tc-labelled tricarbonyl His-CNA35 as an imaging agent for the detection of tumour vasculature. EANM 2011, Birmingham. October 15-19, 2011. Oral presentation.

Acknowledgements

Ookal klinkt een dankwoord steeds een beetje theatraal, here we go...

Eerst en vooral wens ik **Prof. dr. R. Dierckx** te bedanken om me de mogelijkheid te bieden om een doctoraat te starten onder de vleugels van de Rijksuniversiteit Groningen en er tevens op toe te zien dat dit tot een goed einde werd gebracht.

Prof. dr. C. Van de Wiele, Christophe, bedankt om me gedurende deze 4 jaar te begeleiden met deze thesis. Je gave om in alles mogelijkheden in plaats van beperkingen te zien, zette steeds de deur open voor nieuwe inzichten en uitdagingen. Ook voor alle extra-wetenschappelijke mogelijkheden en activiteiten ben ik je oprecht dankbaar. Zou je dan toch gelijk krijgen dat uiteindelijk alles in orde komt? ☺

De **beoordelingscommissie** bestaande uit Prof. dr. J.A. Langendijk (Rijksuniversiteit Groningen, Nederland), Prof. dr. P.M. Kluin (Rijksuniversiteit Groningen, Nederland), Prof. dr. A. Signore (Sapienza Università di Roma, Italië) wens ik te bedanken voor hun bereidheid dit proefschrift te beoordelen. Ook de **promotiecommissie** bestaande uit de leden van de beoordelingscommissie, Prof. dr. A. Maes (Katholieke Universiteit Leuven, België), Prof. dr. P.H. Elsinga (Rijksuniversiteit Groningen, Nederland), Prof. dr. Y. D'Asseler (Universiteit Gent, België) wens ik te bedanken voor hun bereidheid om hier vandaag, ondanks hun ongetwijfeld drukke agenda, aanwezig te zijn.

De gehele **P7** (Nucleaire Geneeskunde, UZ Gent) wil ik graag bedanken voor de voorbije 4 jaar. Ik zal de fijne tijd die ik bij jullie had nooit vergeten.

Een grote dank gaat uit naar de '**mensen van de K12**' (Gastroenterologie, UZ Gent) : Debby, Nancy, Sara, Kim, Ellen, Elien, Evi, Lyndsey, Pieter, Hugo, Hilde, Sarah. Ik ben elk van jullie oprecht dankbaar om mijn sporadische aanwezigheid in jullie labo te tolereren. Vele experimenten uit deze thesis waren niet mogelijk geweest zonder jullie hulp, kennis en/of materiaal. Altijd kon ik bij jullie terecht voor (in vele gevallen stomme en overbodige) vragen, ondersteuning en raad bij experimenten, koffiekletsjes, after-work drinks, ... Bedankt!

Een bedankje aan een aantal mensen die een aandeel in deze thesis hebben gehad: **Thomas** (mn 'pathologie-connection', bedankt voor de hulp met de honderden weefselstalen), **Philippe** (jij hebt me wegwijs gemaakt op het UZ(ot) en leerde me de kneepjes van de immunohistochemie), **Denise** (bij wie ik steeds terecht kon voor allerhande praktische zaken (en dit altijd met de glimlach)), **Yves** en **Johan** (bedankt voor de technische assistentie en de leuke babbels tijdens de lunch), **Prof. dr. W. Ceelen** (bedankt voor de hulp met het uitvoeren van de pO₂-metingen en het gebruik van het labo van de experimentele heekunde), **Prof. dr. P. Pauwels** (bedankt voor de hulp met het interpreteren van de immunohistochemische kleuringen), **Kathelijne Peremans**, **Eva Vandermeulen** en **Simon Vermeire** (bedankt voor de hulp met het scannen van de muizen en het beschikbaar stellen van jullie scanners!), **Ineke ten Have** (bedankt voor de hulp met allerlei praktische zaken in Groningen), **Prof. dr. C. Reutelingsperger** (bedankt voor de samenwerking), iedereen van de **faculteit Diergeneeskunde** met wie ik samenwerkte (Prof. dr. R. Ducatelle, Sarah Loomans, Hilde De

Rooster, Bart Van Goethem) wil ik bedanken voor de vlotte samenwerking, **Magali Van Steenkiste** (bedankt voor de hulp met de HPLC-experimenten).

A big thanks to **Doug Scott** to let me use his picture on the cover of this thesis!

Christel, jij hebt ons nogal vlug verlaten voor de bovenvernoemde Gastro-mensen. Gezien het bureel zonder daglicht waar we toen in zaten, een te begrijpen keuze. Althans, dat maken Koen en ik onszelf toch wijs dat het het gebrek aan daglicht was dat je heeft weggejaagd van bij ons. Bedankt voor alle hulp met experimenten! **Koen**, het gezicht waar ik de voorbije 4 jaar elke dag heb moeten/mogen op kijken. Bedankt voor alles wat je gedaan hebt, van praktische hulp met experimenten, over koffietjes in 't zonnetje tijdens de middag tot pintjes na 't werk en onvergetelijke congressen samen. Bedankt om ... tja, gewoon zo'n leuke collega te zijn! Kben der zeker van dat we elkaar in toekomst nog wel ergens treffen. **Julie en Alexander**, jullie wens ik het beste toe met het verdere verloop van jullie doctoraat en (wetenschappelijke) carrière!

Mama, papa. Ookal lijkt jullie aandeel in deze thesis heel klein, hij is groter dan jullie ooit zouden kunnen vermoeden. Bedankt voor alles.

Ten slotte, **Lies**. Jij was er steeds om me te steunen en te helpen waar mogelijk. Mijn rust en zekerheid in soms woelige tijden. Ook jouw aandeel is groter dan je beseft. Xxx...